Università degli studi di Ferrara

Dottorato di Ricerca in

"FISICA"

ciclo xxiv

Coordinatore Prof. Filippo Frontera

Scaled chiral quark-solitons for nuclear matter

Settore Scientifico Disciplinare: FIS/04

Dottoranda:

Dott.ssa Mantovani Sarti Valentina

Tutore interno:

Dott. Drago Alessandro

Tutore esterno:

Prof. Vento Vicente

Anni 2009/2011

Contents

Introduction

One of the most challenging problems in hadronic and nuclear physics is to study nuclear matter at finite density by using a scheme which includes one of the fundamental properties of QCD, namely *chiral symmetry*. In general, when studying a physical system one would like to use a technique which can allow, at least in principle, for a systematic improvement in the theoretical quantitative analysis. For instance, in the regimes where they are applicable, perturbative techniques are able to provide more and more precise estimates by increasing the order of the calculation. A good example of such a technique applied to this field is the so-called hard thermal loop expansion [1, 2] which is able to provide a good description of the behaviour of matter at temperature larger than the critical one. Another example is chiral perturbation theory [3], which on the other hand is still struggling to provide reliable results at densities of the order of nuclear matter saturation density. At asymptotically large densities one can vice versa imagine that perturbation theory is again applicable and important results have been obtained in that regime showing for instance the relevance of the phenomenon of color superconductivity [4]. On the other hand the deconfinement transition from hadrons to quarks and gluons cannot be described by using a perturbative

approach.[1] At the moment the only non-perturbative technique which is able to describe some aspects of the transition from hadrons to quark and gluons is lattice QCD: this technique can provide rather precise informations about the behaviour of matter at very high temperatures [6–8] but unfortunately these calculations can be performed only for small values of the chemical potential μ.

In this work we will focus on the non-perturbative region of QCD; in the absence of any reliable expansion scheme we have to resort to model Lagrangians, incorporating the degrees of freedom relevant at the energy scale of the phase transition. Chiral symmetry breaking is typically described in terms of chiral Lagrangians including the corresponding Goldstone bosons as the relevant degrees of freedom. At the moment the process of confinement-deconfinement at finite density is much less understood and it is not even clear if it is associated with a phase transition. The simplest choice, which we will also adopt, is to neglect altogether coloured degrees of freedom, by assuming that they are suppressed by the mechanism of confinement. Therefore we take into account quark-antiquark correlations having the quantum numbers of the pion but we do not include coloured quark-antiquark fluctuations: while this simple scheme is maybe correct at relatively low densities, it is certainly questionable at larger densities where the role of coloured diquark condensates can be relevant. While discussing symmetries and confinement one has to recall that scale invariance is an almost exact symmetry of QCD but it is non perturbatively broken in the hadronic phase. On the other hand scale invariance is restored (but for perturbative contributions) in the quark-gluon plasma at large temperatures. One is therefore pressed to investigate the role played by scale invariance in model Lagrangians.

[1] For an attempt to relate large N_c and confinement see e.g. [5]

There are many chiral models able to provide a quite accurate description of the nucleon. We concentrate on models where the fermionic degrees of freedom are coupled to mesons in a chirally invariant way. This type of models can be separated in two main classes: models in which no kinetic energy is attributed to the quark-antiquark fluctuations and models where those correlations are identified with real chiral fields having an explicit kinetic term. The first class includes the Nambu-Jona-Lasinio model [9] and the chiral quark-soliton model [10, 11]. This type of models are very nicely related to QCD but they are not easy to use having in mind to obtain an effective Lagrangian for nuclear physics by starting from a Lagrangian of interacting quarks. In particular the kinetic energy of the physical pion should be obtained by evaluating non trivial contributions coming from the sea. From this viewpoint the second class of models [12–14] is simpler because its Lagrangian already contains the kinetic terms which appear in a typical nuclear physics Lagrangian. These types of models are able to provide *non-topological* solitonic solutions, given by the interaction between quarks and mesons, which yield a good description of the nucleon properties in vacuum.

It is well known that the introduction of chiral symmetry in an effective Lagrangian to describe nuclear matter at finite density and nuclei is not straightforward. For instance models based on the linear σ model fail to describe nuclear matter already at densities $\rho \sim \rho_0$ because the normal solution in which chiral symmetry is broken becomes unstable respect to the so-called Lee-Wick phase [15]. The main problems in these models are due to the constraints on the scalar field dynamics imposed by the Mexican hat potential [16]. The interaction terms of σ and $\boldsymbol{\pi}$ fields in the linear realization of chiral symmetry allows the chiral fields to move away from the chiral circle as the density rises and to reach,

already at ρ_0, the local maximum where $\sigma_v = 0$ and chiral symmetry is restored.

The problem of a too early restoration of chiral symmetry at finite density can be overcame in two different ways. One could implement chiral symmetry into the Lagrangian through a non-linear realization [17] where the scalar fields are forced to stay on the chiral circle. In Ref. [18] the authors use a non-linear realization of chiral symmetry in which a scalar-isoscalar effective field is introduced, as a chiral singlet, to simulate intermediate range attraction and to satisfy broken scale invariance in QCD; in this way the dynamics of the chiral singlet field is no more regulated by the Mexican hat potential and accurate results for finite nuclei are presented. The other approach is still based on a linear realization of chiral symmetry but with a new potential, which includes terms not present in the Mexican hat potential. A possible guideline in building such a potential is *scale invariance*, which is spontaneously broken in QCD due to the presence of the parameter Λ_{QCD} coming from the renormalization process and it is strictly connected to a non vanishing gluon condensate. This fundamental symmetry of QCD can be implemented in the Lagrangian at mean-field level, following the approaches in [19, 20], through the introduction of a new scalar field, the *dilaton* field, whose dynamics is regulated by a potential chosen in order to reproduce the scale divergence of QCD.

In this work we will adopt a Chiral Dilaton Model (CDM) which also includes scale invariance introduced by the nuclear physics group of the University of Minnesota [21–24]. In their first paper [21] the authors have shown that the model with hadronic degrees of freedom is indeed able to provide a good description of nuclear physics at densities about ρ_0. In the following work [25] it is also shown that the model describes the gradual restoration of chiral symmetry at higher

densities and leads to a phase diagram where the interplay between chiral and scale invariance restoration results in a scenario similar to the one proposed by McLerran and Pisarski in [26].This is not too surprising since the large N_c limit explored in [26] should be well represented in chiral models as the one discussed in [25]. It is therefore tempting to explore the scenario presented in [25] at a more microscopic level.

The new idea we develop in this work is to interpret the fermions as quarks, to build the hadrons as solitonic solutions of the fields equations as in [13, 27] and, finally, to explore the properties of the soliton at finite density.

The description of nuclear matter at finite density can be achieved through several approaches. A possibility is to describe the modification of the single nucleon properties when it is embedded in a dense medium [28–30]. Another possibility is to mimic nuclear matter by placing the solitons on a lattice, with a specific geometry and specific boundary conditions. The Wigner-Seitz approximation is one of the most used approaches in this category, since it relies on the simply assumption of a spherical cell in which the fermions move under the action of a periodic potential given by the meson fields. This scheme has been applied in the past [31–37] but one of the problems in those works is that the solitonic solutions are unstable and disappear already at moderate densities when e.g the linear σ model is adopted. We are therefore facing an instability similar to the one discussed and solved when studying nuclear matter with hadronic chiral Lagrangians.

The first aim of this thesis is *to check whether, just by modifying the mesons interaction with the inclusion of scale invariance, the new logarithmic potential allows the soliton crystal to reach higher densities.* Next, since the CDM also

takes into account the presence of vector mesons, the second and more important aim is *to check whether the inclusion of vector mesons in the dynamics of the quarks can provide saturation for chiral matter.* We should remark that no calculation, neither in vacuum nor at finite density, exists at the moment for the CDM with quarks and vector mesons.

The structure of the thesis is the following: in Chapter 1 a brief overview of soliton models in QCD is presented; in Chapter 2 we introduce the CDM and we present the results for the single soliton in vacuum; in Chapter 3 the Wigner-Seitz approximation to nuclear matter is discussed together with the results for the CDM at finite density; in Chapter 4 we show a first attempt to go beyond the Wigner-Seitz approach with the construction of the $B = 2$ soliton system and the study of the inter-soliton energy. Finally in the Conclusions we summarize the main results achieved along with the discussion of future improvements and extensions of the model.

List of publications

The work presented in this thesis is based on the following papers and preprints:

- "A chiral quark-soliton model with broken scale invariance for nuclear matter.".
  Valentina Mantovani Sarti, Alessandro Drago.
  Submitted for publication to Phys.Rev.C.

- "A hybrid-chiral soliton model with broken scale invariance for nuclear matter.".
  Valentina Mantovani Sarti, Alessandro Drago.
  J.Phys.Conf.Ser. 336 (2011) 012028.

- 'The baryon number two system in the Chiral Soliton Model".
  Valentina Mantovani Sarti, Alessandro Drago, Vicente Vento and Byung-Yoon Park.
  Proceedings for the Conference Few-Body Systems (APFB2011) .

Chapter 1

Soliton models in QCD

The description of nucleons and in general of hadrons properties has to take into account the internal structure of these particles, given by the interaction of quarks and gluons. In particular the calculation of nucleons properties in an appropriate theoretical framework, including masses and form factors, has to provide results compatible with phenomenology.

The main difficulty with QCD is that it becomes a free theory at asymptotically large energies. In most cases the experiments cannot be described just in a perturbative approach. For instance the theoretical interpretation of the structure functions of the hadrons, extracted from experiments of deep inelastic scattering, is given in terms of a non-perturbative matrix element and only its evolution in q^2 can be evaluated using perturbative techniques. The non-perturbative matrix element describes physical processes which take place at low energies.

Since low energy phenomenology is directly linked to the non-perturbative behaviour of QCD, the calculation of hadronic observables involves the full complexity of the underlying fundamental theory.

Lattice simulations of QCD [38,39] are able to provide useful informations in this regime but are still affected by large uncertainties due to the difficulties of the chiral extrapolation.

The gap between the exact gauge theory and the phenomenology in this low energy regime can be filled by relativistic *effective field theories*.

The essential idea of these effective models is to include the fundamental symmetries of QCD into the Lagrangian and to realize that the dynamics at low energies is governed by appropriate degrees of freedom depending on the energy scale.
Models for hadrons can be loosely divided in two classes: bag-like models [40,41] in which confinement is imposed via special boundary conditions given on a chosen (and in most cases static) surface and soliton models in which confinement (or at least binding) is the outcome of the internal dynamics of the fields. It is interesting to notice how the interaction between quarks and chiral fields takes place in the two cases: in the MIT bag model the interaction occurs only at the surface, while in the chiral soliton model the energy density of the interaction is peaked close to the extended region which separates the internal from the external part of the nucleon.

The term *soliton* has to be interpreted as a localised non-dissipative solution of the set of non-linear classical field equations, given by the chosen Lagrangian. There are different types of soliton models, depending on how the stability of the solution is obtained. On one side there are non-topological solitons, whose energy is smaller than the free wave solution; here the stability is directly given by an energetically favourable state identified with the soliton. This category includes non-chiral theories as the Friedberg-Lee model [42,43] and also chiral Lagrangians

as the chiral colour dielectric model [44] and linear σ models [45].
On the other hand, the topological solitons are stable because they carry a conserved topological charge q which forbids the decay into plane waves; this is the case of the Skyrme model [46, 47] where the topological charge is identified with the baryon charge B.

At mean-field level, namely treating the field operators as classical fields, all the chiral models admit a solution having a special isospin configuration called *Hedgehog*, which will be discussed in details in chapter 2. The configuration of fields provided by this ansatz is based essentially on spherical symmetry. It can be shown that the Hedgehog state is one element of an infinite class of degenerate solutions of field equations at mean-field level [48] and it provides the lowest energy state [49].
Although the Hedgehog state permits to easily calculate energies and observables, it breaks rotational and isospin symmetries. Hence projection methods are needed to make contact with physical states of good spin and isospin. Moreover mean-fields solitons are by definition localised solutions, and so they also break translational invariance. These configurations contain spurious centre-of-mass motion whose contributions to the energy of the baryon and to other observables should be removed. More details about the approaches used in nuclear physics for projection on linear momentum can be found in [35].
In this chapter we will describe in details all the main features of the models that provide non-topological solitons and we will give a brief review of the Skyrme model.

1.1 Non-topological solitons

Here we will present a class of solitons where the coupling of various boson fields, mesons or glueballs, to fermions leads to an energetically stable solution of field equations. It is interesting to notice that even normal nuclei, in which the fermions are nucleons, can be considered as non-topological solitons. The low energy features of QCD, as chiral symmetry and dynamical confinement, are included in these models through the self-interaction of meson fields and the coupling of fermions to scalar fields.

1.1.1 Non-chiral solitons

In this section we will present the most known soliton models which do not include chiral symmetry but provide confinement through the interaction of quarks and scalar fields.

The Friedberg-Lee model

The soliton bag model presented here [42,43,50] is the most representative one for the class of non-chiral soliton models. The model consists of quarks interacting with a scalar field σ and the Lagrangian density has the following form:

$$\mathcal{L} = \overline{\psi}(i\partial\!\!\!/ - g\sigma)\psi + \frac{1}{2}\partial_\mu\sigma\partial^\mu\sigma - U(\sigma) \tag{1.1}$$

where $U(\sigma)$ is the self-interacting potential of the scalar field.
This potential is usually chosen to have a quartic form:

$$U(\sigma) = \frac{1}{2!}a\sigma^2 + \frac{1}{3!}b\sigma^3 + \frac{1}{4!}c\sigma^4 + p. \tag{1.2}$$

The quartic form makes the model renormalizable and the coefficients a, b, c, p in (1.2) can be chosen so that $U(\sigma)$ has the shapes shown in Fig. 1.1. Here the

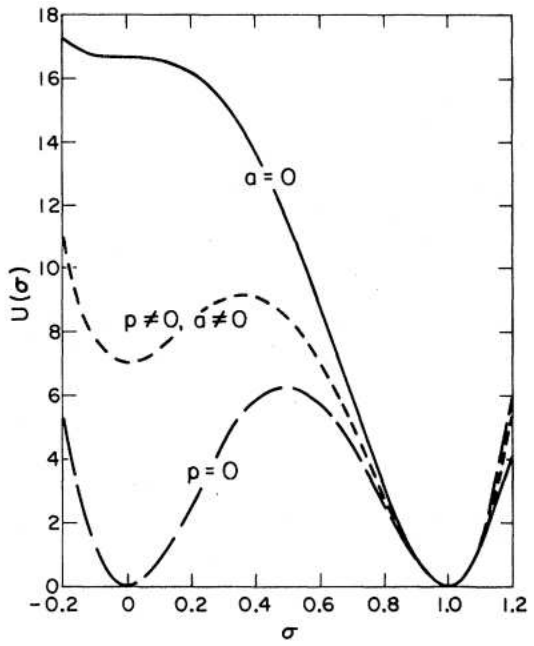

Figure 1.1: Typical forms for the potential $U(\sigma)$ in the soliton bag model [50].

potential always shows two minima: the absolute one at a finite value σ_v and the other one at $\sigma = 0$. The former represents the non-perturbative physical vacuum with a condensate $\sigma = \sigma_v$, while the latter corresponds to a metastable vacuum in which the condensate vanishes. We will see later that for the Linear-σ model the non vanishing condensate is connected to the spontaneous breaking of chiral symmetry, i.e. the vacuum is not invariant under chiral transformations. In other models as e.g in the non-chiral version of the dielectric model, a non vanishing scalar field in the vacuum is instead associated with the breaking of scale invariance: the scalar field is related to the dilaton field which in turns is connected to the gluon condensate.

The coupling between the quarks and the scalar field, $g\sigma\overline{\psi}\psi$, besides acting as the mass term for the quarks, also adds a linear term in the potential $U(\sigma)$. This

means that when the scalar density $\rho_s = \overline{\psi}\psi$ is large enough, this linear term can raise the energy of the non-perturbative vacuum and the perturbative vacuum becomes the stable minimum. In this way the quarks are confined in a finite region by the self-interaction of the scalar field and the quarks density forces the σ field to stay close to zero.

The colour dielectric model

This model is similar to the Friedberg-Lee one but here the coupling of the quarks to the scalar field χ can provide absolute confinement.
In this model the interaction term between χ and fermion is non-linear, but it goes like $\frac{1}{g_\chi \chi}$. Solitons in this model have been studied in different papers as [51–54].
The Lagrangian of the model reads:

$$\mathcal{L} = \overline{\psi}\left(i\partial\!\!\!/ - \frac{m}{g_\chi \chi}\right)\psi + \frac{1}{2}(\partial_\mu \chi)^2 - U(\chi). \tag{1.3}$$

The potential $U(\chi)$ can still have a quartic form, similar to the potential of the soliton bag model in Fig. 1.1 but here the absolute minimum now occurs at $\chi_v = 0$ as shown in Fig. 1.2.

In Fig. 1.3 we show a "one phase" configuration of fields, where the scalar field stays close to zero; here all fields have a smooth behaviour as they approach the surface of the confining region.

In the case of a "two phase" solution (Fig. 1.4), since the χ field can switch from one minimum to the other as shown in Fig. 1.2, the scalar field shows a sharper decrease at the surface and also the quarks wave function G and F are rapidly cut off.

The colour dielectric model can be made chiral invariant by replacing the mass term with the coupling of quarks to the chiral fields, σ and $\boldsymbol{\pi}$. The modified

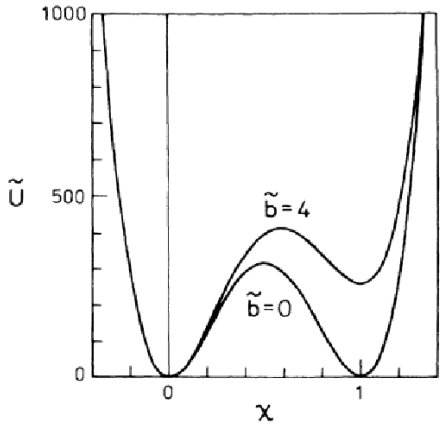

Figure 1.2: Potential $\tilde{U}_\chi$ as given in Ref. [55]. Here $\tilde{b} = b/\sigma_v$ and $\tilde{U}_\chi = U_\chi/\sigma_v^4$. The case with $\tilde{b} = 0$ provides a "one phase" solution (Fig. 1.3), while the case with $\tilde{b} = 4$ gives a "two phase" configuration (Fig. 1.4).

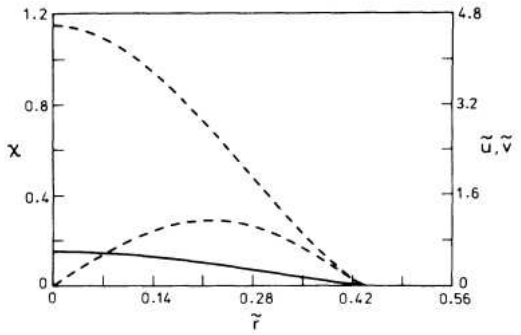

Figure 1.3: Upper and lower Dirac components (dashed line) and scalar field (solid line) in the colour-dielectric model for "one phase" solution [55].

Lagrangian becomes:

$$\begin{aligned}\mathcal{L} =& \overline{\psi}\left(i\partial\!\!\!/ - g_\pi \frac{\sigma + i\boldsymbol{\tau}\cdot\boldsymbol{\pi}\gamma_5}{g_\chi \chi}\right)\psi \\ &+ \frac{1}{2}(\partial_\mu\chi)^2 + \frac{1}{2}(\partial_\mu\sigma)^2 + \frac{1}{2}(\partial_\mu\boldsymbol{\pi})^2 - U(\chi) - U_{mex}(\sigma,\boldsymbol{\pi}) \qquad (1.4)\end{aligned}$$

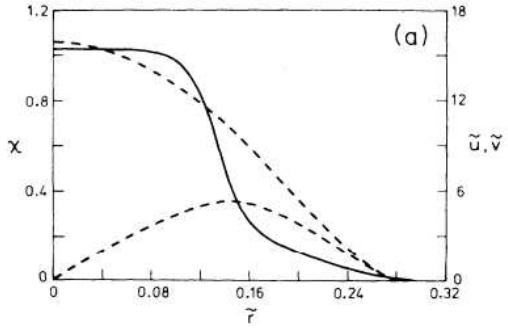

Figure 1.4: Upper and lower Dirac components (dashed line) and scalar field (solid line) in the colour-dielectric model for "two phase" solution [55].

where $U_{mex}(\sigma, \boldsymbol{\pi})$ is the Mexican hat potential which will be described in Sec. 1.1.2. This extension to include chiral symmetry plays anyway a small role in determining the structure and properties of baryons [56].

1.1.2 Chiral solitons

Chiral symmetry is an exact symmetry of QCD in the limit of vanishing quark masses. In this case the quark part of the QCD Lagrangian,

$$\mathcal{L}_q = \overline{\psi}(i\gamma^\mu D_\mu)\psi \tag{1.5}$$

is invariant under ordinary $SU(2)$ rotation in isospin space and also under axial isospin rotations. This whole set of transformations is equivalent to isospin rotations which act independently on right- and left-handed quarks and hence the symmetry group is denoted as $SU(2)_R \times SU(2)_L$.

However, it is well known that current quark masses are finite but, considering only up and down quarks, since their masses are small compared to the hadronic scale, chiral symmetry can be considered as an approximate symmetry of the

strong interactions.

There are two modes to realize chiral symmetry: the Wigner-Weyl mode and the Nambu-Goldstone mode [57].

In the Wigner-Weyl mode we have a chiral-symmetric vacuum which annihilates under the action of isospin Q_α and axial $Q_{\alpha,5}$ charges. In this case if we apply to the proton state $|p\rangle$ the strong interaction Hamiltonian H and the parity operator P (which anti-commutes with the axial charge) we obtain:

$$\begin{aligned} HQ_{\alpha,5}|p\rangle &= Q_{\alpha,5}H|p\rangle = m_p Q_{\alpha,5}|p\rangle \\ PQ_{\alpha,5}|p\rangle &= -Q_{\alpha,5}P|p\rangle = -Q_{\alpha,5}|p\rangle\,. \end{aligned} \tag{1.6}$$

Hence, from here it is clear that if chiral symmetry is an exact symmetry realized in the Wigner-Weyl mode, there should exist a chiral partner of the proton with same mass m_p but opposite parity. This realization of chiral symmetry has already been used in several σ-models [58–60] especially to study matter at high density and temperatures.

In the Nambu-Goldstone realization of chiral symmetry in QCD the symmetry is spontaneously broken, due to the fact that now the vacuum is not chiral invariant. From Goldstone theorem it follows that there exist a boson for each broken symmetry. Since there are three axial charges, then there should be three massless pseudoscalar bosons, identified with the pion, which are the corresponding Goldstone bosons. The existence of massless particles in the chirally broken phase has to be taken into account in any effective low-energy Lagrangian.

In this section we will present the best known chiral soliton models used in hadronic and nuclear physics. In these models the quarks are coupled to the chiral fields, a scalar-isoscalar σ and a pseudoscalar-isovector π, in a chirally invariant

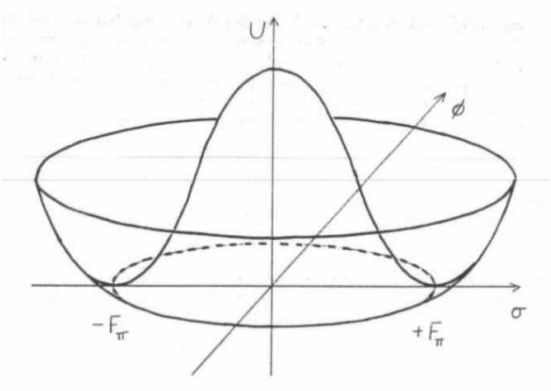

Figure 1.5: The Mexican hat potential for the meson fields in the Linear-σ model [35].

way. The meson potential provides the suitable mechanism for the spontaneous breakdown of chiral symmetry.

The linear σ model

The linear σ model [45] includes a fermionic massless isodoublet field ψ, a triplet of pseudoscalar pions π and a scalar field σ. The chirally symmetric Lagrangian involving these fields has the form:

$$\mathcal{L} = \overline{\psi}[i\partial\!\!\!/ + g(\sigma + i\boldsymbol{\pi}\cdot\boldsymbol{\tau}\gamma_5)]\psi + \frac{1}{2}(\partial_\mu\sigma)^2 + +\frac{1}{2}(\partial_\mu\boldsymbol{\pi})^2 - U(\sigma,\boldsymbol{\pi}). \tag{1.7}$$

The potential in (1.7) is chosen to have a Mexican hat form:

$$U_{mex}(\sigma,\boldsymbol{\pi}) = \frac{\lambda^2}{4}(\sigma^2 + \boldsymbol{\pi}^2 - \nu^2)^2. \tag{1.8}$$

As can be seen in Fig. 1.5, the potential admits degenerate minima, which satisfy the chiral circle equation $\sigma^2 + \boldsymbol{\pi}^2 = \nu^2$. By imposing that the physical vacuum is parity even, it follows that $\sigma_v = \pm\nu$, $\boldsymbol{\pi}_v = 0$. The pionic vacuum excitations are then massless particles, the three Goldstone bosons of the model, while the sigma excitations acquire a mass.

Explicit symmetry breaking can be included in the model by adding to the potential a term linear in σ:

$$U_{mex,SB}(\sigma, \boldsymbol{\pi}) = U_{mex}(\sigma, \boldsymbol{\pi}) + c\sigma \tag{1.9}$$

The linear term tilts the potential and allows the pion to have a finite mass. The three parameters λ, ν and c can be fixed by requiring that:

- the pion has the physical mass $m_\pi = 139$ MeV,
- the pion decay constant (which can be estimated by using the divergence of the axial current inside the matrix element of the pion decay) has the physical value $f_\pi = 93$ MeV,
- finally λ can be related to the mass of the sigma by the equation:

$$\lambda^2 = \frac{m_\sigma^2 - m_\pi^2}{2f_\pi^2} \ , \tag{1.10}$$

  and after this parameter fixing :

$$\nu^2 = \frac{m_\sigma^2 - 3m_\pi^2}{2f_\pi^2}. \tag{1.11}$$

The label linear used in this section distinguishes this model from the non-linear one, where the sigma and the pion fields are tied to the chiral circle. Under this constraint, the sigma field reads:

$$\sigma = f_\pi \left(1 - \frac{\boldsymbol{\pi}^2}{f_\pi^2}\right)^{1/2} \tag{1.12}$$

and by substituting it in (1.7) we obtain the Lagrangian for the non-linear model.

The σ model has been fully analysed in many papers, both in its linear [12,61] and non linear form [13]. It has been shown that, with a proper choice of the

parameters g and m_σ, good results can be obtained for both baryon masses and nucleon observables.

The basic model has been extended in several directions, in particular in [62] the authors include also the vector mesons. The new Lagrangian incorporates the idea of universal coupling [63], which couples the vector mesons to the appropriate currents: the ρ meson to the isospin current, the a_1 to the axial isospin current and the ω to the baryon one.

1.2 Topological solitons

In the large-N_c limit, it has been proved [64] that QCD reduces to a local field theory of weakly interacting mesons, and baryons may emerge as solitons of this theory. Many of these properties of large-N_c are satisfied by the meson-sector of the non-linear sigma model and are included in the Skyrme model [46, 47].

The Skyrme model does not have explicit quarks and gluons degrees of freedom but it is based only on meson fields and their interaction.

The Lagrangian of the model reads:

$$\mathcal{L} = \frac{f_\pi^2}{16} Tr(\partial_\mu U^\dagger \partial^\mu U) + \frac{1}{32e^2} Tr[U^\dagger \partial_\mu U, U^\dagger \partial_\nu U] + \frac{1}{8} m_\pi^2 f_\pi^2 (TrU - 2) \qquad (1.13)$$

where $U = \frac{1}{f_\pi}(\sigma + i\boldsymbol{\tau} \cdot \boldsymbol{\pi})$, f_π is the pion decay constant and e is an adjustable parameter of the model. The first term in the Lagrangian represents the kinetic energies of the meson fields, the second one is the necessary fourth-order term that stabilizes the solitonic configurations and the last term takes into account the explicit symmetry breaking.

The solutions of fields equations of (1.13) are called Skyrmions and are classified according to a positive integer n, the *topological charge*. This conserved charge can be identified with the baryon number B, once the Wess-Zumino term is

included [65]. It has been shown that a skyrmion with $n = 1$ has the same properties of a fermion; hence starting from a pure bosonic model, we can obtain solitonic solutions which behave as nucleons thanks to its topological properties.

Chapter 2

The Chiral Dilaton Model

At present we are still far from being able to describe the phenomenology of the non-perturbative regime of QCD with an effective Lagrangian involving mesons and quarks, and which could be used for nuclear physics starting from the fundamental constituents. A possible guideline to the construction of such a Lagrangian is to incorporate in it all the fundamental symmetries of the exact theory, such as the spontaneous breakdown of chiral and scale symmetry. In the previous chapter we presented an overview of the non-topological soliton models used in QCD, where quarks degrees of freedom are explicitly included and where chiral symmetry plays a fundamental role in building up the nucleon.

In this chapter we will describe an effective Lagrangian, introduced by the nuclear physics group of the University of Minnesota [21–24], which reproduces the chiral dynamics together with the breaking of scale invariance, given by the introduction in the model of the gluon condensate as an additional scalar field.

In the next sections we will introduce scale invariance and the so-called scale anomaly, which is responsible for the breaking of scale invariance in QCD. Later

on we will discuss in detail the Chiral Dilaton Model, in particular how chiral symmetry and scale invariance are implemented in the Lagrangian. Subsequently we will review the mean-field approximation and the Hedgehog ansatz, used for computing the soliton properties. We will also give a brief description of the projection technique adopted for obtaining the nucleon observables. Finally we will present the results for the single soliton in vacuum.

2.1 Scale invariance in QCD

2.1.1 Invariance under dilatations

A classical massless theory is invariant under scale transformations if its action remains constant when fields, denoted generically as ϕ, and coordinates transform as follows [66, 67] :

$$\begin{aligned} x &\to \lambda^{-1}x \ , \ \lambda > 0, \\ \phi(x) &\to U(\lambda)\phi(\lambda x) \end{aligned} \tag{2.1}$$

where $U(\lambda)$ is the scale operator assumed to be fully reducible. This means that it can be written as:

$$U(\lambda) = e^{D \ln \lambda} \tag{2.2}$$

with D a matrix that can be diagonalized. In a classical massless theory these transformations are symmetries if all non-dimensionless parameters (coupling constants and masses) are set equal to zero and if the eigenvalues of D are equal to $d = 1$ for bosons and $d = 3/2$ for fermions.

From Noether's theorem we know that the scale invariance of the action is associated with the conservation of the so called *dilatation* current. In order to take into account also the case of a massive theory, an improved energy-momentum

tensor is defined so that its trace vanishes for vanishing masses. Recalling the fact that the equations of motions do not change when a total derivative is added to the Lagrangian, a similar possibility exists for the definition of the energy-momentum tensor. As shown in [68], the improved expression of the energy-momentum tensor does not change the form of the global generators of the Poincarè group. It can than be proved that the divergence of the dilatation current corresponds to the trace of the 'improved' energy momentum tensor, i.e.:

$$\partial_\mu D^\mu = \widetilde{T}^\mu_\mu \,. \tag{2.3}$$

For instance, in the case of the Lagrangian of a scalar field ϕ the improved energy-momentum tensor is obtained by adding to the canonical energy-momentum tensor the term:

$$\frac{1}{6}(g_{\mu\nu}\partial^2 - \partial_\mu\partial_\nu)\phi^2 \,. \tag{2.4}$$

The following expression for the 'improved' tensor is then obtained:

$$\widetilde{T}_{\mu\nu} = T_{\mu\nu} + \frac{1}{6}(g_{\mu\nu}\partial^2 - \partial_\mu\partial_\nu)\phi^2 = \frac{\partial\mathcal{L}_\phi}{\partial(\partial^\mu\phi)}(\partial_\nu\phi) - g_{\mu\nu}\mathcal{L}_\phi + \frac{1}{6}(g_{\mu\nu}\partial^2 - \partial_\mu\partial_\nu)\phi^2 \,. \tag{2.5}$$

2.1.2 Scale anomaly

The concept of quantum anomaly is simple: when the Lagrangian of a classical field theory is invariant under a given symmetry, it can happen that, after the quantization of the fields, the symmetry is no more exact, since the associated Noether currents are no longer conserved. In this case it is said that there is a quantum anomaly, since the symmetry of the Lagrangian is broken at a quantum level.

Let us now concentrate on scale invariance. In the case of QCD, in the approximation of massless quarks the Lagrangian is scale invariant due to the absence of any dimensional parameter. The renormalization process, in the case of asymptotic free theories as e.g. QCD, allows only to determine how the coupling constant varies with the scale, but not the absolute value itself. An alternative procedure is to introduce a dimensional parameter Λ directly into the definition of the running coupling. The numerical value of Λ can then be determined by comparison with experimental values and it turns out to be of the order of a few hundred MeV. In this way, and at variance with QED, scale invariance is broken due to quantum corrections coming from the appearance of a dimensional parameter. Notice also that, since the masses of the up and down quarks are small, all dimensional quantities in hadronic physics should be related to the numerical value of Λ.

In order to quantify the breaking of scale symmetry, one computes the divergence of the dilatation current, which is given by the trace of the 'improved' energy-momentum tensor. In QCD the trace of the energy-momentum tensor reads [69–71]:

$$(\widetilde{T}_{QCD})^{\mu}_{\mu}(x) = \frac{\beta(g)}{2g} F^{a}_{\mu\nu}(x) F^{a\mu\nu}(x)\,, \tag{2.6}$$

where $F^{a}_{\mu\nu}$ is the field strength and $\beta(g)$ is the QCD beta function:

$$\beta(g) = -\frac{11g^3}{16\pi^2}(1 - \frac{2n_f}{33}) + \mathcal{O}(g^5)\,. \tag{2.7}$$

Here the first number in parentheses arises from the anti-screening self-interaction of the gluons and the second, proportional to the number of active flavours n_f, is the screening contribution of quark pairs.

It has been speculated that the vacuum expectation value of the r.h.s of

eq. (2.6) does not vanish, generating a gluon condensate [72]. It is then possible to relate the value of such a condensate to various observables, by using QCD sum rules [73].

2.2 The dilaton potential

In the previous section we showed that quantum corrections in QCD violate scale symmetry. The first attempt of building up a Lagrangian able to mimic the scale anomaly of QCD at mean-field level has been done by Schechter [19] and subsequently by Migdal and Shifman [20]. Here we start developing the potential in the pure gauge sector and later on we will add the quarks.
The fundamental ingredient is a new scalar-isoscalar field ϕ, called the *dilaton*, whose Lagrangian reads:

$$\mathcal{L}_{dil} = \frac{1}{2}\partial_\mu\phi\partial^\mu\phi - \mathcal{V}_{dil}(\phi) \tag{2.8}$$

where $\mathcal{V}_{dil}(\phi)$ represents the dilaton potential. In order to get the explicit expression for the dilaton potential we compute the trace of the improved energy-momentum tensor:

$$\widetilde{T}^\mu_\mu = \frac{\partial\mathcal{L}_{dil}}{\partial\phi}\phi + 2\frac{\partial\mathcal{L}_{dil}}{\partial(\partial^\mu\phi)}(\partial_\nu\phi) - 4\mathcal{L}_{dil} = 4\mathcal{V}_{dil} - \frac{\partial\mathcal{V}_{dil}}{\partial\phi}\phi\,. \tag{2.9}$$

Recalling that the non conservation of the dilatation current is directly connected to the trace of (2.9), we request that the trace is not vanishing and in particular that it is proportional to ϕ^4 through a dimensionless constant $-B$. This constraint permits us to obtain the dilaton potential by solving the differential equation:

$$4\mathcal{V}_{dil} - \frac{\partial\mathcal{V}_{dil}}{\partial\phi}\phi = -B\phi^4\,. \tag{2.10}$$

By imposing the boundary condition $\mathcal{V}(0) = 0$ one gets:

$$\mathcal{V}_{dil}(\phi) = B\phi^4 \left(\ln \frac{\phi}{\phi_0} - \frac{1}{4} \right) . \tag{2.11}$$

This potential admits a minimum for $\phi = \phi_0$ where $\mathcal{V}(\phi_0) = \epsilon_{vac} = -\frac{1}{4} B {\phi_0}^4$. Expanding $\mathcal{V}_{dil}(\phi)$ around ϕ_0 one obtains:

$$\begin{aligned} \mathcal{V}_{dil}(\phi) &\simeq \epsilon_{vac} + 2B\phi_0^2(\phi - \phi_0)^2 + O[(\phi - \phi_0)^3] \\ &\equiv \epsilon_{vac} + \frac{1}{2} M_\phi^2 (\phi - \phi_0)^2 + O[(\phi - \phi_0)^3] , \end{aligned} \tag{2.12}$$

where the mass of the dilaton field is $M_\phi = 2\phi_0\sqrt{B}$. Since the dilaton field represents the gluon condensate, its fluctuation around ϕ_0 can be associated with the scalar glueball. In this way M_ϕ can be associated with the mass of the scalar glueball [74]. The numerical value of the parameters ϕ_0 and B can be fixed in terms of the values of the gluon condensate and of the scalar glueball mass.
In order to mimic QCD scale anomaly at a mean-field level the vacuum expectation value of the trace of the "improved" energy-momentum tensor computed in the model must equal the same quantity computed in QCD (eq.(2.6)):

$$\langle \widetilde{T}^{\mu}_{\mu_{dil}} \rangle = \langle \widetilde{T}^{\mu}_{\mu_{QCD}} \rangle . \tag{2.13}$$

2.2.1 The modified glueball potential

Here we will discuss how to modify the effective potential (2.11) when we introduce the quarks degrees of freedom in the Lagrangian.

Basically the potential should again reproduce at mean-field level the QCD scale anomaly of eq. (2.6) but now taking into account also the quarks, as described by the β-function of eq. (2.7). A way to build up such potential has been

shown in [19, 20].

A generalization of the glueball potential is needed when the single scalar field is replaced by the set $\{\sigma, \boldsymbol{\pi}, \phi\}$ [75]. The divergence of the dilatation current including the chiral fields, becomes:

$$(\widetilde{T}_{dil})^{\mu}_{\mu} = 4V_{dil}(\Phi_i) - \sum_i \Phi_i \frac{\partial V_{dil}}{\partial \Phi_i} = 4\epsilon_{vac}\left(\frac{\phi}{\phi_0}\right)^4 \tag{2.14}$$

where Φ_i runs over the scalar and pseudo-scalar fields $\{\sigma, \boldsymbol{\pi}, \phi\}$. The proportionality $(\widetilde{T}_{dil})^{\mu}_{\mu} \propto \phi^4$ is suggested by the form of the QCD trace anomaly in eq. (2.6). Here again $\epsilon_{vac} = \frac{1}{4}B\phi_0^4(1-\delta)$ is the value of the potential at minimum, where the parameter $\delta = 2n_f/33$ weights the contribution of the quarks to the trace anomaly.

In order to have an explicit form of the potential $V_{dil}(\Phi_i)$, we should impose a further constraint, namely that the modified potential has to be chirally invariant. This means that the dependency on chiral fields has to occur only through the combination $\sigma^2 + \pi^2$ and moreover the contribution arising from the chiral fields has to be weighted by the δ parameter, in order to reproduce the same result obtained in QCD.

The final form of the potential introduced in Ref. [75] reads:

$$\begin{aligned} \mathcal{V}_{dil}(\phi, \sigma, \boldsymbol{\pi}) &= B\phi^4\left(\ln\frac{\phi}{\phi_0} - \frac{1}{4}\right) - \frac{1}{2}B\delta\phi^4 ln\frac{\sigma^2 + \boldsymbol{\pi}^2}{f_\pi^2} \\ &+ \frac{1}{2}B\delta\zeta^2\phi^2\left(\sigma^2 + \boldsymbol{\pi}^2 - \frac{1}{2}\frac{\phi^2}{\zeta^2}\right). \end{aligned} \tag{2.15}$$

Here the first term on the right hand side is the usual dilaton potential introduced by Schechter [19] and discussed in the previous section, while the second term provides the contribution of the chiral fields to the violation of scale invariance. A "new" dimensional parameter f_π is introduced, which as usual can be interpreted as the pion decay constant. The third term does not contribute to the

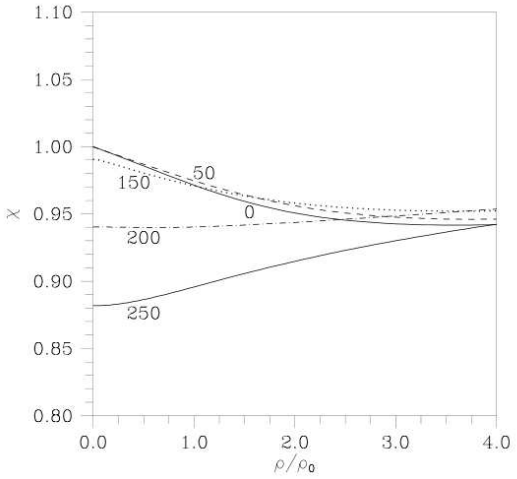

Figure 2.1: The glueball mean-field ratio χ as a function of density for various temperatures in MeV [22].

trace anomaly, and it is needed to ensure that in the vacuum $\phi = \phi_0$, $\sigma = \frac{\phi_0}{\zeta} = f_\pi$ and $\boldsymbol{\pi} = 0$, where $\mathcal{V}_{dil}(\phi_0, \sigma_0, 0) = \epsilon_{vac} = -\frac{1}{4}B\phi_0^4(1-\delta)$.

In this work we will kept the dilaton field frozen to its vacuum value ϕ_0. This choice of not including at the moment the dilaton in the dynamics of the model can be justified by the results provided in [22,25]. In particular in [22] the authors show that the ratio $\chi = \phi/\phi_0$ at low temperatures remains close to unity, even at large densities, as can be seen in Fig. 2.1. Under this assumption, the dilaton potential reads:

$$\mathcal{V}_{dil}(\sigma, \pi) = \lambda_1^2(\sigma^2 + \boldsymbol{\pi}^2) - \lambda_2^2 \ln(\sigma^2 + \boldsymbol{\pi}^2) \tag{2.16}$$

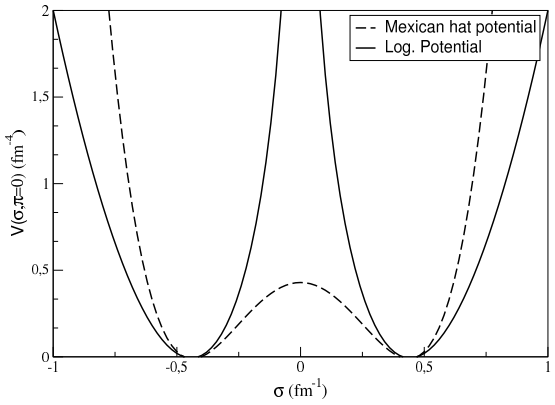

Figure 2.2: Comparison between the logarithmic (solid line) and the Mexican hat potential (dashed line).

where:

$$\lambda_1^2 = \frac{1}{2}\frac{B\delta\phi_0^4 + \epsilon_1}{\sigma_0^2} = \frac{1}{4}(m_\sigma^2 + m_\pi^2) \tag{2.17}$$

$$\lambda_2^2 = \frac{1}{2}B\delta\phi_0^4 = \frac{\sigma_0^2}{4}(m_\sigma^2 - m_\pi^2). \tag{2.18}$$

It is interesting to compare the logarithmic with the Mexican hat potential. In Fig. 2.2 it can be seen that in the case of the Mexican hat potential it is relatively easy to restore chiral symmetry by climbing the maximum located at the center. This is not possible in the case of the logarithmic potential as long as the dilaton field remains frozen. Since only at large temperatures the dilaton field changes significantly [25] we can expect that at large densities and moderate temperatures this model provides more stable solitonic solutions. This is a crucial point which will be investigated in the next chapter.

2.3 The Lagrangian of the Chiral Dilaton Model

In this section we will present the full Lagrangian of the model with the inclusion of the vector mesons.

An important point in our approach is that we aim at describing the dynamics of nuclear matter by incorporating all the interactions already at a quark level. This is at variance with e.g. the approach of Ref. [76, 77] where the vector field ω was introduced only at the nucleon level, but was not present in the dynamics of the quarks.

First of all we will provide a brief review, both phenomenological and theoretical, concerning the introduction of vector mesons in nuclear models; next we will describe in detail the Lagrangian of the model, at first in its chiral invariant realization and later on including also an explicit chiral breaking term.

2.3.1 Vector Meson Dominance

The first measurements of the electromagnetic form factors of the nucleons were performed during the fifties. The experimental data suggested that the electromagnetic structure of the nucleon is dominated by vector mesons, namely that the exchanged photon does not interact directly with the nucleon but rather transforms into a neutral vector meson which next couples to the nucleon, as shown in Fig. 2.3. The picture of a nucleon surrounded by a pion cloud allowed to interpret the data on electromagnetic form factors for the existence of a vector-isoscalar meson $\omega \to 3\pi$ [78] and of a vector-isovector meson $\rho^0 \to 2\pi$. [79].

The nucleon-photon interaction is shown in Fig. 2.3, where N and N' are the initial and final nucleon states and the line between the photon and the fermion lines is the meson propagator for the ρ^0 and the ω. The so-called *vector mesons*

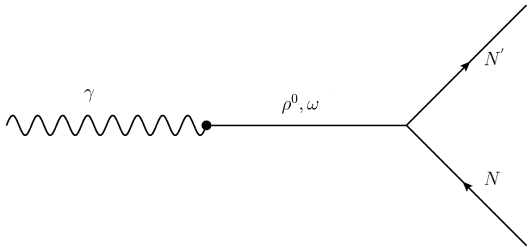

Figure 2.3: Diagram of nucleon-photon interaction through exchange of a vector meson.

dominance is based on the fact that the coupling between the nucleon and the vector mesons is treated as an interaction between elementary particles.

From the theoretical point of view this concept can be expressed through the current field identities [80], which basically permit to write the electromagnetic current proportional to the isovector and isoscalar currents coupled to the neutral vector mesons.

The presence of vector mesons also plays an important role in the description of the nucleon-nucleon interaction. This feature is clearly present in the one-boson exchange model, where a coupling between nucleons and vector fields is included in the Lagrangian in order to go beyond the one-pion exchange potential and provide the necessary repulsion at short distances. This approach has been extremely successful in reproducing the experimental data [81].
Hence it is quite evident that one way to improve the description of nucleon properties and nucleon-nucleon interactions seems to include in the effective Lagrangian explicitly vector degrees of freedom. This extension is however not unique and additional principles have to be invoked in order to reduce the number of coupling constants. One possible solution lies in the principle of universal-

ity [63], which states that the ρ meson couples to the conserved isospin current and the ω meson couples to the baryonic one. For further insight into this fundamental request, let us consider the case for the ρ meson. The isovectorial contribution to the electromagnetic form factor given by the process in Fig. 2.3 is proportional to:

$$\langle N^{'}(p')|J_{\mu}^{iv}(0)|N(p)\rangle \propto \overline{u}(p')[F_1^{iv}(q^2)\gamma_{\mu}]\frac{\tau_3}{2}u(p) \tag{2.19}$$

where p and p' are the momentum for the initial and final state and $q = p' - p$ is the transferred momentum. Let us define $g_{\gamma\rho}$ and $g_{\rho NN}$ the respective couplings for the vertices $\gamma - \rho^0$ and $\rho^0 - N$. From the Feynman rules applied on Fig. 2.3 we obtain:

$$F_1^{iv}(q^2) = g_{\gamma\rho}\frac{-1}{m_{\rho}^2 - q^2}g_{\rho NN} \tag{2.20}$$

which contains the propagator of the massive meson fields. Considering the limit $q^2 \to 0$ of the expression (2.20), which has to be equal to the unitary charge of the proton:

$$F_1^{iv}(0) = -\frac{g_{\gamma\rho}g_{\rho NN}}{m_{\rho}^2} = 1 \tag{2.21}$$

we get the following relation between the coupling constants:

$$g_{\rho NN} = -\frac{m_{\rho}^2}{g_{\gamma\rho}}. \tag{2.22}$$

This latter formula explicitly shows that if we consider the interaction of photons with particles carrying an isospin charge (such as quarks, pions), since the process is still dominated by the ρ^0 meson exchange and the universality of charge imposes again $F_{particle}^{iv}(0) = 1$, we can obtain:

$$g_{\rho NN} = g_{\rho qq} = g_{\rho\pi\pi} = g_{\rho\rho\rho} \ , (q^2 = 0) \tag{2.23}$$

This last equality formally explains the *principle of universality* which simply states that *in the limit of* $q^2 \to 0$ the coupling between the ρ^0 meson and isovector particles is the same.
An analogous argument can be obtained for the ω meson which couples to the baryonic current. In the case of quarks, since they carry $B = 1/3$, the universality imposes $g_{\omega qq} = \frac{1}{3} g_{\omega NN}$.

The next step consists in realizing the vector meson dominance and the principle of universality in an effective chiral Lagrangian. Actually vector mesons can be introduced in chiral Lagrangians following two approaches which can be proved to be equivalent and both fulfil low-energy hadronic relations, such as the Weinberg sum rule [17] and the KSFR relation [82, 83].
In the first scheme, a hidden local symmetry is shown to be present in chiral Lagrangians [84–87] and vector mesons represent the gauge fields of this local symmetry. This approach relies on the understanding, firstly proposed in super gravity theories [88,89], that any non-linear sigma model based on the manifold G/H is gauge equivalent to another model with $G_{global} \otimes H_{local}$ symmetry; in particular for the case of massless two-flavoured QCD we will have the global symmetry $G = SU(2)_L \otimes SU(2)_R$ to be spontaneously broken to the subgroup $H = SU(2)_V$ and the candidate gauge boson will be the ρ meson. In the second strategy, which is the one adopted in the present work, the vector mesons are treated as massive Yang-Mills fields of the chiral $SU(2)_L \otimes SU(2)_R$ symmetry [90–92]. This approach was initially suggested by Sakurai for isospin symmetry [93] and then extended to the chiral symmetric case by Lee and Nieh [94]. Focusing on the context of chiral quark-meson soliton models the massive Yang-Mills Lagrangian with valence quarks coupled to the mesons was first proposed by Broniowski and

Banerjee [62]. In this work the authors extended the Linear-σ model to the vector mesons sector, by including the ρ^0, the ω and the a_1 mesons which play the role of gauge bosons of the symmetry group $SU(2)_L \otimes SU(2)_R \otimes U(1)$, locally broken by mass terms.

2.3.2 Chiral symmetric Lagrangian

Following Refs. [21–25] the chiral symmetric Lagrangian including the vector mesons reads:

$$\begin{aligned}
\mathcal{L}_{VM} = & \bar{\psi}\left(i\gamma^\mu\partial_\mu - g_\pi(\sigma + i\boldsymbol{\pi}\cdot\boldsymbol{\tau}\gamma_5) + g_\rho\gamma^\mu\frac{\boldsymbol{\tau}}{2}\cdot(\boldsymbol{\rho}_\mu + \gamma_5\boldsymbol{A}_\mu) - \frac{g_\omega}{3}\gamma^\mu\omega_\mu\right)\psi \\
& + \frac{\beta}{2}(D_\mu\sigma D^\mu\sigma + D_\mu\boldsymbol{\pi}\cdot D^\mu\boldsymbol{\pi}) \\
& - \frac{1}{4}(\boldsymbol{\rho}_{\mu\nu}\cdot\boldsymbol{\rho}^{\mu\nu} + \boldsymbol{A}_{\mu\nu}\cdot\boldsymbol{A}^{\mu\nu} + \omega_{\mu\nu}\omega^{\mu\nu}) \\
& + \frac{1}{2}m_\rho^2(\boldsymbol{\rho}_\mu\cdot\boldsymbol{\rho}^\mu + \boldsymbol{A}_\mu\cdot\boldsymbol{A}^\mu) + \frac{1}{2}m_\omega^2\omega_\mu\omega^\mu \\
& - V(\phi_0,\sigma,\pi). \qquad (2.24)
\end{aligned}$$

Here ψ stands for quark fields and in addition to chiral fields σ and $\boldsymbol{\pi}$ there is the vector field ω_μ responsible for the short-range repulsion, the vector-isovector $\boldsymbol{\rho}_\mu$ and the axial-vector-isovector field $\boldsymbol{A}_\mu$. The potential $V(\phi_0,\sigma,\pi)$ is given by the expression (2.16).

The covariant derivatives of the chiral fields and the field tensors for vector mesons

are given by:

$$
\begin{aligned}
D_\mu\sigma &= \partial_\mu\sigma + g_\rho \boldsymbol{A}_\mu \cdot \boldsymbol{\pi}, \\
D_\mu\boldsymbol{\pi} &= \partial_\mu\boldsymbol{\pi} + g_\rho(\boldsymbol{\rho}_\mu \wedge \boldsymbol{\pi} - \boldsymbol{A}_\mu\sigma), \\
\omega_{\mu\nu} &= \partial_\mu\omega_\nu - \partial_\nu\omega_\mu, \\
\boldsymbol{\rho}_{\mu\nu} &= \partial_\mu\boldsymbol{\rho}_\nu - \partial_\nu\boldsymbol{\rho}_\mu + g_\rho(\boldsymbol{\rho}_\mu \wedge \boldsymbol{\rho}_\nu + \boldsymbol{A}_\mu \wedge \boldsymbol{A}_\nu), \\
\boldsymbol{A}_{\mu\nu} &= \partial_\mu\boldsymbol{A}_\nu - \partial_\nu\boldsymbol{A}_\mu + g_\rho(\boldsymbol{\rho}_\mu \wedge \boldsymbol{A}_\nu + \boldsymbol{A}_\mu \wedge \boldsymbol{\rho}_\nu).
\end{aligned} \tag{2.25}
$$

First of all we notice that in the Lagrangian (2.24) there are terms which mix $\boldsymbol{\rho}_\mu$ and $\boldsymbol{A}_\mu$ with the chiral fields. These terms arise form the covariant derivatives and from the tensor fields and are due to the fact that vector mesons are introduced as massive gauge bosons of the local symmetry $SU(2)_L \otimes SU(2)_R$.

Chiral symmetry requires that the masses of $\boldsymbol{\rho}_\mu$ and *bare* $\boldsymbol{A}_\mu$ mesons to be equal.

The presence of the β parameter requires a brief explanation and more details can be found in [95, 96]. Let us consider the kinetic term for the pions $\frac{\beta}{2} D_\mu\boldsymbol{\pi} D^\mu\boldsymbol{\pi}$, where the covariant derivative is given by (2.25). In vacuum the sigma field develops a non vanishing value $\sigma_v = f_\pi$, hence the pion kinetic term introduces in the Lagrangian terms proportional to $f_\pi \boldsymbol{A}_\mu \cdot \partial^\mu\boldsymbol{\pi}$ which do not correspond to any physical process. The solution to this problem is given by a redefinition of the $\boldsymbol{A}_\mu$ field, by identifying it with the new physical field $\boldsymbol{A}_\mu^{ph}$ such that the pion kinetic term recovers the usual form:

$$
\begin{aligned}
&\frac{m_\rho^2}{2}\boldsymbol{A}_\mu^2 + \frac{\beta}{2}\left[\partial_\mu\boldsymbol{\pi} + g_\rho(\boldsymbol{\rho}_\mu \times \boldsymbol{\pi} - f_\pi \boldsymbol{A}_\mu)\right]^2 = \\
&\qquad \frac{1}{2}(m_\rho^2 + \beta g_\rho^2 f_\pi^2)(\boldsymbol{A}_\mu^{ph})^2 + \frac{1}{2}\frac{\beta m_r ho^2}{m_r ho^2 + \beta g_\rho^2 f_\pi^2}(\partial_\mu\boldsymbol{\pi} + g_\rho\boldsymbol{\rho}_\mu \times \boldsymbol{\pi})^2
\end{aligned} \tag{2.26}
$$

where:

$$\boldsymbol{A}_\mu^{ph} = \boldsymbol{A}_\mu - \frac{\beta g_\rho f_\pi}{m_\rho^2 + \beta g_\rho^2 f_\pi^2}(\partial_\mu \boldsymbol{\pi} + g_\rho \boldsymbol{\rho}_\mu \times \boldsymbol{\pi}). \tag{2.27}$$

Requiring now that the coefficient of the pion kinetic terms equals $\frac{1}{2}$, the β parameter becomes:

$$\beta = \frac{m_\rho^2}{m_\rho^2 - g_\rho^2 f_\pi^2} \tag{2.28}$$

and from eq. (2.26) we obtain the relation between the masses of the physical field A and m_ρ, namely $m_A = \sqrt{\beta} m_\rho$ which agrees with the Weinberg sum rule [17]. In the following we assign the physical masses to the meson fields π, ρ and ω; $m_\pi = 139$ MeV, $m_\rho = 776$ MeV and $m_\omega = 782$ MeV.

2.3.3 Explicit chiral symmetry breaking term

Up to now we have introduced a Lagrangian which is exactly invariant under chiral transformations. It is well known that this limit holds as long as the quarks are massless and consequently the pion mass is zero. In order to describe in a realistic way nuclear matter phenomenology we must take into account that chiral symmetry is not an exact symmetry and the PCAC (Partially Conserved Axial Current) relation implies:

$$\partial_\mu \boldsymbol{a}^\mu = -f_\pi m_\pi^2 \boldsymbol{\pi} \tag{2.29}$$

and relates the non conservation of the axial current $\boldsymbol{a}^\mu$ to the finite pion mass and decay constant.

To do so we need to add another term in the Lagrangian (2.24) which is able to break explicitly the chiral symmetry and give a finite mass to the pion. In order to restrict the range of possibilities, we recall that chiral symmetry, at a quark level, is explicitly broken by terms like $V_{SB} = m(\overline{u}u + \overline{d}d)$ where m is the averaged (u, d) quark mass. In [24] the authors provide three forms for the

symmetry breaking term, requesting that it should also contributes to the trace anomaly. The most general symmetry breaking term in the potential (2.16) may be written as:

$$V_{SB} = -\epsilon_1\sigma - \epsilon_2\sigma(\sigma^2 + \boldsymbol{\pi}^2) + \epsilon_3\overline{\psi}\psi. \tag{2.30}$$

Moreover, in order to recover the vacuum conditions $\sigma = f_\pi$ and $\boldsymbol{\pi} = 0$, we add a term which does contribute to the symmetry breaking, hence obtaining:

$$\begin{aligned} V'_{SB} = \; & - \frac{1}{4} f_p i \phi_0^2 \epsilon_1 \left[4\nu - 2\left(\frac{\sigma^2 + \boldsymbol{\pi}^2}{f_\pi} \right) - 1 \right] \\ & - \frac{1}{4} f_\pi^3 \epsilon_2 \left[(4\nu - 6\phi_0^2) \left(\frac{\sigma^2 + \boldsymbol{\pi}^2}{f_\pi^2} \right) - 3 \right] \\ & + \epsilon_3 \bar{N} N - \frac{3}{4} f_\pi (\phi_0^2 \epsilon_1 + f_\pi^2 \epsilon_2) \,, \end{aligned} \tag{2.31}$$

where $\nu = \sigma / f_\pi$. In [24] the authors showed that only the term proportional to ϵ_1 provides a correct phenomenology of nuclei, thus is the only term which is taken into account. Keeping only $\epsilon_1 \neq 0$ the trace anomaly now reads:

$$(\widetilde{T}_{dil})^\mu_\mu = -\left(\frac{1}{4} B \phi_0^4 (1 - \delta) + \epsilon_1 \right) \left(\frac{\phi}{\phi_0} \right)^4 = 4\epsilon_{vac} \left(\frac{\phi}{\phi_0} \right)^4 \tag{2.32}$$

where $\epsilon_{vac} = -\frac{1}{4} B \phi_0^4 (1 - \delta) - \epsilon_1$. It is easy to verify that the pion vacuum mass is related to the value of ϵ_1 by the following equation:

$$\epsilon_1 = (\sigma_0 m_\pi)^2 \,. \tag{2.33}$$

Now the final expression of the potential becomes:

$$V(\sigma, \pi) = \lambda_1^2 (\sigma^2 + \boldsymbol{\pi}^2) - \lambda_2^2 \ln(\sigma^2 + \boldsymbol{\pi}^2) - \sigma_0 m_\pi^2 \sigma. \tag{2.34}$$

2.3.4 Hamiltonian of the model and field equations

The Lagrangian of the model, including the symmetry breaking term given in the previous section, reads:

$$\begin{aligned}\mathcal{L} = \bar{\psi}\big(&i\gamma^\mu\partial_\mu - g_\pi(\sigma + i\boldsymbol{\pi}\cdot\boldsymbol{\tau}\gamma_5) + g_\rho\gamma^\mu\frac{\boldsymbol{\tau}}{2}\cdot(\boldsymbol{\rho}_\mu + \gamma_5\boldsymbol{A}_\mu)\\ &- \frac{g_\omega}{3}\gamma^\mu\omega_\mu\big)\psi + \frac{\beta}{2}(D_\mu\sigma D^\mu\sigma + D_\mu\boldsymbol{\pi}\cdot D^\mu\boldsymbol{\pi})\\ &- \frac{1}{4}(\boldsymbol{\rho}_{\mu\nu}\cdot\boldsymbol{\rho}^{\mu\nu} + \boldsymbol{A}_{\mu\nu}\cdot\boldsymbol{A}^{\mu\nu} + \omega_{\mu\nu}\omega^{\mu\nu})\\ &+ \frac{1}{2}m_\rho^2(\boldsymbol{\rho}_\mu\cdot\boldsymbol{\rho}^\mu + \boldsymbol{A}_\mu\cdot\boldsymbol{A}^\mu) + \frac{1}{2}m_\omega^2\omega_\mu\omega^\mu\\ &- V(\sigma,\pi).\end{aligned} \tag{2.35}$$

The Euler-Lagrangian equations that follow from this Lagrangian are:

$$\begin{aligned}&[i\partial\!\!\!/ - g_\pi(\sigma + i\boldsymbol{\pi}\cdot\boldsymbol{\tau}\gamma_5) + g_\rho\frac{\boldsymbol{\tau}}{2}\cdot(\boldsymbol{\rho\!\!\!/} + \gamma_5\boldsymbol{A\!\!\!/}) - \frac{g_\omega}{3}\omega\!\!\!/]\psi = 0,\\ &\beta\partial_\mu D^\mu\sigma = -\beta g_\rho\boldsymbol{A}_\mu\cdot\boldsymbol{\pi} - g\bar{\psi}\psi - \frac{\partial V}{\partial\sigma},\\ &\beta\partial_\mu D^\mu\boldsymbol{\pi} = \beta g_\rho(-\boldsymbol{\rho}_\mu\times D^\mu\boldsymbol{\pi} + \boldsymbol{A}_\mu D^\mu\sigma) - ig\bar{\psi}\boldsymbol{\tau}\gamma_5\psi - \frac{\partial V}{\partial\boldsymbol{\pi}},\\ &-\partial^\mu\boldsymbol{\rho}_{\mu\nu} = g_\rho\boldsymbol{v}_\nu + m_\rho^2\boldsymbol{\rho}_\nu,\\ &-\partial^\mu\boldsymbol{A}_{\mu\nu} = g_\rho\boldsymbol{a}_\nu + m_\rho^2\boldsymbol{A}_\nu,\\ &-\partial^\mu\omega_{\mu\nu} = -\frac{1}{3}g_\omega b_\nu + m_\omega^2\omega_\nu.\end{aligned} \tag{2.36}$$

Here $\boldsymbol{v}_\nu$, $\boldsymbol{a}_\nu$ and b_ν are respectively the vector, the axial-vector and the baryonic currents:

$$\begin{aligned}&\boldsymbol{v}_\nu = \boldsymbol{\rho}_\mu\times\boldsymbol{\rho}_{\mu\nu} + \boldsymbol{A}_\mu\times\boldsymbol{A}_{\mu\nu} + \beta\boldsymbol{\pi}\times D^\nu\boldsymbol{\pi} + \bar{\psi}\gamma_\nu\frac{\boldsymbol{\tau}}{2}\psi,\\ &\boldsymbol{a}_\nu = \boldsymbol{\rho}_\mu\times\boldsymbol{A}_{\mu\nu} + \boldsymbol{A}_\mu\times\boldsymbol{\rho}_{\mu\nu} + \beta\boldsymbol{\pi}\times D^\nu\sigma - \beta\sigma D_\nu\boldsymbol{\pi} + \bar{\psi}\gamma_5\gamma_\nu\frac{\boldsymbol{\tau}}{2}\psi\\ &b_\nu = \overline{\psi}\gamma_\nu\psi.\end{aligned} \tag{2.37}$$

It can be easily verified that for these currents hold the following relations:

$$\partial^\nu \boldsymbol{a}_\nu = -f_\pi m_\pi^2 \boldsymbol{\pi} \ (PCAC) \tag{2.38}$$

$$\partial^\nu \boldsymbol{v}_\nu = 0 \ (CVC) \tag{2.39}$$

Using these relations and taking the divergence of the vector mesons field equations in (2.36), we obtain:

$$\begin{aligned} \partial^\nu \boldsymbol{\rho}_\nu &= -\frac{g_\rho}{m_\rho^2}\partial^\nu \boldsymbol{v}_\nu = 0 \ , \\ \partial^\nu \boldsymbol{A}_\nu &= -\frac{g_\rho}{m_\rho^2}\partial^\nu \boldsymbol{a}_\nu = -\frac{g_\rho f_\pi m_\pi^2}{m_\rho^2}\boldsymbol{\pi} \ , \\ \partial^\nu \omega_\nu &= \frac{g_\omega}{3m_\omega^2}\partial^\nu \overline{\psi}\gamma_\nu\psi = 0 \end{aligned} \tag{2.40}$$

which just underline the fact that, for spin 1 fields, only three components are linearly independent.

Now in order to evaluate the Hamiltonian density $\mathcal{H} = \varphi p_\varphi - \mathcal{L}$ we need to compute the conjugate momenta p_φ for every field φ:

$$\begin{aligned} p_\psi &= \frac{\partial \mathcal{L}}{\partial \dot{\psi}} = i\psi^\dagger \ , \\ p_\sigma &= \frac{\partial \mathcal{L}}{\partial \dot{\sigma}} = \beta D^0 \sigma \\ \boldsymbol{p}_\pi &= \frac{\partial \mathcal{L}}{\partial \dot{\boldsymbol{\pi}}} = \beta D^0 \boldsymbol{\pi} \ , \\ p_\omega^\mu &= \frac{\partial \mathcal{L}}{\partial \dot{\omega}_\mu} = -\omega^{0\mu} \ , \\ \boldsymbol{p}_\rho^\mu &= \frac{\partial \mathcal{L}}{\partial \dot{\boldsymbol{\rho}}_\mu} = -\boldsymbol{\rho}^{0\mu} \ , \\ \boldsymbol{p}_A^\mu &= \frac{\partial \mathcal{L}}{\partial \dot{\boldsymbol{A}}_\mu} = -\boldsymbol{A}^{0\mu} \ . \end{aligned} \tag{2.41}$$

Due to the antisymmetry of the field tensors the time components of the canonical conjugate momenta vanish, namely the time component of the vector meson fields

is not a dynamical variable and has to be eliminated. In order to do so we consider the time components of the vector mesons field equations in (2.36):

$$\begin{aligned} -\partial^\mu \boldsymbol{\rho}_{\mu 0} &= g_\rho \boldsymbol{v}_0 + m_\rho^2 \boldsymbol{\rho}_0 \ , \\ \partial^\mu \boldsymbol{A}_{\mu 0} &= g_\rho \boldsymbol{a}_0 + m_\rho^2 \boldsymbol{A}_0 \ , \\ \partial^\mu \omega_{\mu 0} &= -\frac{g_\omega}{3} b_0 + m_\omega^2 \omega_0 \ , \end{aligned} \tag{2.42}$$

which allow to express the time component of fields in terms of fields themselves and momenta:

$$\begin{aligned} \boldsymbol{\rho}_0 &= -\frac{1}{m_\rho^2}(\partial^\mu \boldsymbol{\rho}_{\mu 0} + g_\rho \boldsymbol{v}_0) \ , \\ \boldsymbol{A}_0 &= -\frac{1}{m_\rho^2}(\partial^\mu \boldsymbol{A}_{\mu 0} + g_\rho \boldsymbol{a}_0) \ , \\ \omega_0 &= -\frac{1}{m_\omega^2}(\partial^\mu \omega_{\mu 0} - \frac{g_\omega}{3} b_0). \end{aligned} \tag{2.43}$$

The Hamiltonian density of the model hence reads:

$$\begin{aligned} \mathcal{H} = \overline{\psi} \Big[&-i\boldsymbol{\gamma}\cdot\boldsymbol{\nabla} + g_\pi(\sigma + i\boldsymbol{\pi}\cdot\boldsymbol{\tau}\gamma_5) + g_\rho \gamma^i \frac{\boldsymbol{\tau}}{2}(\boldsymbol{\rho}_i + \gamma_5 \boldsymbol{A}_i) + \frac{g_\omega}{3}\gamma^i \omega_i \Big] \\ &+ \frac{1}{2\beta}(p_\sigma^2 + \boldsymbol{p}_\pi^2) + \frac{1}{2}(p_{\omega_i}^2 + \boldsymbol{p}_{\rho_i}^2 + \boldsymbol{p}_{A_i}^2) + V(\sigma, \boldsymbol{\pi}) \\ &+ \frac{\beta}{2}[(D_i\sigma)^2 + (D_i\boldsymbol{\pi})^2] + \frac{1}{4}(\boldsymbol{\rho}_{ij}\cdot\boldsymbol{\rho}_{ij} + \boldsymbol{A}_{ij}\cdot\boldsymbol{A}_{ij} + \omega_{ij}\omega ij) \\ &+ \frac{1}{2}m_\rho^2(\boldsymbol{\rho}_i^2 + \boldsymbol{A}_i^2) + \frac{1}{2}m_\omega^2\omega_i^2 + \frac{1}{2}m_\rho^2(\boldsymbol{\rho}_0^2 + \boldsymbol{A}_0^2) + \frac{1}{2}m_\omega^2\omega_0^2 \end{aligned} \tag{2.44}$$

2.4 Mean-field approximation

The fields equations in (2.36) involve quantum meson fields. The *mean-field approximation* (MFA) consists of describing the mesons as time-independent classical fields and of replacing powers and products of these fields by powers and

products of their expectation value on the vacuum state. This means that all fluctuations in the meson fields are neglected in the dynamics and only tree graphs are included

The mean-field state is defined as a Slater determinant of quarks fields and coherent mesons states:

$$|B\rangle = |N_c\psi\rangle|\sigma\rangle|\pi\rangle|\omega\rangle|\rho\rangle|A\rangle \tag{2.45}$$

where the quark part reads:

$$|N_c\psi\rangle = \prod_{\alpha=1}^{N_c} \int d^3x \psi_\alpha^+(x)\psi_{val}(x)|0\rangle \tag{2.46}$$

and the valence quarks ψ_{val} are in a 1s-state. The meson fields are written in terms of coherent states:

$$|\sigma\rangle = U(\sigma, p_\sigma)|0\rangle \tag{2.47}$$

where $U(\sigma, p_\sigma)$ is a unitary transformation given by:

$$U(\sigma, p_\sigma) = \exp\left(-i \int d^3x[\sigma_{cl}(x)p_\sigma(x) + p_{\sigma,cl}(x)\sigma(x)]\right). \tag{2.48}$$

Here σ_{cl} and $p_{\sigma,cl}$ are respectively the expectation values of the field operators $\sigma(x)$ and $p_\sigma(x)$ in the mean-field state $|\sigma\rangle$. Basically the coherent state is a Gaussian wave packet in the functional space of the quantum field we study, and it is centered at the field configuration corresponding to the classical mean-field. Similar expressions hold for the other mesons and more details can be found in [35, 97] and in Appendix I. In the next section we will introduce a field configuration which allows us to obtain a classical solution which minimizes the mean-field energy of the soliton [49, 98].

2.4.1 The Hedgehog ansatz

The Hedgehog configuration for quark spinor in the spin-isospin space reads:

$$\psi = \frac{1}{\sqrt{4\pi}} \begin{pmatrix} u(r) \\ iv(r)\boldsymbol{\sigma} \cdot \hat{\boldsymbol{r}} \end{pmatrix} \chi_h \tag{2.49}$$

where the spin or χ_h, defined as:

$$\chi_h = \frac{1}{\sqrt{2}}(\chi_u \chi_\downarrow - \chi_d \chi_\uparrow) \tag{2.50}$$

satisfies the condition for the Grand Spin $\boldsymbol{G} = \boldsymbol{I} + \boldsymbol{J}$:

$$\boldsymbol{G}\chi_h = 0. \tag{2.51}$$

This last relation means that there is a mixing between angular momentum and isospin, and this holds for all the fields. The corresponding Hedgehog baryon $|B\rangle = |N_c q\rangle|\sigma\rangle|\pi\rangle|\omega\rangle|\rho\rangle|A\rangle$ hence should be a linear combination of states with $I = 1/2$ and $I = 3/2$.

Once the form of the quark wave function is defined, the self-consistent configuration for the meson fields follows from the invariance of the Hedgehog ansatz under "grand reversal" transformation $\mathcal{R}$, namely the product of time reversal and isorotation about the axis 2 by π. Since the quark field in (2.49) is invariant under $\mathcal{R}$, we deduce that only mean-field mesons which are even under grand reversal couple to quarks. In this way we can obtain the sources for the mesons, by evaluating the matrix element of the meson fields on the state (2.49):

$$\sigma(r) \to -\frac{1}{4\pi}(u^2 - v^2)\,,$$
$$\pi^a \to -\frac{1}{4\pi} 2uv\hat{r}^a\,,$$

$$
\begin{aligned}
\omega^{\mu} &\to \begin{cases} \frac{1}{4\pi}(u^2+v^2)\,, \mu = 0 \\ 0\,, \mu = i = 1,2,3 \end{cases} \\
\rho^a_{\mu} &\to \begin{cases} 0\,, \mu = 0 \\ \frac{1}{4\pi} 2uv\epsilon^{aij}\hat{r}^j\,, \mu = i = 1,2,3 \end{cases} \\
A^a_{\mu} &\to \begin{cases} 0\,, \mu = 0 \\ -\frac{1}{4\pi}\left[(u^2 - \frac{1}{3}v^2)\delta^{ai} + 2v^2(\hat{r}^a\hat{r}^i - \frac{1}{3}\delta^{ai})\right]\,, \mu = i = 1,2,3. \end{cases}
\end{aligned}
\tag{2.52}
$$

The profiles of the chiral and the vector meson fields are hence given by:

$$
\begin{aligned}
&\frac{\langle B|\sigma|B\rangle}{\langle B|B\rangle} = \sigma_h(r), \quad \frac{\langle B|\boldsymbol{\pi}_a|B\rangle}{\langle B|B\rangle} = \widehat{r}_a h(r) \\
&\frac{\langle B|\omega_{\mu}|B\rangle}{\langle B|B\rangle} = \delta_{\mu 0}\omega_{\mu}(r) = \omega(r) \\
&\frac{\langle B|\boldsymbol{\rho}_a|B\rangle}{\langle B|B\rangle} = \rho^a_i(r) = \rho(r)\epsilon^{ika}\widehat{r}^k \\
&\frac{\langle B|\boldsymbol{A}_a|B\rangle}{\langle B|B\rangle} = A^a_i(r) = A_S(r)\delta^{ai} + A_T(r)(\widehat{r}^a\widehat{r}^i - \frac{1}{3}\delta^{ai})
\end{aligned}
\tag{2.53}
$$

where $\sigma_h(r)$, $h(r)$, $\omega(r)$, $\rho(r)$, $A_S(r)$ and $A_T(r)$ are radial functions.

Using the Hedgehog ansatz for the quarks in (2.49) and for the mesons in (2.53), the fields equations (2.36) for the Dirac components read:

$$
\frac{du}{dr} = (g_{\pi}h - g_{\rho}\rho)u + \left[-\epsilon - g_{\pi}\sigma_h + \frac{g_{\omega}}{3}\omega + \frac{g_{\rho}}{2}\left(A_S - \frac{4}{3}A_T\right)\right]v \ , \tag{2.54}
$$

$$
\frac{dv}{dr} = -\frac{2}{r}v + (-g_{\pi}h + g_{\rho}\rho)v + \left[\epsilon - g_{\pi}\sigma_h - \frac{g_{\omega}}{3}\omega + \frac{3}{2}g_{\rho}A_S\right]u \ , \tag{2.55}
$$

while for the chiral fields, the equations become:

$$\begin{aligned}\frac{d^2\sigma_h}{dr^2} =& -\frac{2}{r}\frac{d\sigma_h}{dr} + \frac{g_\pi}{\beta}\frac{3}{4\pi}(u^2-v^2) + \frac{1}{\beta}\frac{\partial V}{\partial \sigma_h} \\ &+ 2g_\rho\left[-\frac{dh}{dr}\left(A_S+\frac{2}{3}A_T\right) - \frac{2}{r}h\left(A_S-\frac{1}{3}A_T\right)\right] \\ &+ g_\rho^2\left[\sigma_h\left(3A_S^2+\frac{2}{3}A_T^2\right) + 2\rho h\left(A_S-\frac{1}{3}A_T\right) - \frac{f_\pi m_\pi^2}{m_\rho^2}h^2\right] \qquad (2.56)\end{aligned}$$

$$\begin{aligned}\frac{d^2h}{dr^2} =& -\frac{2}{r}\frac{dh}{dr} + \frac{2}{r^2}h + \frac{g_\pi}{\beta}\frac{3}{2\pi}uv + \frac{1}{\beta}\frac{\partial V}{\partial h} \\ &+ 2g_\rho\left[\frac{d\sigma_h}{dr}\left(A_S+\frac{2}{3}A_T\right) - \frac{2}{r}h\rho\right] \\ &+ g_\rho^2\left[2\rho h^2 + 2\sigma_h\rho\left(A_S-\frac{1}{3}A_T\right) + h\left(A_S+\frac{2}{3}A_T\right)^2 + \frac{f_\pi m_\pi^2}{m_\rho^2}\sigma_h h\right]. \qquad (2.57)\end{aligned}$$

Finally for the vector mesons we obtain the following:

$$\frac{d^2\omega}{dr^2} = -\frac{2}{r}\frac{d\omega}{dr} - g_\omega\frac{u^2+v^2}{4\pi} + m_\omega^2\omega \qquad (2.58)$$

$$\begin{aligned}\frac{d^2\rho}{dr^2} =& -\frac{2}{r}\frac{d\rho}{dr} + \frac{2}{r^2}\rho - \frac{3g_\rho}{4\pi}uv + m_\rho^2\rho \\ &+ g_\rho\left\{2\left(A_S+\frac{2}{3}A_T\right)\left(\frac{dA_S}{dr}-\frac{1}{3}\frac{dA_T}{dr}\right) - \frac{1}{r}\left[3\rho^2+\beta h^2 + A_T\left(2A_S+\frac{1}{3}A_T\right)\right]\right\} \\ &+ g_\rho^2\left\{\beta\rho h^2\beta\sigma_h h\left(A_S-\frac{1}{3}A_T\right) + \rho^3 + \rho\left[\left(A_S+\frac{2}{3}A_T\right)^2 + \left(A_S-\frac{1}{3}A_T\right)^2\right]\right. \\ &\left.+\frac{f_\pi m_\pi^2}{m_\rho^2}h\left(A_S-\frac{1}{3}A_T\right)\right\} \qquad (2.59)\end{aligned}$$

$$\begin{aligned}\frac{d^2A_S}{dr^2} =& -\frac{2}{r}\frac{dA_S}{dr} - \frac{3g_\rho}{8\pi}\left(u^2-\frac{1}{3}v^2\right) + m_\rho^2 A_S \\ &+ 2g_r ho\left[-\frac{d\rho}{dr}\left(A_S+\frac{1}{3}A_T\right) - \frac{2}{r}\rho A_S + \frac{\rho}{3}\left(\frac{dA_S}{dr}-\frac{1}{3}\frac{dA_T}{dr}\right)\right.\end{aligned}$$

$$
\begin{aligned}
&-\frac{f_\pi m_\pi^2}{6m_\rho^2}\left(\frac{dh}{dr}+\frac{2}{r}h\right)+\frac{\beta}{6}\left(h\frac{d\sigma_h}{dr}-\sigma_h\frac{dh}{dr}-\frac{2}{r}\sigma_h h\right)\Bigg] \\
&+g_\rho^2\left\{\frac{\beta}{3}\left[h^2\left(A_S+\frac{2}{3}A_T\right)+3\sigma_h^2A_S+2\sigma_h h\rho\right]\right. \\
&\left.+\frac{2}{3}\rho^2\left(2A_S+\frac{1}{3}A_T\right)+2\left(A_S^3-\frac{1}{27}A_T^3\right)-\frac{2}{3}\frac{f_\pi m_\pi^2}{m_\rho^2}\rho h\right\} \qquad (2.60)
\end{aligned}
$$

$$
\begin{aligned}
\frac{d^2A_T}{dr^2}=&-\frac{2}{r}\frac{dA_T}{dr}+\frac{6}{r^2}A_T+m_\rho^2A_T-\frac{3g_\rho}{4\pi}v^2 \\
&+g_\rho\left[\beta\left(\frac{d\sigma_h}{dr}h-\sigma_h\frac{dh}{dr}+\frac{1}{r}\sigma_h h\right)-\frac{4}{r}\rho A_T+2\frac{d\rho}{dr}A_T\right. \\
&\left.+2\rho\left(\frac{dA_S}{dr}-\frac{1}{3}\frac{dA_T}{dr}\right)-\frac{f_\pi m_\pi^2}{m_\rho^2}\left(-\frac{dh}{dr}+\frac{1}{r}h\right)\right] \\
&+g_\rho^2\left\{\beta\left[h^2\left(A_S+\frac{2}{3}A_T\right)+\sigma_h^2A_T-\sigma_h\rho h\right]\right. \\
&\left.+\rho^2\left(A_S+\frac{5}{3}A_T\right)-A_T^2\left(A_S-\frac{1}{3}A_T\right)+\frac{f_\pi m_\pi^2}{m_\rho^2}h\rho\right\} \qquad (2.61)
\end{aligned}
$$

At mean-field level the meson fields are classical and the differential equations governing their dynamics have to be supplemented by the appropriate boundary conditions.

For the single nucleon case we impose the following boundary conditions to the fields:

$$
\begin{aligned}
u'(0)=v(0)=0,\\
\sigma_h'(0)=h(0)=0,\\
\rho(0)=\omega'(0)=A_S'(0)=A_T(0)=0,
\end{aligned} \qquad (2.62)
$$

while at infinity the boundary conditions read:

$$
\begin{aligned}
&\sigma_h(\infty)=\sigma_0,\ h(\infty)=0,\\
&\frac{v(\infty)}{u(\infty)}=\sqrt{\frac{-g\sigma_0+\epsilon}{-g\sigma_0-\epsilon}},
\end{aligned} \qquad (2.63)
$$

$$\omega'(\infty) = \rho'(\infty) = A_S'(\infty) = A_T'(\infty) = 0,$$

where ϵ is the quark eigenvalue.

The total energy of the soliton at mean-field level is given by:

$$E_{MFA} = 4\pi \int r^2 dr (E_{int} + E_{kin,Q} + E_\sigma + E_\pi + E_\omega + E_\rho + E_A + E_{pot}) \quad (2.64)$$

where the quark-mesons interaction and the quark kinetic energies are:

$$\begin{aligned} E_{int} = \quad & \frac{3}{4\pi}\Big\{ g_\pi \sigma_h (u^2 - v^2) + 2 g_\pi h u v - \frac{g_\omega}{3}\omega(u^2+v^2) - 2 g_\rho \rho u v \\ & + g_\rho \left[\frac{3}{2} A_S \left(u^2 - \frac{1}{3} v^2 \right) + \frac{2}{3} v^2 A_T \right] \Big\} \end{aligned} \quad (2.65)$$

$$E_{kin,Q} = \frac{3}{4\pi}\left(u \frac{dv}{dr} - v \frac{du}{dr} + \frac{2}{r} u v \right) \quad (2.66)$$

and the energy density of the meson fields and of the potential read:

$$E_\sigma = \frac{\beta}{2}\left[-\frac{d\sigma_h}{dr} - g_\rho h \left(A_S + \frac{2}{3} A_T \right) \right]^2 \quad (2.67)$$

$$\begin{aligned} E_\pi = & \frac{\beta}{2}\left[\frac{dh}{dr} + g_\rho \sigma_h \left(A_S + \frac{2}{3} A_T \right) \right]^2 \\ & + \beta \left[-\frac{h}{r} + g_\rho h + g_\rho \sigma_h \left(A_S - \frac{1}{3} \right) \right]^2 \end{aligned} \quad (2.68)$$

$$E_\omega = -\frac{1}{2}\left(\frac{d\omega}{dr} \right)^2 - \frac{1}{2} m_\omega^2 \omega^2 \quad (2.69)$$

$$\begin{aligned} E_\rho = & \left[\frac{d\rho}{dr} + \frac{\rho}{r} - g_\rho \left(A_S + \frac{2}{3} A_T \right) \left(A_S - \frac{1}{3} A_T \right) \right]^2 \\ & + \frac{1}{2}\left[\frac{2}{r}\rho - g_\rho \rho^2 - g_\rho \left(A_S - \frac{1}{3} A_T \right)^2 \right]^2 + m_\rho^2 \rho^2 \end{aligned} \quad (2.70)$$

$$\begin{aligned} E_A = & \left[\left(\frac{dA_S}{dr} - \frac{1}{3}\frac{dA_T}{dr} \right) - \frac{A_T}{r} + g_\rho \rho \left(A_S + \frac{2}{3} A_T \right) \right]^2 \\ & + \frac{1}{2} m_\rho^2 \left(3 A_S^2 + \frac{2}{3} A_T^2 \right) \end{aligned} \quad (2.71)$$

$$E_{pot} = V(\phi_0, \sigma_h, h) \tag{2.72}$$

2.4.2 Static observables at mean-field level

The static properties of the Hedgehog baryon at mean-field level are presented in this section. In particular, for both CDM and linear σ model with and without vector mesons, we calculate the electric isoscalar radius $\langle r_E^2 \rangle_{I=0}$, the isovector magnetic moment $\mu_{I=1}$, the isovector magnetic radius $\langle r_M^2 \rangle_{I=1}$ and the axial coupling constant g_a.

The formulae for the observables in the mean-field approximation read:

$$\begin{aligned}
\langle r_E^2 \rangle_{I=0} &= \int r^4 (u^2 + v^2) dr \ , \\
\langle r_m^2 \rangle_{I=1} &= \frac{1}{\mu_{I=1}} \int r^5 dr \frac{2\pi}{9} (G_m^Q(r) + G_m^\pi(r) + G_m^\rho(r) + G_m^A(r)) \ , \\
\mu_{I=1} &= \int r^3 dr \frac{2\pi}{9} (G_m^Q(r) + G_m^\pi(r) + G_m^\rho(r) + G_m^A(r)) \ , \\
g_a &= \int r^2 dr \frac{2\pi}{9} (G_{a,0}^Q(r) + G_{a,0}^\sigma(r) + G_{a,0}^\pi(r) + G_{a,0}^\rho(r) + G_{a,0}^{\rho_0}(r) + G_{a,0}^A(r)) \ .
\end{aligned} \tag{2.73}$$

The expressions for each term G_i^{field} are given by:

$$\begin{aligned}
G_m^Q(r) &= \frac{3}{\pi} uv \ , \\
G_m^\pi(r) &= 4\beta \left[\frac{1}{r} h^2 - g_\rho h \sigma_h \left(A_S - \frac{1}{3} A_T \right) - g_\rho h^2 \rho \right] \ , \\
G_m^\rho(r) &= 4 \left\{ \frac{2}{r} \rho^2 - g_\rho \rho \left[\rho^2 + \left(A_S - \frac{1}{3} A_T \right)^2 \right] \right\} \ , \\
G_m^A(r) &= (-1) \left[4 \left(A_S' - \frac{1}{3} A_T' - \frac{A_T}{r} \right) \left(A_S + \frac{2}{3} A_T \right) + 4 g_\rho \rho \left(A_S + \frac{2}{3} A_T \right)^2 \right] \ ,
\end{aligned} \tag{2.74}$$

while the contributions in the axial coupling constant are:

$$
\begin{aligned}
G^{Q}_{a,0}(r) &= \frac{9}{2\pi}\left(u^2 - \frac{1}{3}v^2\right) \ , \\
G^{\sigma}_{a,0}(r) &= -4\beta h\left[\sigma_h' + g_\rho h\left(A_S + \frac{2}{3}A_T\right)\right] \ , \\
G^{\pi}_{a,0}(r) &= 4\beta\sigma_h\left(h' + \frac{2}{r}h - 2g_\rho\rho h - 3g_\rho\sigma_h A_S\right) \ , \qquad (2.75) \\
G^{\rho}_{a,0}(r) &= -8\rho\left(A_S' - \frac{1}{3}A_T' - \frac{A_T}{r}\right) - 8g_\rho\rho^2\left(A_S + \frac{2}{3}A_T\right) \ , \\
G^{\rho_0}_{a,0}(r) &= \frac{g_\rho}{\pi m_\rho^2}\tilde{A}_S(u^2 + v^2) \ , \\
G^{A}_{a,0}(r) &= 8\left\{\rho^2 + \left(2A_S + \frac{1}{3}A_T\right) + \frac{\rho}{r}\left(4A_S - \frac{1}{3}A_T\right)\right. \\
&\quad \left. -g_\rho\left(A_S - \frac{1}{3}A_T\right)\left[\rho^2 + 3\left(A_S - \frac{1}{3}A_T\right)^2 + 3A_S A_T\right]\right\} \ . \qquad (2.76)
\end{aligned}
$$

For the model without vector mesons the corresponding observables can be obtained from the above formulae by putting $g_\rho = 0$.

2.5 Projection of the Hedgehog baryon

The Hedgehog baryon defined in Sec. 2.4.1, since it is an eigenstate of the grand spin $\boldsymbol{G}$, violates both rotational and isospin symmetry of the Hamiltonian. The baryon state can be written as:

$$
|B\rangle = \sum_{JMM_I} (-)^{J+M} C_J \delta_{M,-M_I} |J = I, M, M_I\rangle \qquad (2.77)
$$

where C_J are the coefficients of the expansion which will be defined later.

The constraint $J = I$ follows from the fact that, since the Hedgehog states are eigenstates of the Grand Spin $\boldsymbol{G}$, it is equivalent to rotate either in spin or in isospin space.

One way to restore these symmetries is to use the so-called Peierls-Yoccoz projection approach [99, 100]. In this approach we introduce generator coordinates and construct the physical states with correct quantum numbers, starting from a linear combination of all the broken-symmetry mean-field states. In the case of the spin-isospin symmetry, the states of good spin and isospin can be built starting from a linear combination of all possible orientations of the Hedgehog ansatz. The states are thus:

$$|JMM_I\rangle = N_{JM_I} \int d^3\Omega D^J_{M,-M_I}(\Omega)^* \widehat{R}(\Omega)|B\rangle. \tag{2.78}$$

where N_{JM_I} is a normalization factor, the weight functions D are the Wigner functions and the integral is done over the volume element:

$$\int d^3\Omega = \int_0^{2\pi} d\alpha \int_0^{2\pi} d\gamma \int_0^{\pi} \sin\beta d\beta \tag{2.79}$$

The rotation matrix $\widehat{R}(\Omega)$ is a spatial rotation through Euler angles $\Omega \equiv (\alpha, \beta, \gamma)$ given by:

$$\widehat{R}(\Omega) = e^{-iJ_x\alpha} e^{-iJ_y\beta} e^{-iJ_z\gamma}. \tag{2.80}$$

When studying diagonal matrix elements of nucleon states, it is customary to work with states where the third component of the angular momentum M is equal to $-M_I$ since in this case the expression of the Wigner function is particularly simple. In this way the projection operator becomes:

$$P_{JM} = \frac{2J+1}{8\pi^2} \int d^3\Omega D^J_{M,M}(\Omega)^* \widehat{R}(\Omega). \tag{2.81}$$

and it has the basic properties:

$$(P_{JM})^{\dagger} = P_{JM} \ , \tag{2.82}$$

$$(P_{JM})^2 = P_{JM}. \tag{2.83}$$

The normalization factor has been determined by using (2.78)-(2.81):

$$N^2_{J,-M} = \left(\frac{2J+1}{8\pi^2}\right)^2 (\langle B|P_{JM}|B\rangle)^{-1}. \tag{2.84}$$

Finally, the coefficients C_J in eq. (2.77) are given by the expression:

$$\begin{aligned} C_J^2 &= \langle B|P_{JM}|B\rangle \\ &= \frac{2J+1}{8\pi^2}\int d^3\Omega a D^J_{M,M}(\Omega)\langle B|\widehat{R}(\Omega)|B\rangle. \end{aligned} \tag{2.85}$$

In this way the projected state reads:

$$|JM\ -M\rangle = N_{J,-M}P_{JM}|B\rangle \tag{2.86}$$

Once we obtain the projected state, we proceed to evaluate the corresponding energy. Basically we need to calculate the expectation value of the Hamiltonian in (2.44) on the projected state given by (2.86). The projected energy can be written as:

$$\begin{aligned} E_J =&\langle JM - M| : H : |JM - M\rangle \\ =&4\pi \int r^2 dr(E_{int} + E_{kin,Q} + E_{J,\sigma} + E_{J,\pi} + E_{\omega} \\ &+ E_{J,\rho} + E_{J,\rho_0} + E_{J,A} + E_{J,A_0} + E_{J,pot}) \end{aligned} \tag{2.87}$$

where the energy densities E_{int}, $E_{kin,Q}$ and E_{ω} are not affected by the projection and are given by their expressions at mean-field level in eqs. (2.65)-(2.67) . The

projected energies for the other meson fields are given by:

$$\begin{aligned}
E_{J,\sigma} =& \frac{1}{2}\beta\left\{\sigma_h^{'2} + g_\rho\sigma_h'\pi\left(A_S+\frac{2}{3}A_T\right)\left(1+\frac{1}{3}G_1^J\right)\right.\\
&+ g_\rho^2h^2\left[\left(A_S+\frac{2}{3}A_T\right)^2\frac{1}{30}(10+5G_1^J+G_2^J)\right.\\
&\left.\left.+\left(A_S-\frac{1}{3}A_T\right)^2\frac{1}{120}(10+5G_1^J+G_2^J)\right]\right\} \qquad (2.88)\\
E_{J,\pi} =& \frac{\beta}{4}\left(h^{'2}+\frac{2}{r^2}h^2\right)\left(1+\frac{1}{3}G_1^J\right) - \frac{1}{4\beta}\left(h^{'2}+\frac{2}{r^2}h^2+m_\pi h^2\right)\left(1-\frac{1}{3}G_1^J\right)\\
&- \frac{1}{2}\beta g_\rho\left\{\sigma_h\left[h\left(A_S+\frac{2}{3}A_T\right)+\frac{2}{r}h\left(A_S-\frac{1}{3}A_T\right)\right]\left(1+\frac{1}{3}G_1^J\right)+\rho\frac{h^2}{r}(1+G_1^J)\right\}\\
&+ \frac{1}{4}\beta g_\rho^2\left\{\rho^2h^2\frac{1}{12}(10+11G_1^J+G_2^j)+2\sigma_h h\rho\left(A_S-\frac{1}{3}A_T\right)(1+G_1^J)\right.\\
&\left.+\sigma_h^2\left[\left(A_S+\frac{2}{3}A_T\right)^2+2\left(A_S-\frac{1}{3}A_T\right)^2\right]\left(1+\frac{1}{3}G_1^J\right)\right\} \qquad (2.89)\\
E_{J,\rho} =& \left(\rho^{'2}+\frac{2}{r^2}\rho^2+m_\rho^2\rho^2\right)\frac{1}{3}G_1^J - g_\rho\left[\left(rho'+\frac{\rho}{r}\right)\left(A_S+\frac{2}{3}A_T\right)\left(A_S-\frac{1}{3}A_T\right)\right.\\
&\left.+\frac{\rho}{r}\left(A_S-\frac{1}{3}A_T\right)^2+\frac{\rho^3}{r}\right]\frac{1}{2}(1+G_1^J)+g_\rho^2\left\{\frac{1}{2}\left[\rho^2+\left(A_S-\frac{1}{3}A_T\right)^2\right]^2\right.\\
&\left.+\left(A_S-\frac{1}{3}A_T\right)^2\left(A_S+\frac{2}{3}A_T\right)^2\right\}\frac{1}{48}(10+11G_1^J+G_2^J) \qquad (2.90)\\
E_{J,A} =& \left[\left(A_S'-\frac{1}{3}A_T'-\frac{A_T}{r}\right)^2+\frac{1}{2}m_\rho^2\left(3A_S^2+\frac{2}{3}A_T^2\right)\right]\frac{G_1^J}{3}\\
&+\frac{1}{2}g_\rho\left(A_S'-\frac{1}{3}A_T'-\frac{A_T}{r}\right)\left(A_S+\frac{2}{3}A_T\right)\rho(1+G_1^J)\\
&+g_\rho^2\left(A_S+\frac{2}{3}A_T\right)^2\rho^2\frac{1}{48}(10+11G_1^J+G_2^J) \qquad (2.91)
\end{aligned}$$

$$
\begin{aligned}
E_{J,\rho_0} =& \frac{g_\rho^2}{m_\rho^2}\frac{1}{120}\left\{\left[\rho\tilde{\rho}+\left(A_S-\frac{1}{3}A_T\right)\left(\tilde{A}_S-\frac{1}{3}\tilde{A}_T\right)\right]^2(7G_2^J-5G_1^J-20)\right.\\
&+2\left[\rho\tilde{\rho}+\left(A_S-\frac{1}{3}A_T\right)\left(\tilde{A}_S-\frac{1}{3}\tilde{A}_T\right)\right]\left[h\tilde{h}+\left(A_S+\frac{2}{3}A_T\right)\left(\tilde{A}_S+\frac{2}{3}\tilde{A}_T\right)\right]\\
&\times(3G_2^J-5G_1^J)+2\left[h\tilde{h}+\left(A_S+\frac{2}{3}A_T\right)\left(\tilde{A}_S+\frac{2}{3}\tilde{A}_T\right)\right]^2(G_2^J-5)\\
&+\frac{N_c}{4\pi}(u^2+v^2)\left(h\tilde{h}+2\rho\tilde{\rho}+3A_S\tilde{A}_S+\frac{2}{3}A_T\tilde{A}_T\right)10(G_1^J-3)\\
&\left.+15N_c(N_c-1)\left(\frac{u^2+v^2}{4\pi}\right)^2(1-G_N^J)\right\} \qquad (2.92)
\end{aligned}
$$

$$
\begin{aligned}
E_{J,A_0} =& \frac{1}{12m_\rho^2}\left\{g_\rho^2\left[\rho\left(\tilde{A}_S-\frac{1}{3}\tilde{A}_T\right)-\tilde{\rho}\left(A_S-\frac{1}{3}A_T\right)-\sigma_h\tilde{h}\right]^2\right.\\
&+2g_\rho\left(\tilde{A}'_S+\frac{2}{3}\tilde{A}'_T+\frac{2}{r}\tilde{A}_T\right)\\
&\left.\times\left[\rho\left(\tilde{A}_S-\frac{1}{3}\tilde{A}_T\right)-\tilde{\rho}\left(A_S-\frac{1}{3}A_T\right)-\sigma_h\tilde{h}\right]\right\}(G_1^J-3). \qquad (2.93)
\end{aligned}
$$

In these expressions the coefficients G_1^J, G_2^J and $G_N^J$are given by:

$$
\begin{aligned}
G_1^J &= \frac{F_1^J(N_c,N_B)}{F^J(N_c,N_B)}\\
G_1^J &= \frac{F_2^J(N_c,N_B)}{F^J(N_c,N_B)} \qquad (2.94)\\
G_N^J &= \frac{F^J(N_c-2,N_B)}{F^J(N_c,N_B)},
\end{aligned}
$$

where $F^J(N_c,N_B)=\langle B|P_{JJ}|B\rangle$ is the projected Hedgehog norm and:

$$
F_1^J = \sum_{J'=|J-1|}^{J+1} F^{J'}(N_c,N_B) \qquad (2.95)
$$

$$
F_2^J = \sum_{J'=|J-2|}^{J+2} F^{J'}(N_c,N_B). \qquad (2.96)
$$

The evaluation of the generic fields $\tilde{\phi}$ is given in detail in Appendix I and in Ref. [97]. More details about the projection technique and the evaluation of these projection coefficients can be found in [27, 97].

The projected potential energy needs a detailed explanation, since this kind of of calculation has never been performed before for a logarithmic potential but only for the Mexican hat potential. The matrix element for which we need to develop a full calculation is:

$$E_{J,pot} = \langle JM - M| : \int d^3 r V(\sigma_h, h) : |JM - M\rangle \tag{2.97}$$

It has already been shown in [27] that terms which do not involve the pion field (such as the quark-pion interaction energy and the σ and quark kinetic energies) are not affected by projection. The main issue is the evaluation of the matrix elements of the chiral fields between rotated and unrotated Hedgehog states.

These matrix elements for the sigma field $\sigma(\boldsymbol{r})$ are:

$$\langle B|\widehat{R}(\Omega)^{-1}\sigma(\boldsymbol{r})^n|B\rangle = \overline{\sigma}(\boldsymbol{r})^n\langle B|\widehat{R}(\Omega)^{-1}|B\rangle\,, \tag{2.98}$$

where:

$$\overline{\sigma}(\boldsymbol{r}) = \frac{1}{2}\left(\sigma(\boldsymbol{r}) + \widehat{R}(\Omega)^{-1}\sigma(\boldsymbol{r})\right) \equiv \sigma_h(r)\,. \tag{2.99}$$

In an analogous way, for the pion field the matrix elements become:

$$\langle B|\widehat{R}(\Omega)^{-1}\boldsymbol{\pi}(\boldsymbol{r})|B\rangle = \overline{\boldsymbol{\pi}}(\boldsymbol{r})h(r)\langle B|\widehat{R}(\Omega)^{-1}|B\rangle\,, \tag{2.100}$$

$$\overline{\boldsymbol{\pi}}(\boldsymbol{r}) = \frac{1}{2}\left(\widehat{\boldsymbol{r}} + \widehat{R}(\Omega)^{-1}\widehat{\boldsymbol{r}}\right)\,. \tag{2.101}$$

Since the potential is a function of the pion only through quadratic terms, by

using the previous relation we get:

$$\begin{aligned}
&\langle B|\widehat{R}(\Omega)^{-1}\boldsymbol{\pi}^2(\boldsymbol{r})|B\rangle = g(\Omega,\theta,\phi)\langle B|\widehat{R}(\Omega)^{-1}|B\rangle\,, \\
&g(\Omega,\theta,\phi) = \frac{1}{2}h(r)^2\left(1+\widehat{\boldsymbol{r}}\cdot\widehat{R}(\Omega)^{-1}\widehat{\boldsymbol{r}}\right)\,,
\end{aligned} \tag{2.102}$$

where the function g depends on Euler angles Ω and on the polar and azimuthal angles.

For a generic function F of the quadratic pionic terms, the following relation holds:

$$\langle B|\widehat{R}(\Omega)^{-1}F[\boldsymbol{\pi}^2(\boldsymbol{r})]|B\rangle = F[g(\Omega,\theta,\phi)]\langle B|\widehat{R}(\Omega)^{-1}|B\rangle. \tag{2.103}$$

Therefore the projection of the potential term can be obtained by leaving the pure σ terms unchanged and by replacing the quadratic terms of the pion with the function g given in eq. (2.102):

$$\begin{aligned}
V(\sigma_h,&h,g(\Omega,\theta,\phi)) = \\
&\lambda_1^2\left(\sigma_h^2+h^2g(\Omega,\theta,\phi)\right)-\lambda_2^2\ln\left(\sigma_h^2+h^2g(\Omega,\theta,\phi)\right) \\
&-f_\pi m_\pi^2\sigma_h\,.
\end{aligned} \tag{2.104}$$

The expectation value of the potential between the projected states, eq. (2.104), becomes:

$$\begin{aligned}
E_{J,pot} = \langle JJ-J|:\int d^3rV(\sigma_h,h,g(\Omega,\theta,\phi)):|JJ-J\rangle = \\
\frac{1}{N_{JJ}}\int_0^\infty r^2dr\int_0^\pi\sin\theta d\theta\int_0^{2\pi}d\phi \\
\times\int d\Omega^3D^J_{J,J}(\Omega)V(\sigma_h,h,g(\Omega,\theta,\phi))\langle B|\widehat{R}(\Omega)^{-1}|B\rangle
\end{aligned} \tag{2.105}$$

where the Wigner function is equal to:

$$D^J_{J,J}(\Omega) = e^{-iJ(\alpha+\gamma)} \left(\cos\frac{\beta}{2}\right)^{2J} . \tag{2.106}$$

Finally, the overlap between rotated and unrotated Hedgehog states reads:

$$\begin{aligned}\langle B|\widehat{R}(\Omega)^{-1}|B\rangle = \\ \left(\cos\frac{\beta}{2}\cos\frac{\alpha+\gamma}{2}\right)^3 \\ \times \exp\left(\overline{N}_\sigma + \frac{\overline{N}_\pi}{3}\left(4\cos^2\frac{\beta}{2}\cos^2\frac{\alpha+\gamma}{2} - 1\right)\right) .\end{aligned} \tag{2.107}$$

Here $\overline{N}_\sigma$, $\overline{N}_\pi$ are the average numbers of σ and π mesons in the Hedgehog state [97] (see Appendix I) and N_{JJ} is a normalization integral given by eq.(2.84). Besides the rotation and the isospin symmetries the semi-classical Hedgehog solution also breaks the translational symmetry of the Lagrangian, since the localized soliton is not an eigenstate of the linear momentum, either. The soliton hence contains spurious center-of-mass motion, whose kinetic contribution adds to the total energy. In addition to that, this intrinsic motion also contributes to the nucleon observables, such as radii and magnetic moments. In literature there are many techniques that allow to handle the problem of collective motion, such as the Peierls-Yoccoz projection on linear momentum [99, 100].

In the present work we do not perform a projection on the linear momentum, but we adopt an easier approach [101], which provides a rough estimate of the center-of-mass corrections to the baryon total energy. Using this approach, the masses for the J state read:

$$M_J = (E_J - \boldsymbol{P}^2)^{1/2} \tag{2.108}$$

where the momentum operator $\boldsymbol{P}^2$ is defined as:

$$\boldsymbol{P}^2 = \int d^3r \left[\left(\frac{du}{dr}\right)^2 + \left(\frac{dv}{dr}\right)^2 + 2v^2 \right] \tag{2.109}$$

2.5.1 Projected observables

In this section we present the explicit expressions for the projected observables, such as electric and magnetic radii and momenta, for the model with only chiral fields and for the model with vector mesons. The projected formulae read:

$$\begin{aligned}
\langle r_E^2\rangle_p &= \int r^4 dr \left\{ (u^2+v^2) + \frac{1}{2} G_\tau^{1/2} [2\pi(h\tilde{h} + 2\rho\tilde{\rho} + 3A_S\tilde{A}_S + \frac{2}{3}A_T\tilde{A}_T - N_B(u^2+v^2)] \right\} \\
\langle r_E^2\rangle_n &= \int r^4 dr \left\{ \frac{1}{2} G_\tau^{1/2} [2\pi(h\tilde{h} + 2\rho\tilde{\rho} + 3A_S\tilde{A}_S + \frac{2}{3}A_T\tilde{A}_T - N_B(u^2+v^2)] \right\} \\
\mu_p &= \frac{1}{3}\int r^3 dr \left\{ \frac{1}{3} uv(1 - N_B G_\tau^{1/2}) + \frac{\pi}{3}(G_m^Q(r) + G_m^\pi(r) \right. \\
&\qquad \left. + G_m^\rho(r) + G_m^{\rho_0}(r) + G_m^A(r) + G_m^{A_0}(r)) \right\} \\
\mu_n &= \frac{1}{3}\int r^3 dr \left\{ \frac{1}{3} uv(1 - N_B G_\tau^{1/2}) - \frac{\pi}{3}(G_m^Q(r) + G_m^\pi(r) \right. \\
&\qquad \left. + G_m^\rho(r) + G_m^{\rho_0}(r) + G_m^A(r) + G_m^{A_0}(r)) \right\} \\
\langle r_M^2\rangle_p &= \frac{1}{\mu_p}\int r^5 dr \frac{1}{5} \left\{ \frac{1}{3} uv(1 - N_B G_\tau^{1/2}) + \frac{\pi}{3}(G_m^Q(r) + G_m^\pi(r) \right. \\
&\qquad \left. + G_m^\rho(r) + G_m^{\rho_0}(r) + G_m^A(r) + G_m^{A_0}(r)) \right\} \\
\langle r_M^2\rangle_n &= \frac{1}{\mu_n}\int r^5 dr \frac{1}{5} \left\{ \frac{1}{3} uv(1 - N_B G_\tau^{1/2}) - \frac{\pi}{3}(G_m^Q(r) + G_m^\pi(r) \right. \\
&\qquad \left. + G_m^\rho(r) + G_m^{\rho_0}(r) + G_m^A + G_m^{A_0}(r)) \right\} \\
g_a &= \int r^2 dr \frac{2\pi}{9} [G_{a,0}^Q(r) + G_{a,0}^\sigma(r) + G_{a,0}^\pi(r) \\
&\qquad + G_{a,0}^\rho(r) + G_{a,0}^{\rho_0}(r) + G_{a,0}^A(r)]
\end{aligned} \tag{2.110}$$

where the radial functions $G_i(r)$ for the quarks and the chiral fields are given by:

$$\begin{aligned}
G^Q_m(r) =& \frac{1}{\pi} uv(5 - 2N_B G_\tau^2) \ , \\
G^\pi_m(r) =& \beta \left[\left(\frac{h^2}{r} - g_\rho \sigma_h h \left(A_S - \frac{1}{3} A_T \right) \right) (2 + G_1^{1/2} - W_{1/2}) \right. \\
& \left. - g_\rho h^2 \rho \frac{1}{2} (3 + 2G_1^{1/2} - W_{1/2}) \right] , \\
G^Q_{a,0}(r) =& \frac{3}{2\pi} \left(u^2 - \frac{1}{3} v^2 \right) (5 - 2N_B G_\tau^2) \ , \\
G^\sigma_{a,0}(r) =& - \beta h \left\{ 4\sigma_h' + g_\rho h \left[\left(A_S - \frac{1}{3} A_T \right) (3 + W_{1/2}) \right. \right. \\
& \left. \left. + A_T \frac{2}{5} (6 + W_{1/2} + G_1^{1/2}) \right] \right\} \ , \\
G^\pi_{a,0}(r) =& 2\beta \sigma_h \left[2 \left(h' + \frac{2}{r} h \right) - g_\rho \rho h (2 + G_1^{1/2} - W_{1/2}) - 6 g_\rho \sigma_h A_S \right] . \qquad (2.111)
\end{aligned}$$

For the magnetic terms of vector mesons we have:

$$\begin{aligned}
G^\rho_m(r) =& \left\{ \frac{2}{r} \rho^2 (2 + G_1^{1/2} - W_{1/2}) \right. \\
& \left. - \frac{1}{2} g_\rho \rho \left[\rho^2 + \left(A_S + \frac{2}{3} A_T \right)^2 \right] (3 + 2G_1^{1/2} - W_{1/2}) \right\} \ , \\
G^{\rho_0}_m(r) =& \frac{g_\rho}{5 m_\rho^2} \left\{ \tilde{\rho} \left[h\tilde{h} + \left(A_S + \frac{2}{3} A_T \right) \left(\tilde{A}_S + \frac{2}{3} \tilde{A}_T \right) \right] (1 + G_1^{1/2} - 4W_{1/2}) \right. \\
& - \rho \tilde{\rho}^2 (G_1^{1/2} + 6W_{1/2} - 9) - \tilde{\rho} \left(A_S - \frac{1}{3} A_T \right) \left(\tilde{A}_S - \frac{1}{3} \tilde{A}_T \right) \\
& \left. \times (G_1^{1/2} + 6W_{1/2} - 9) + \frac{5}{\pi} (u^2 + v^2) \tilde{\rho} (1 - N_B G_\tau^{1/2}) \right\} \ ,
\end{aligned}$$

$$
\begin{aligned}
G_m^A(r) =&(-1)\left[\left(A_S' - \frac{1}{3}A_T' - \frac{A_T}{r}\right)\left(A_S + \frac{2}{3}A_T\right)(2 + G_1^{1/2} - W_{1/2})\right. \\
&\left. + \frac{1}{2}g_\rho\rho\left(A_S + \frac{2}{3}A_T\right)^2(3 + 2G_1^{1/2} - W_{1/2})\right] \ , \\
G_m^{A_0}(r) =&(-1)\frac{1}{m_\rho^2}\left\{g_\rho\left[\tilde{\rho}\left(A_S - \frac{1}{3}A_T\right) - \rho\left(\tilde{A}_S - \frac{1}{3}\tilde{A}_T\right)\right]\right. \\
&\times\left(\tilde{A}_S - \frac{1}{3}\tilde{A}_T\right)(2 - G_1^{1/2} + W_{1/2}) \\
&\left. - \left(\tilde{A}_S - \frac{1}{3}\tilde{A}_T\right)\left(\tilde{A_S}' + \frac{2}{3}\tilde{A_T}' + \frac{2}{r}\tilde{A}_T - g_\rho\sigma_h\tilde{h}\right)(2 - G_1^{1/2} + W_{1/2})\right\} \ ,
\end{aligned}
\tag{2.112}
$$

while the axial components read:

$$
\begin{aligned}
G_{a,0}^{\rho}(r) =& -2\rho\left(A_S' - \frac{1}{3}A_T' - \frac{A_T}{r}\right)(2 + G_1^{1/2} - W_{1/2}) \\
&- g_\rho\rho^2\left(A_S + \frac{2}{3}A_T\right)(3 + 2G_1^{1/2} - W_{1/2}) \\
G_{a,0}^{\rho_0}(r) =& -2\frac{g_\rho}{m_\rho^2}\left\{h\tilde{h}\left[\left(\tilde{A}_S - \frac{1}{3}\tilde{A}_T\right)(W_{1/2} - 1) + \tilde{A}_T\frac{1}{5}(G_1^{1/2} + W_{1/2} - 4)\right]\right. \\
&+\rho\tilde{\rho}\left[2\left(\tilde{A}_S + \frac{1}{6}\tilde{A}_T\right)(W_{1/2} - 1) - \tilde{A}_T\frac{1}{5}(G_1^{1/2} + W_{1/2} - 4)\right] \\
&+\left(\tilde{A}_S - \frac{1}{3}\tilde{A}_T\right)\left[3\left(\tilde{A}_S - \frac{1}{3}\tilde{A}_T\right)\left(A_S - \frac{1}{3}A_T\right) + 2A_S\tilde{A}_T + A_T\tilde{A}_S\right](W_{1/2} - 1) \\
&+\frac{1}{5}\left(A_S\tilde{A}_T + A_T\tilde{A}_S + \frac{1}{3}A_T\tilde{A}_T\right)\tilde{A}_T(G_1^{1/2} + W_{1/2} - 4) \\
&\left. -\frac{3}{2\pi}\tilde{A}_S(u^2 + v^2)\left(1 - \frac{2}{3}N_B G_\tau^{1/2}\right)\right\} \ ,
\end{aligned}
$$

$$
\begin{aligned}
G^{A}_{a,0}(r) =& 2\left[\rho'\left(2A_S+\frac{1}{3}A_T\right)+\frac{\rho}{r}\left(4A_S-\frac{1}{3}A_T\right)\right](2+G_1^{1/2}-W_{1/2}) \\
&-g_\rho\left(A_S-\frac{1}{3}A_T\right)\left[\rho^2+3\left(A_S-\frac{1}{3}A_T\right)^2-3A_SA_T\right](3+2G_1^{1/2}-W_{1/2}) \ , \\
G^{A_0}_{a,0}(r) =& \frac{2}{m_\rho^2}\left\{g_\rho\tilde{\rho}\left[\tilde{\rho}\left(A_S-\frac{1}{3}A_T\right)-\rho\left(\tilde{A}_S-\frac{1}{3}\tilde{A}_T\right)\right](2-G_1^{1/2}+W_{1/2})\right. \\
&\left.-\tilde{\rho}\left(\tilde{A_S}'+\frac{2}{3}\tilde{A_T}'+\frac{2}{r}\tilde{A}_T-g_\rho\sigma_h\tilde{h}\right)(2-G_1^{1/2}+W_{1/2})\right\}. \qquad (2.113)
\end{aligned}
$$

The definition of fields $\tilde{\phi}$ is given in Appendix I. In these expressions N_B represents the total number of mesons given by $\overline{N}_\pi+\overline{N}_\rho+\overline{N}_A$ (see Appendix I) and the coefficients $G_1^{1/2}$, $W_{1/2}$ and $G_\tau^{1/2}$ are defined as:

$$
G_1^{1/2}=\frac{F1^{1/2}(3,N_B)}{F^{1/2}(3,N_B)}, \qquad W_{1/2}=\frac{1}{3}\left(2\frac{F^{3/2}}{F^{1/2}}-1\right), \ G_\tau^{1/2}=\frac{2}{9}\left(2-\frac{F^{3/2}}{F^{1/2}}\right).
$$

2.6 Single soliton in vacuum

In this section we present the results for the single soliton in vacuum, obtained in the Chiral Dilaton Model with only chiral fields and then with the inclusion of the vector mesons. First we will show the results at mean-field level for both models and in particular we will compare them with the ones obtained in the Linear-σ model. Finally we will show the results after projection and the comparison with experimental values.

In this section the main aim is to check that the model can provide a reasonable description of the nucleon properties with the chosen parameter set. In particular we present here the results for the Lagrangian without vector mesons $\mathcal{L}_0$, obtained by putting $g_\omega=g_\rho=0$ in eq. (2.35), for the set $m_\sigma=550$ MeV and the typical

value $g_\pi = 5$ [27,75]. For the model including vector mesons we present here the results for the set $m_\sigma = 1200$ MeV, $g_\pi = 3.9$, $g_\omega = 12$ and $g_\rho = 4$, denoted as set I. This set has been chosen in order to both get saturation at finite density (as will be shown in Chapter 3) and a reasonable description of the nucleon in vacuum. Anyway, since the calculation of nuclear matter properties by using the Wigner-Seitz approximation is affected by large uncertainties we also present a second set of results with parameters better fitted to single nucleon properties, namely $m_\sigma = 1200$ MeV, $g_\pi = 3.6$, $g_\omega = 13$ and $g_\rho = 4$ (set II).

2.6.1 Mean-field results

We start the analysis of the CDM in vacuum by showing the behaviour of the fields at zero density. In Fig. 2.4 we plot the Dirac and the chiral fields for the model without vector mesons and we compare them with the ones obtained form the linear σ model. The field configurations provided by the two models are very similar and show the usually trend. The same result is given for the model including vector mesons in Fig. 2.5, where for this reason we just show the fields in the logarithmic model.

In Tables 2.1 and 2.2 we present the static properties of the Hedgehog baryon at mean-field level,calculated with the formulae (2.73), and we compare them with results obtained in the linear σ model [61, 62].

The results are very similar for the CDM and the linear σ model; nevertheless it should be noticed that, already at mean-field level, on one hand the repulsion of the ω field provides a Hedgehog mass too large compared to the experimental value, but on the other hand the contributions of the isovector fields, as the ρ and the a_1, leads to better results for the corresponding radii and magnetic moment.

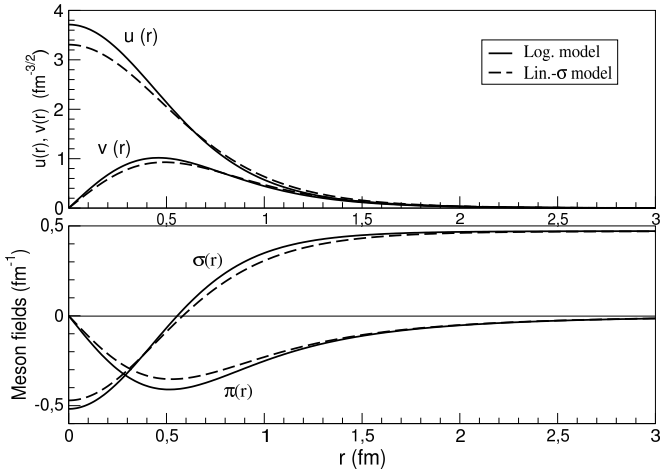

Figure 2.4: Upper panel: Dirac components in the CDM (solid line) and in the linear σ model (dashed line) without vector mesons. Lower panel: chiral fields in the CDM (solid line) and in the linear σ model (dashed line) without vector mesons.

Table 2.1: Various nucleon properties at mean-field level in the present work without vector mesons and in the σ-model [61]. The experimental value for the mass is given by $(M_N + M_\Delta)/2$.

Quantity	Log. Model	σ-Model	Exp.
$M\,(MeV)$	1176	1136	1085
$\langle r_e^2 \rangle_{I=0}$	$(0.76\,fm)^2$	$(0.78\,fm)^2$	$(0.72\,fm)^2$
$\mu_{I=1}\ (\mu_N)$	3.83	3.63	4.70
$\langle r_m^2 \rangle_{I=1}$	$(1.12\,fm)^2$	$(1.14\,fm)^2$	$(0.80\,fm)^2$
g_A	1.27	1.22	1.26
$\overline{N}_\pi$	2.4	1.9	$\diagup$

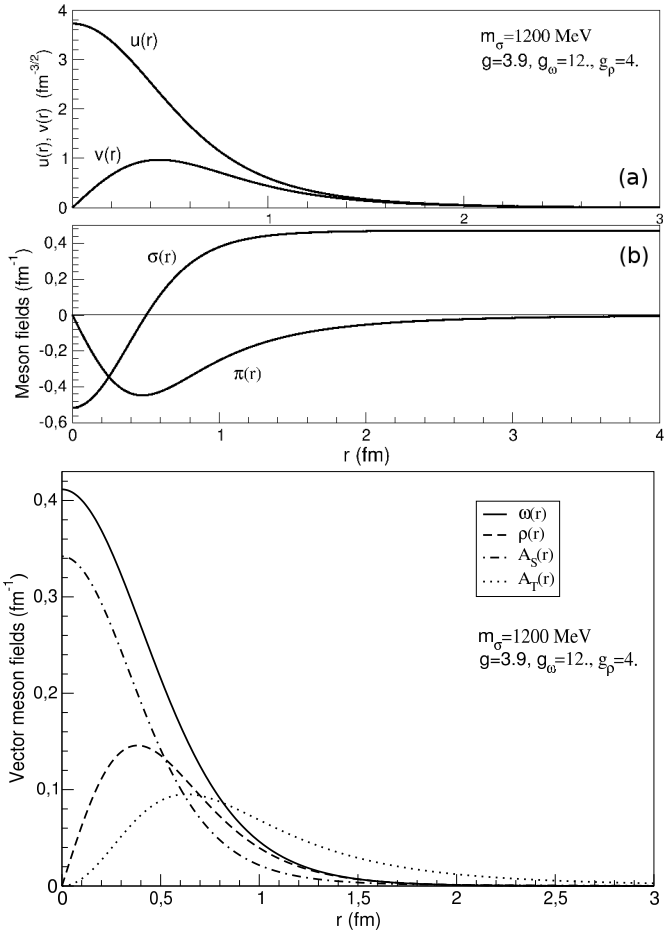

Figure 2.5: Upper panel: Dirac components (panel (a)) and chiral fields (panel (b)) in the CDM with vector mesons for set I. Lower panel: vector mesons profiles in the CDM for set I.

In Tables 2.3 and 2.4 we show the decomposition of the soliton total energy in its various contributions and again we compare with the linear σ model [61, 62].

We see that the contributions to the total energy coming from chiral fields and from vector mesons are comparable: as expected vector mesons play an important role in the dynamics of the soliton. It is also interesting to notice that the results

Table 2.2: Various nucleon properties at mean-field level in the present model and in the σ-model [62] with vector mesons and set I. The experimental value for the mass is given by $(M_N + M_\Delta)/2$.

Quantity	Log. Model	σ-Model	Exp.
$M\,(MeV)$	1329.5	1331.7	1085
$\langle r_e^2\rangle_{I=0}$	$(0.78\,fm)^2$	$(0.76\,fm)^2$	$(0.72\,fm)^2$
$\mu_{I=1}\ (\mu_N)$	4.49	4.51	4.70
$\langle r_m^2\rangle_{I=1}$	$(0.99\,fm)^2$	$(1.01\,fm)^2$	$(0.80\,fm)^2$
g_A	1.34	1.35	1.26
$\overline{N}_\pi$	2.62	2.66	$\diagup$

for the energy contributions obtained with the logarithmic model are very similar to the ones obtained with the Mexican hat potential, at zero density, especially when vector mesons are included.

2.6.2 Results after projection

In Tables 2.5 and 2.6 we present the results after projection in both models, with and without vector mesons. Moreover, in Table 2.7 we present the results obtained for the model with vector mesons using set II, better fitted to the nucleon and Delta masses. It is important to stress that our results in the model with only chiral fields are consistent with the ones obtained in [102]. There, a different approach based on the coherent pair approximation was used. Their results are similar to ours when the coherence length parameter x is taken to be of the order of one, as suggested in [103].

Table 2.3: Contributions to the soliton total energy at mean-field level in the Logarithmic model and in the linear σ model [61]. All quantities are in MeV.

Quantity	Log. Model	linear σ model
Quark eigenvalue	83.1	107.4
Quark kinetic energy	1138.0	1056.9
E_σ (mass+kin.)	334.5	320.3
E_π (mass+kin.)	486.0	373.1
Potential energy $\sigma - \pi$	105.7	120.7
$E_{q\sigma}$	-101.4	-62.3
$E_{q\pi}$	-787.0	-673.2
Total energy	1175.6	1136.2

The results obtained both without and with the vector mesons in general overestimate the experimental values, particularly for the magnetic observables, once the parameters are chosen so that the projected mass of the nucleon is close to its physical value. One has anyway to recall that for the mass an approximate correction for the spurious center of mass motion has been taken into account (see eq.(2.108)), while no center of mass correction has been done for the other observables. When this further corrections are taken into account the value of some observables typically reduces.

Table 2.4: Contributions to the soliton total energy at mean-field level in the Logarithmic model and in the linear σ model with vector mesons [62]. All quantities are in MeV.

Quantity	Log. Model	linear σ model
Quark eigenvalue	114.5	112.9
Quark kinetic energy	1075.8	1080.6
E_σ (mass+kin.)	213.8	212.2
E_π (mass+kin.)	393.2	397.3
Potential energy $\sigma - \pi$	81.2	80.4
E_ω (mass+kin.)	-194.4	-196.5
E_ρ (mass+kin.)	162.6	165.4
E_A (mass+kin.)	329.5	334.1
$E_{q\sigma}$	6.54	4.74
$E_{q\pi}$	-621.9	-627.1
$E_{q\omega}$	388.9	393.0
$E_{q\rho}$	-163.8	-165.9
E_{qA}	-341.8	-346.4
Total energy	1329.5	1331.7

Table 2.5: Projected nucleon properties in the present work without vector mesons and in the linear σ-model and comparison with experimental values.

Quantity	Log. Model	σ-Model	Exp.
$E_{1/2}\,(MeV)$	1075	1002	
$M_N\,(MeV)$	960	894	938
$E_{3/2}\,(MeV)$	1140	1075	
$M_\Delta\,(MeV)$	1032	975	1232
$\langle r_E^2\rangle_p\,(fm^2)$	0.55	0.61	0.74
$\langle r_E^2\rangle_n\,(fm^2)$	-0.02	-0.02	-0.12
$\langle r_M^2\rangle_p\,(fm^2)$	0.7	0.72	0.74
$\langle r_M^2\rangle_n\,(fm^2)$	0.72	0.75	0.77
$\mu_p\ (\mu_N)$	2.25	2.27	2.79
$\mu_n\ (\mu_N)$	-1.97	-1.92	-1.91
g_a	1.52	1.10	1.26
$\langle N_\pi\rangle_J$	1.6 $(J=1/2)$ 2. $(J=3/2)$	1.2 $(J=1/2)$ 1.6 $(J=3/2)$	/

Table 2.6: Projected nucleon properties in the present work and in the linear σ-model with vector mesons and comparison with experimental values.

Quantity	Log. Model	σ-Model	Exp.
$E_{1/2}\,(MeV)$	892	882	
$M_N\,(MeV)$	763	750	938
$E_{3/2}\,(MeV)$	1030	1029	
$M_\Delta\,(MeV)$	918	917	1232
$\langle r_E^2\rangle_p\,(fm^2)$	0.59	0.58	0.74
$\langle r_E^2\rangle_n\,(fm^2)$	-0.03	-0.02	-0.12
$\langle r_M^2\rangle_p\,(fm^2)$	0.69	0.69	0.74
$\langle r_M^2\rangle_n\,(fm^2)$	0.70	0.71	0.77
$\mu_p\ (\mu_N)$	2.72	2.71	2.79
$\mu_n\ (\mu_N)$	-2.49	-2.5	-1.91
g_a	1.6	1.48	1.26
$\langle N_\pi\rangle_J$	1.1 $(J=1/2)$	1.8 $(J=1/2)$	/
	1.3 $(J=3/2)$	2.2 $(J=3/2)$	

Table 2.7: Projected nucleon properties in the present work and in the linear σ-model with vector mesons and comparison with experimental values for the parameter set: $g = 3.6$, $g_\omega = 13$, $g_\rho = 4$ and $m_\sigma = 1200$ MeV.

Quantity	Log. Model	σ-Model	Exp.
$E_{1/2}\,(MeV)$	1020	1008	
$M_N\,(MeV)$	926	912	938
$E_{3/2}\,(MeV)$	1148	1147	
$M_\Delta\,(MeV)$	1066	1063	1232
$\langle r_E^2\rangle_p\,(fm^2)$	0.67	0.66	0.74
$\langle r_E^2\rangle_n\,(fm^2)$	-0.05	-0.05	-0.12
$\langle r_M^2\rangle_p\,(fm^2)$	0.77	0.76	0.74
$\langle r_M^2\rangle_n\,(fm^2)$	0.78	0.77	0.77
$\mu_p\ (\mu_N)$	2.63	2.64	2.79
$\mu_n\ (\mu_N)$	-2.37	-2.38	-1.91
g_a	1.58	1.46	1.26

Chapter 3

The Wigner-Seitz approximation to nuclear matter

In the previous chapters we described how to build up a single soliton, starting from quarks interacting with mesons. Now to go further in our analysis and to test the behaviour of the CDM at finite density, we need to mimic a dense system of solitons.

The description of nuclear matter, starting from effective Lagrangians, has been widely discussed in literature and it has been applied to models including both nucleons or quarks degrees of freedom. One approach consists of considering the fermion, a nucleon or a quark, embedded in a uniform mean meson field which simulates interactions with the surrounding medium. This method has been applied to the $\sigma - \omega$ model [104–107] achieving remarkable results in describing nuclear matter as composed of hadrons. The same method has been used for soliton models, such as the colour dielectric model, with fermions as quarks and mesons acting as confining forces [44, 54, 108, 109].

The other approach we adopt in this work is a technique, the so-called *Wigner-Seitz approximation* [110], coming from solid state physics which is based on the construction of a lattice of spherical cells, each one containing a soliton. For sake of completeness, we should mention that in the literature one can find also attempts to treat nuclear matter as a crystal, by letting the particles sit on a regular lattice [31, 111–113], but since nuclear matter looks like a fluid, the Wigner-Seitz approach seems to provide a better physical picture.

Specifically the Wigner-Seitz method consists of replacing the cubic lattice by a spherical symmetric one where each soliton sits on a spherical cell of radius R with specific boundary conditions imposed on fields at the surface of the sphere. The configuration of the meson fields, centered at each lattice point, generates a periodic potential in which the quarks move. In this way a many-body system, such as a dense nuclear system, is reduced to a single particle one where the effects of finite density enter through the imposition of proper boundary conditions. This method has been used in the past to describe finite density systems in non-topological soliton models [34, 36, 114], chiral soliton models [36, 37, 115, 116] and Skyrme models [117, 118].

In the next sections we will describe in detail the main features of the Wigner-Seitz approximation, such as the choice of boundary conditions and the definition of a band width.

3.1 The Wigner-Seitz cell

Before introducing the main features of the Wigner-Seitz cell, we briefly review the case of a regular lattice, e.g an fcc lattice [119], in which quarks interact with a scalar field σ. The assumption of periodicity of the lattice leads to the following

constraint on the scalar field:

$$\sigma(\boldsymbol{r}) = \sigma(\boldsymbol{r} + \boldsymbol{L}) \tag{3.1}$$

where $\boldsymbol{L}$ is the lattice vector. The σ field will possess the symmetries of the lattice. Under this configuration for the σ field, the spinor of the quark field must satisfy the Bloch theorem:

$$\psi_{\boldsymbol{k}}(\boldsymbol{r}) = e^{i\boldsymbol{k}\cdot\boldsymbol{r}}\Phi_{\boldsymbol{k}}(\boldsymbol{r}), \tag{3.2}$$

where $\boldsymbol{k}$ is the crystal momentum (which for the ground state is equal to zero) and $\Phi_{\boldsymbol{k}}(\boldsymbol{r})$ is a spinor that has the same periodicity of the lattice, namely:

$$\Phi_{\boldsymbol{k}}(\boldsymbol{r}) = \Phi_{\boldsymbol{k}}(\boldsymbol{r} + \boldsymbol{L}). \tag{3.3}$$

The quark spinor satisfies the Dirac equation:

$$[\boldsymbol{\alpha}\cdot(\boldsymbol{p} + \boldsymbol{k}) + g\beta\sigma(\boldsymbol{r})\Phi_{\boldsymbol{k}} = \epsilon_{\boldsymbol{k}}\Phi_{\boldsymbol{k}} \tag{3.4}$$

where for a given $\boldsymbol{k}$ corresponds an eigenvalue $\epsilon_{\boldsymbol{k}}$.

In the case of the Wigner-Seitz cell, we replace the cubic lattice with a spherical cell of radius R. The spherical symmetry imposes that for the lowest band all the fields should have an s-wave form. This requirement is naturally satisfied by the fields configuration in the Hedgehog ansatz, shown in Sec. 2.4.1, where only an extra quantum number k for the linear momentum of the cell has to be

added. Therefore the quarks spinor for example will read:

$$\psi_k = \frac{1}{\sqrt{4\pi}} \begin{pmatrix} u_k(r) \\ iv_k(r)\boldsymbol{\sigma} \cdot \hat{\boldsymbol{r}} \end{pmatrix} \chi_h. \tag{3.5}$$

In this work we will limit the calculation to the ground state for which $k = 0$.

3.1.1 Boundary conditions

The translational invariance by multiples of the cell radius R, given by the periodicity of the lattice, allows to impose appropriate boundary conditions for the fields on the surface of the sphere.
In the literature various sets of possible boundary conditions have been discussed [36, 37]. In our work we adopt the choice of Ref. [36] which relates the boundary conditions at R to the parity operation, $\boldsymbol{r} \to -\boldsymbol{r}$. With respect to this symmetry the lower component $v(r)$ of quark spinor, the pion $h(r)$ and the rho $\rho(r)$ are odd, and therefore they have to vanish at R:

$$v(R) = h(R) = \rho(R) = 0. \tag{3.6}$$

Similarly, for the σ field, the upper Dirac component, the ω and the A fields the argument based on parity provides the conditions:

$$u'(R) = \sigma_h'(R) = \omega'(R) = A_S'(R) = A_T'(R) = 0. \tag{3.7}$$

The boundary conditions at $r = 0$ remain the ones given in eq. (2.62). Basically the calculation consists in solving the set of coupled field equations in a self-consistent way for a given value R; practically we start from $R = 4$ fm, for

which the periodic solutions are indistinguishable from the vacuum ones, and we slowly decrease the cell radius down to the smallest radius for which self-consistent solutions can be obtained.

In Fig. 3.1 we plot the Dirac and the chiral fields in the model without vector mesons for different values of R; down to $R = 2$ fm, the solutions do not change significantly, but as the cell radius shrinks to lower values, we see that all the fields are deeply modified by the finite density.

For the model including vector mesons, we present in Fig. 3.2 the trend of the vector meson fields. To better clarify the difference between the models without

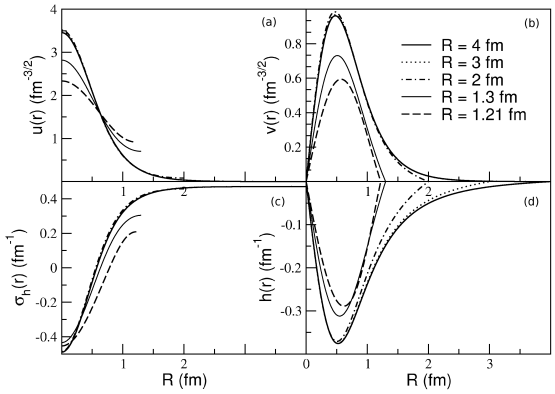

Figure 3.1: In panel (a) and in panel (b) we plot the upper and lower components of the Dirac spinor, also σ (panel (c)) and pion (panel (d)) fields are shown for different values of the cell radius R in the model without vector mesons.

and with vector mesons, in Fig. 3.3 we show the baryon density profiles in the two cases. The relevant feature is that in the model without vector mesons the shape of the soliton becomes significantly more flat, at large densities, than in the case with vector mesons. This effect is due to the repulsion between the two solitons provided by the ω field, which prevents the baryon density from becoming large

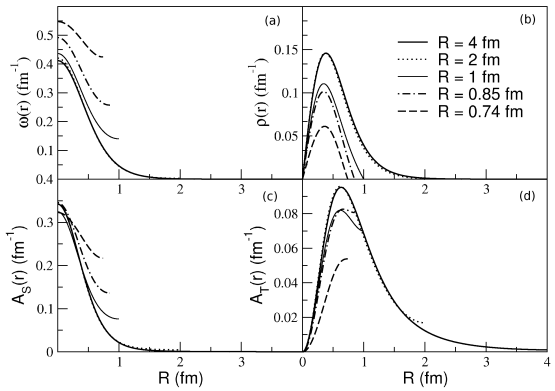

Figure 3.2: Vector meson fields, as functions of the cell radius R. In (a) we plot the ω field, in (b) the ρ field, in (c) the A_S field and in (d) the A_T field.

in the inter-nucleon region. This feature will have an important consequence on the dependence of the radii on the density, as discussed in Section 3.2.2.

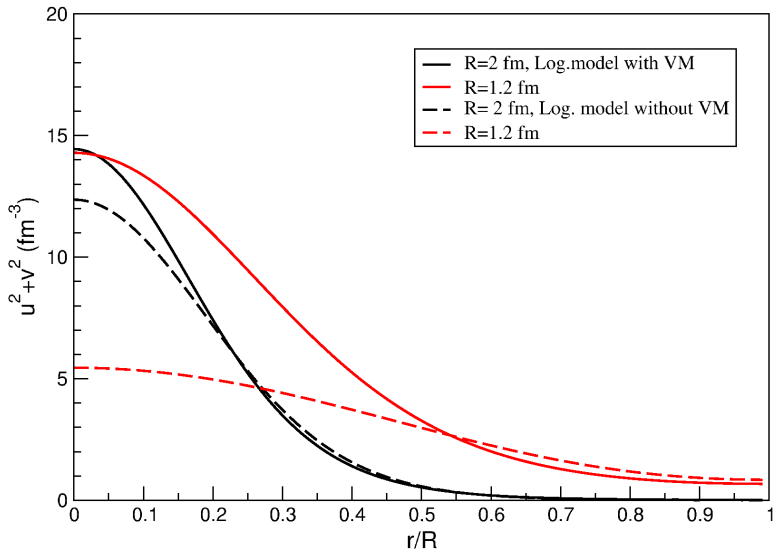

Figure 3.3: Baryon density as a function of the ratio r/R for the model without (dashed line) and with vector mesons (solid line). Two values of the cell radius R are shown, namely $R = 2$ fm and $R = 1.2$ fm.

3.1.2 Band width

The formation of a band structure, namely a continuous set of states with an energy gap above the highest state, comes directly from the Bloch wave function for the quark fields defined in eq. (3.2). By solving the Dirac equation in (3.4) for a single cell, we can obtain the energy eigenvalues $\epsilon_{\boldsymbol{k}}$ for all values of crystal momentum $\boldsymbol{k}$ within the first Brillouin zone and hence define a band where the lowest energy state is given by $\boldsymbol{k} = 0$. For the spherical symmetric cell, how to define the width of the band is highly not trivial. The assumption that inside the cell the potential is spherically symmetric implies that the bottom of the band will therefore be spherically symmetric and the upper Dirac component will be flat on the boundary. Nevertheless to define a band we need all the states, not only the bottom one, so a full calculation of non-spherical symmetric states with $k \neq 0$ should be performed. Many attempts have been made in the field of soliton matter in order to provide the full spectrum of Dirac states and to define the top the band. The most sophisticated technique is the one provided in [36]. Here the authors impose a Bloch-like boundary condition to relate the values of the quark wave function at any pair of opposite points lying on the sphere $\mathcal{S}$:

$$\psi(\boldsymbol{r}) = e^{2i\boldsymbol{k}\cdot\boldsymbol{r}}\psi(-\boldsymbol{r}) \ \ , \forall \boldsymbol{r} \in \mathcal{S} \tag{3.8}$$

and then they solve self-consistently the meson and quark fields equations which obviously depend on $\boldsymbol{k}$.

In this work we adopt two much simpler procedures. The first method is taken from [116], where the authors estimate the top of the band from the momentum connected to the size of the cell, $k_{top} = \frac{\pi}{2R}$. The explicit expressions for the band

and the top eigenvalue read:

$$\Delta = \sqrt{\epsilon_0^2 + \left(\frac{\pi}{2R}\right)^2} - |\epsilon_0|, \tag{3.9}$$

$$\epsilon_{top} = \epsilon_0 + \Delta, \tag{3.10}$$

where ϵ_0 is the eigenvalue of the ground state.

An alternative approximation to the band width is obtained, following [34], by imposing the conditions that the upper Dirac component vanishes at the boundary:

$$u(R) = 0. \tag{3.11}$$

In [36] the authors show that this approximation leads to an upper limit on the energy of the top of the band; the true top is typically about halfway between the bottom and this upper limit.

Now we address the question of how to fill the band. Since we are considering chiral solitons at mean-field level, as shown in Chapter 2, the relevant quantum number is the grand-spin G and the lower band corresponds to $G = G_3 = 0$. For this value of grand-spin, the only degeneracy left is the colour and hence the three quarks per soliton are completely filling the band.

The total energy of the soliton in the cell is estimated by assuming a uniform filling and by averaging the energy within the band.

3.2 Solitons at finite density

In this section we present the results obtained by studying a Wigner-Seitz lattice of solitons for the logarithmic model with only chiral fields and also with vector mesons. We first discuss the energy of the system at finite density and we then

present the effect of the density on the single nucleon properties.

We will show the two main purposes of this thesis:

- the modification of the chiral field interaction, with the inclusion of *scale invariance* and the presence of a *logarithmic* term in the potential, allows to reach higher densities in comparison to the linear σ model;
- the introduction of *vector mesons* in the dynamics of the model stabilises the soliton at high densities and also partially provides the necessary repulsion to obtain saturation.

3.2.1 Energy of the lattice

Let us start by showing in Fig. 3.4 the results for the total energy per unit cell of the soliton at mean-field level in the CDM and in the linear σ model without vector mesons. For each given value of the sigma mass, it can be seen that the logarithmic model allows the system to reach higher densities in comparison to the σ-model. Moreover it should be noticed that as m_σ rises, the system remains stable to lower R since the model is approaching the non-linear limit and the chiral fields are more and more constrained to lie on the chiral circle.

The same result is shown in Fig. 3.5 for both models with the inclusion of vector mesons.

The introduction of vector mesons also leads to more stable solutions at high densities as can be seen in Fig. 3.6, where we present the total energy of the soliton in the logarithmic model with vector mesons and we compare it to the one obtained in the case with only chiral fields.

The other effect obtained by the introduction of vector mesons is to partially provide the repulsion that leads to the saturation of chiral matter. In order to

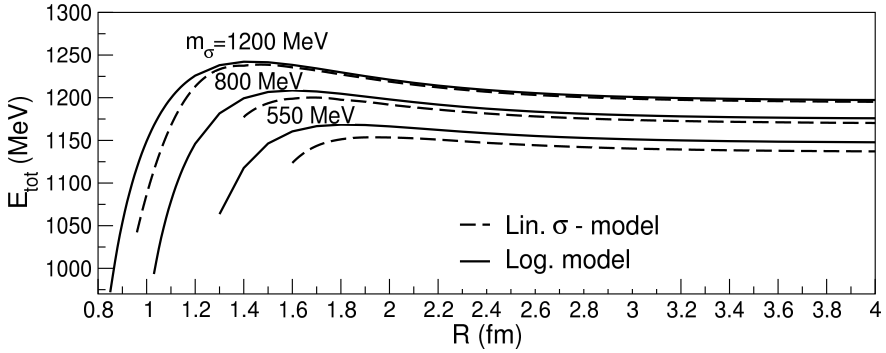

Figure 3.4: Total energy of the soliton as a function of cell radius R for the linear σ-model [36] and for the present model without vector mesons with $g = 5$. Different values of m_σ are considered.

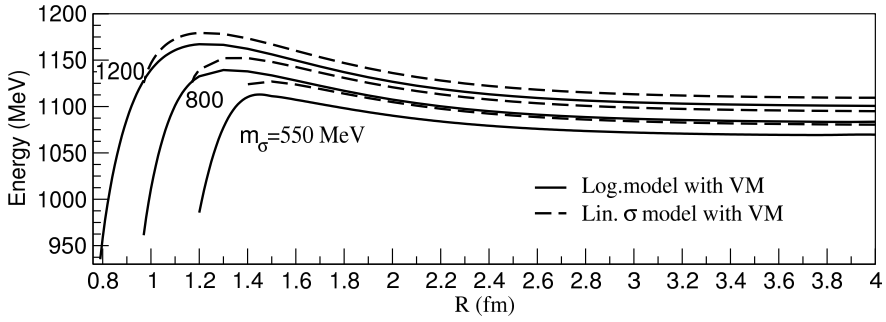

Figure 3.5: Total energy of the soliton as a function of cell radius R for the linear σ-model [36] and for the present model with vector mesons. The parameter set is $g = 5$, $g_\omega = 12$ and $g_\rho = 4$. Different values of m_σ are considered.

show the origin of this saturation mechanism we show in Figs. 3.7 and 3.8 the behaviour of the quark eigenvalue in the CDM with and without vector mesons as a function of the cell radius R. Here we plot the eigenvalue ϵ_0 for the bottom of the band and corresponding to the state $G^P = 0^-$. We also plot the estimates of the top of the band calculated with the eqs. (3.9) and (3.11), denoted respectively with $\epsilon_{top}^{(a)}$ and $\epsilon_{top}^{(b)}$. In addition to that we also show the lower state of the upper

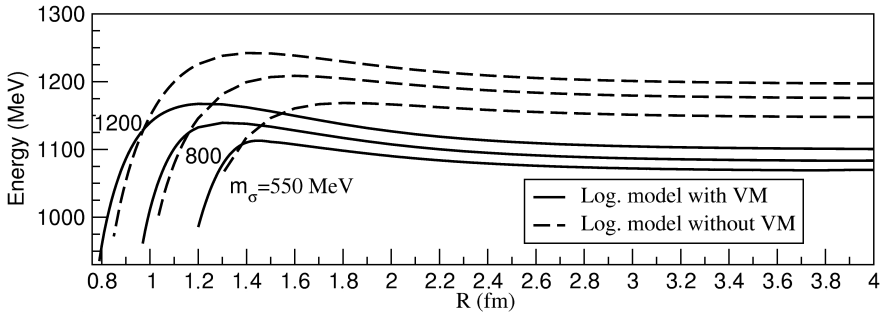

Figure 3.6: Total energy of the soliton as a function of cell radius R for the present model with and without vector mesons. The parameter set is $g = 5$, $g_\omega = 12$ and $g_\rho = 4$. Different values of m_σ are considered.

band, given by the first excited state 1^+. It is clear that in absence of vector mesons we never obtain saturation. Moreover to change the value of m_σ does not modify this result. The band structure is quite similar in both cases. The band

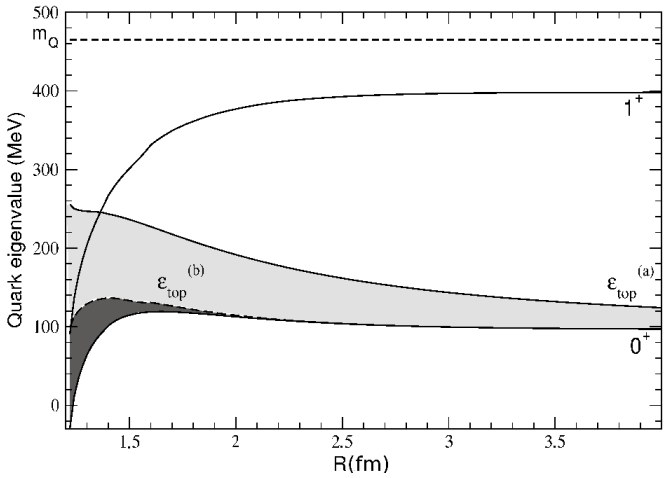

Figure 3.7: Lower panel: quark eigenvalue as a function of the cell radius R, in the model without vector mesons. The shaded areas represent the band as estimated in eq.(3.9) and in eq. (3.11). The quark mass in vacuum, here 465 MeV, is indicated by the dashed line.

is narrower at low densities, where the soliton is well localized within the cell. As proposed in Ref. [33], one can picture this scenario as a colour insulator, with the quarks not free to move across the lattice. While the density rises, the band gets wider up to the density where solution is lost; in this case the chiral matter would act as a colour conductor and the quarks would be free to move from one soliton cell to the other. The main difference between the model without and with vector mesons is given by a significant increase of the top of the band at higher densities which allows us to obtain saturation.

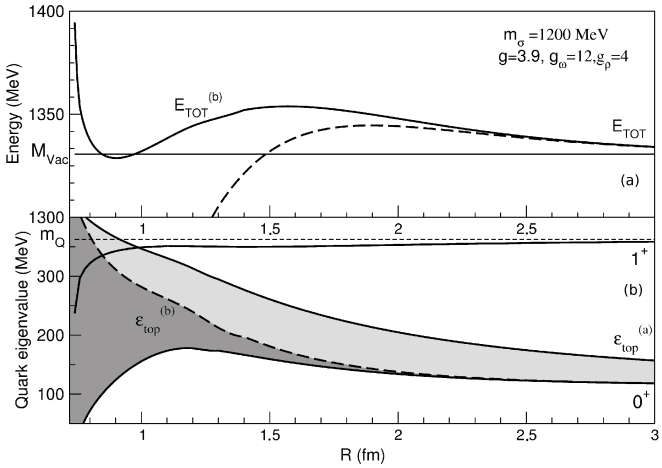

Figure 3.8: Panel (a): total energy of the soliton with band effects (solid line) and without band effects (dashed line) as a function of the cell radius R for the model with vector mesons. Panel (b): the quark eigenvalue as a function of the cell radius R for the model with vector mesons. The shaded areas represent the band as estimated in eq.(3.9) and in eq. (3.11). The quark mass, here 362.7 MeV, is indicated by the dashed line.

To better understand our result which indicates the possibility of getting saturation, in Fig. 3.9 we compare the total energy of the soliton at mean-field

without the contribution associated with the band. In order to emphasize the effect of the density on the energy we subtracted the mass of the nucleon in vacuum. It is clear that the exchange of vector mesons plays a crucial role, by contributing ~ 100 MeV at $R = 1$ fm, but it is not sufficient to get saturation.

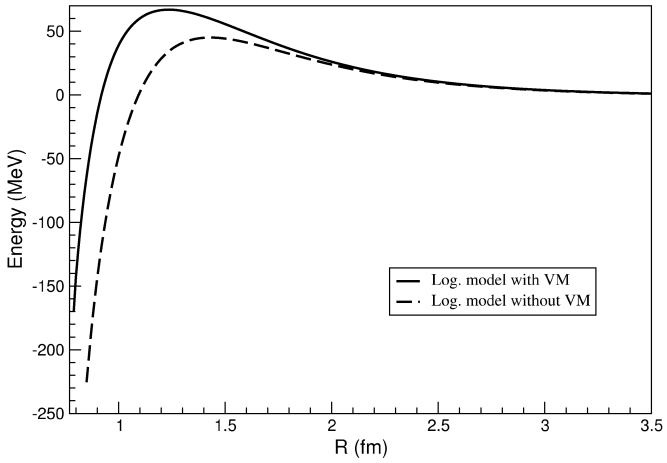

Figure 3.9: Total energy of the soliton at mean-field level in the logarithmic model without vector mesons (dashed line) and with vector mesons (solid line). The parameter values are: $m_\sigma = 1200$ MeV, $g_\pi = 5$, $g_\omega = 12$ and $g_\rho = 4$.

To determine which ingredient of the model is actually providing the repulsion at high densities, in Fig. 3.10 we plot the interaction energies for each term contributing to the total energy at finite density. The plotted quantities are defined as the value of the chosen energy contribution at R minus the corresponding vacuum value:

$$\tilde{E}_i(R) = E_i(R) - E_i(\infty). \tag{3.12}$$

From the figure it is clear that the band effect is strongly influencing the total energy of the soliton, by providing the largest contribution to repulsion at high densities. This is not surprising, because the band is associated with the sharing

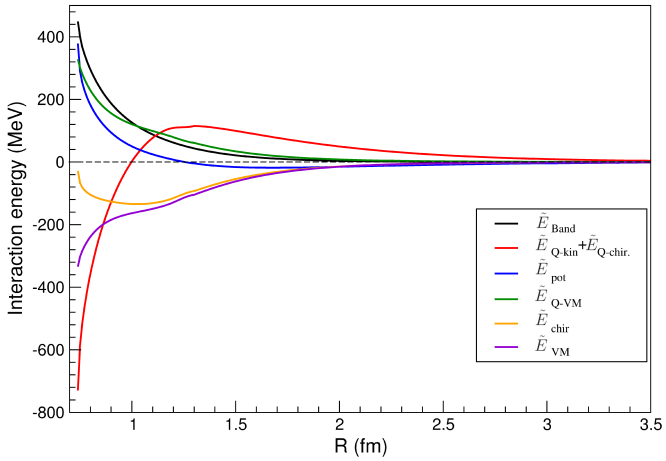

Figure 3.10: Interaction energies $\tilde{E}_i$, as defined in text, as a function of the cell radius R in the model with vector mesons. Parameters as in Fig. 3.8.

of quarks between nucleons. It is well known [120, 121] that in calculations of the $N-N$ potential based on quark models the short-range repulsion is associated with the formation of a six-quark bag. In our calculation the exchange of vector mesons is the dominant effect at densities up to ρ_0, but at very high densities the band effect dominates. The total amount of these contributions leads to the repulsive mechanism responsible for the steep rising of the total energy at high densities, as it can be seen in the upper panel of Fig. 3.8.

In more detail this is also shown in Figs. 3.11 and 3.12, where we focus on the mesons contributions and we leave aside the band term. In the upper panels we plot the contributions of the chiral mesons to the total energy (without the band effect) and the quark-chiral mesons interaction energies, respectively, and in the lower panels we present a similar analysis but for the vector mesons. It is clear that the ω meson provides the short-range repulsion, partially compensated by

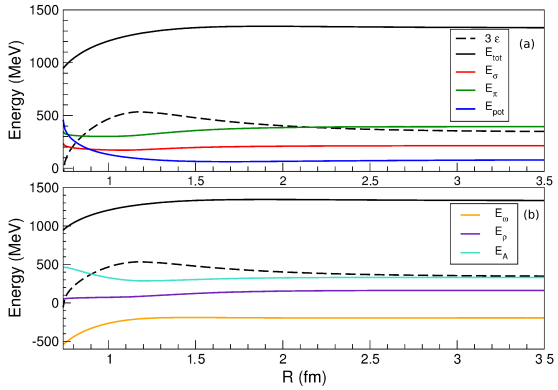

Figure 3.11: Panel (a): contributions of the chiral fields to the total energy of the soliton as a function of the cell radius R in the model with vector mesons. Panel (b): contributions of the vector meson fields to the total energy of the soliton as a function of the cell radius R. Parameters as in Fig. 3.8.

the interaction of the quarks with the A meson.

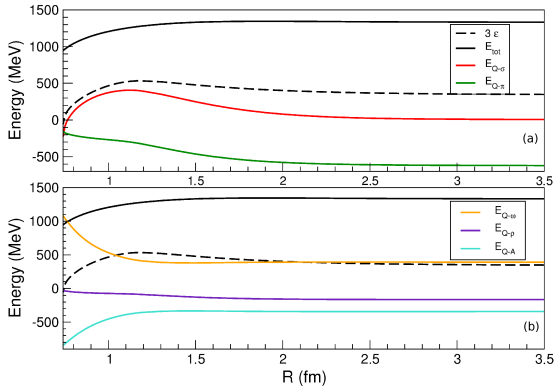

Figure 3.12: Panel (a): interaction energies of the chiral fields with quarks as a function of the cell radius R in the model with vector mesons. Panel (b): interaction energies with the vector mesons as a function of the cell radius R. Parameters as in Fig. 3.8.

It has been discussed in the literature how to interpret the results obtained

using the Wigner-Seitz lattice and in particular which should be the indications of quark deconfinement. In [33] it has been suggested that deconfinement takes place when the upper band, which corresponds to $G = 1$, merges with the lower band. In the case with vector mesons this occurs roughly at densities slightly larger than the saturation density. We should keep in mind that the estimate of the width of the band is affected by large uncertainties and it is well possible that in a more refined calculation saturation density and deconfinement density turn out to be well separated.

The scenario depicted by the results presented so far leads for the very first time to saturation by making use of the interplay between attraction from chiral fields and repulsion from the vector fields. The logarithmic turns out to play a fundamental role, by allowing the solitons to remain stable at densities large enough that the vector mesons can start acting on the dynamics.

At this point it is important to prove that this result can be obtained not only in a tiny parameters' range but that the mechanism leading to saturation is rather stable respect to the choice of parameter values. his analysis is shown in Fig. 3.13 where we plot, as a function of the density, the value of the total energy, including the band effects, at the "saturation density" point minus the energy in vacuum for different values of the parameters, at fixed $m_\sigma = 1200$ MeV. Here "saturation density" means the density at which a local minimum in the total energy appears, even if that minimum is not the global one.

The minimum is global when the energy plotted in Fig. 3.13 is negative and in that situation we are getting real saturation. Instead, when the plotted energy is positive the local minimum corresponds to a sort of metastable state. Since

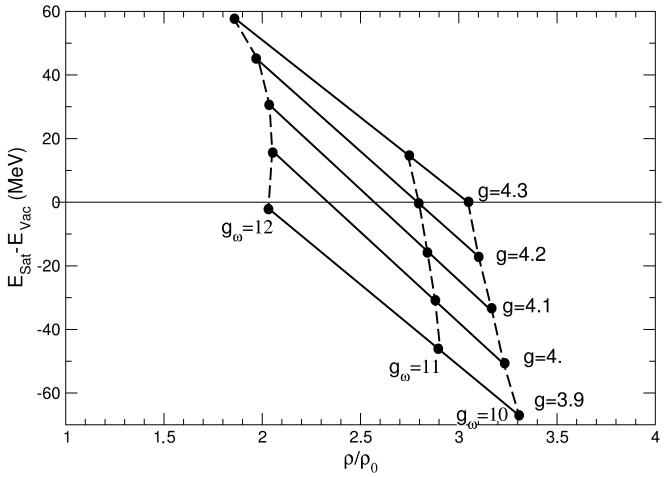

Figure 3.13: Minimum of the total energy as a function of the density. Different sets of couplings are shown, for which the model admit saturation. See the text for more details.

our calculation is affected by large uncertainties we think it is interesting to show also the parameters leading to this "false" minimum, since in a more sophisticated calculation (based for instance on a better estimate of the band) those energies could easily become negative. For parameter values significantly outside the indicated range no local minimum exist. For instance for values of $g_\omega > 12$ the local minimum of the energy disappears because the energy keeps raising as the density increases while for small values of g_ω the repulsion cannot contrast the attraction and the energy gets smaller and smaller at large densities. It is important to notice that the range of parameter values providing "saturation" is at least in part overlapping with the range of parameter values for which a reasonable description of the single soliton in vacuum can be obtained. Finally, we have to recall that we are not really studying nuclear matter, but rather $G = 0$ matter, which is composed of degenerate nucleons and deltas. Obviously,

no experimental data exist for that type of theoretical matter, but we can expect it to be saturating, probably with a larger saturation energy than that of nuclear matter. The corresponding saturation density is also obviously unknown.

3.2.2 Nucleon properties at finite density

The question about the modification of the nucleon properties at finite density have been investigated in many analysis, both experimental [122] and theoretical [77, 123–126]. In Figs. 3.14 and 3.15 we show how the values of a few observables evolve as a function of the spherical cell density. The mean-field observables evaluated as a function of the density cell are the isoscalar electric and the isovector magnetic radius and the number of pions. The formulae for these quantities for the model without and with vector mesons read [97, 127]:

$$\begin{aligned}\langle r_E^2\rangle_{I=0} &= \int r^4(u^2+v^2)dr \\ \langle r_M^2\rangle_{I=1} &= \frac{1}{\mu_{I=1}}\int r^5\frac{2\pi}{9}(G_M^Q+G_M^\pi+G_M^\rho+G_M^A)\,,\end{aligned} \tag{3.13}$$

$\mu_{I=1}$ and the radial functions G_m^{field} are given in eq.(2.73) and in eq.(2.74) in Chapter 2.

The problem with our evaluation is that in the Wigner-Seitz approach we are forcing a unit of baryon number in every cell of the lattice. Therefore, at densities large enough that the fields start occupying most of the cell and their value is no more strongly varying inside the cell, the various radii all simply scale with the size of the cell. The results we are obtaining are therefore indicative only at densities low enough that the fields are still relatively well contained inside each cell. As shown in Figs. 3.1 and 3.2 all the fields are well confined up to values of density close to ρ_0. This implies that the behaviour of the observables, evaluated

from these fields, have no physical relevance at densities of the order or above nuclear matter saturation density ρ_0.

The problem we are facing is deeply associated with the Wigner-Seitz approximation in which the effect of the finite density to the various observables is due only to Hartree contributions. In the real case two neighbouring nucleons interact also via the Fock term. Notice that at densities large enough that the field fluctuations are suppressed, the Hartree contributions associated e.g with the pion field vanishes. On the contrary the Fock term becomes relevant at those densities and it provides to the electromagnetic observables contributions which in nuclear physics are sometimes called pion-in-flight. These terms, of course, cannot be evaluated in the Wigner-Seitz approach.

Another problem with the Wigner-Seitz approach is that it imposes spherical boundary conditions on the fields. This is particularly dangerous in the case of the chiral fields, since at mean-field level directions in ordinary space are connected with directions in isospin space, a situation which is certainly quite far from reality. Due to these problems a work is in progress [128] in which a real lattice will be studied, with boundary conditions which can change depending on the direction. We think it is nevertheless worthy to present our results in Figs. 3.14-3.15 so to compare them with future more precise estimates.

For the model containing σ and π only, our results can be meaningful at low densities where the dynamics is dominated by chiral fields. The introduction of vector mesons affects in quite a interesting way the isoscalar radius: as shown in Fig. 3.3, the repulsion provided by the ω field, for densities smaller than ρ_0, prevents the swelling of the nucleons. The qualitative effect of the inclusion of the vector mesons is to stabilize the shape of the solitons respect to compression.

This can be seen also in the case of the magnetic radius where the reduction of this quantity as a function of the density is less marked than in the case without vector mesons. It is also possible to evaluate the so-called "super-ratio" defined as $(G_E/G_M)^{\rho}/(G_E/G_M)^{vac}$, where $G_{E,M}$ are the electric and magnetic form factors. In our calculation we obtain a reduction of this quantity as a function of the density, similarly to what obtained in other works, although the effect here is much larger. Although the model with vector mesons allows to reach much higher densities, we do not attribute too much significance to the behaviour of the observables at $\rho \gtrsim \rho_0$ for the reasons explained above. In the lowest panel of Figs. 3.14 and 3.15 we also show the behaviour of the number of pions $\overline{N}_{\pi}$ per unit cell at finite density. The possibility of an enhancement of the pion cloud, when the nucleon is not isolated, has been discussed in the literature [124]. In the present approach we obtain instead a decrease of $\overline{N}_{\pi}$. This result stems from the behaviour of the pionic field on the Wigner-Seitz lattice as shown in Fig. 3.1. The strong reduction of the pionic field is due to the boundary conditions requested by the spherical symmetry. It will be interesting to see if this result survives when a real lattice is used in the calculation.

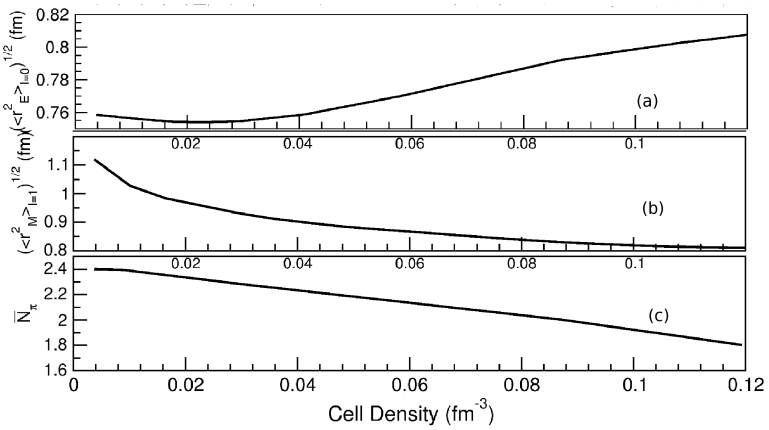

Figure 3.14: Isoscalar electric radius (panel (a)), isovector magnetic radius (panel (b)) and average number of pions (panel (c)) as a function of cell density ρ_C for the model without vector mesons.

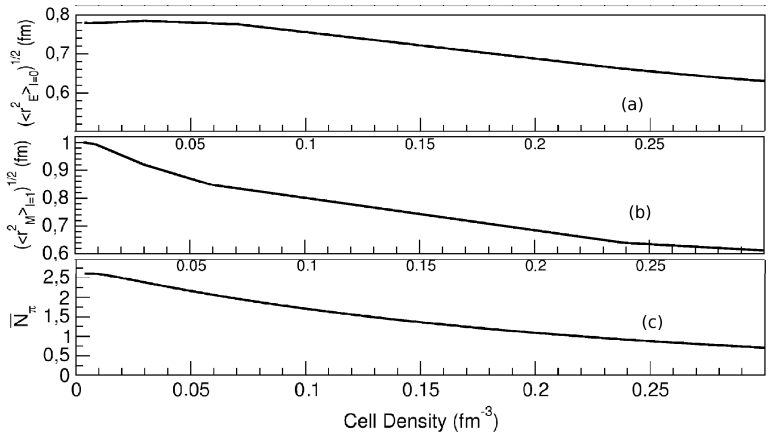

Figure 3.15: Isoscalar electric radius (panel (a)), isovector magnetic radius (panel (b)) and average number of pions (panel (c)) as a function of cell density ρ_C for the model with vector mesons.

Chapter 4

The $B = 2$ system in the Chiral Dilaton Model

The Wigner-Seitz approximation, presented in the previous chapter, does not permit us to study the inter-soliton interaction including a possible dependence on isospin. The Wigner-Seitz lattice represents a group of static field configurations with a precise symmetry connected to the boundary conditions imposed on the edge of each cell. Since the Hedgehog solution contains also isospin degrees of freedom, it would be interesting to check if rotating the relative isospin orientation between solitons could lead to a lower energy configuration.

In this chapter we present a first attempt to go beyond the Wigner-Seitz approximation in order to study the interaction between two solitons in the Chiral Dilaton Model without vector mesons. Starting from the $B = 1$ Hedgehog solution, using a *product ansatz*, we build a $B = 2$ system and we study the interaction of the two solitons by changing the relative orientation of the Hedgehog quills.

The product ansatz approach has been used in the past in the Skyrme model to

describe the deuteron [129–132]. All these works start from the Hedgehog solution in the $B = 1$ sector and then the product ansatz is used to build different bi-skyrmions configurations where the isospin configuration plays a crucial role in providing the lowest energy state. The results given by the Skyrme model in this scheme are quite satisfactory and lead to a suitable description, concerning the quantum numbers, of the deuteron as a skyrmion. More sophisticated approaches, including specific symmetries of the lattice, have been adopted to build skyrmionic matter and to describe on one side multy-baryon systems [133] and on the other to study hot and dense baryonic matter [134, 135].

In soliton models including quark degrees of freedom, the $B = 2$ system has been already studied in previous papers [11, 136, 137] starting from the self-consistent solution of field equations for six quarks.

In this section we will present the first description of the $B = 2$ system in the Chiral Dilaton Model in the product ansatz scheme and the dependence of the soliton-soliton interaction on the isospin relative orientation. First in Sec. 4.1 we will present the $B = 1$ Hedgehog solution and the results for the single soliton in vacuum. Next in Sec. 4.2 we introduce the $B = 2$ soliton system and we will describe in detail the product ansatz. Finally in Sec. 4.2.2 we will show the results obtained.

4.1 The one baryon system

For our analysis we use the simplified Chiral Dilaton Model, including just quarks and chiral fields, σ and π. The Lagrangian of the model reads:

$$\mathcal{L} = \bar{\psi}[i\gamma^\mu\partial_\mu - g_\pi(\sigma + i\boldsymbol{\pi}\cdot\boldsymbol{\tau}\gamma_5)]\psi + \frac{1}{2}(\partial_\mu\sigma\partial^\mu\sigma + \partial_\mu\boldsymbol{\pi}\cdot\partial^\mu\boldsymbol{\pi}) - V(\phi_0,\sigma,\pi). \tag{4.1}$$

The potential, already introduced in Chapter 2, is given by:

$$V(\sigma,\boldsymbol{\pi}) = \lambda_1^2(\sigma^2+\boldsymbol{\pi}^2) - \lambda_2^2\,\ln(\sigma^2+\boldsymbol{\pi}^2) - \sigma_0 m_\pi^2\sigma \tag{4.2}$$

where:

$$\lambda_1^2 = \frac{1}{2}\frac{B\delta\phi_0^4+\epsilon_1}{\sigma_0^2} = \frac{1}{4}(m_\sigma^2+m_\pi^2) \tag{4.3}$$

$$\lambda_2^2 = \frac{1}{2}B\delta\phi_0^4 = \frac{\sigma_0^2}{4}(m_\sigma^2-m_\pi^2) \tag{4.4}$$

$$\epsilon_1 = m_\pi^2\sigma_0^2. \tag{4.5}$$

Here σ is the scalar-isoscalar field, $\boldsymbol{\pi}$ is the pseudoscalar-isotriplet meson field and ψ describes the isodoublet quark fields. The vacuum state is chosen, as usually, at $\sigma_v = f_\pi$ and $\boldsymbol{\pi} = 0$. In the following calculations we use: $g_\pi = 5$, $m_\sigma = 550$ MeV, $m_\pi = 139$ MeV and $f_\pi = 93$ MeV. The self-consistent $B = 1$ solution for the Lagrangian in eq. (4.1) has been obtained by adopting the Hedgehog ansatz, namely:

$$\begin{aligned}
&\sigma_{B=1}(\vec{r}) = \sigma_h(r) \quad , \quad \vec{\pi}_{B=1}(\vec{r}) = h(r)\hat{r}\ , \\
&\psi_{B=1}(\boldsymbol{r}) = \frac{1}{\sqrt{4\pi}}\begin{pmatrix} u(r) \\ i\boldsymbol{\sigma}\cdot\hat{\boldsymbol{r}}v(r)\end{pmatrix}\frac{1}{\sqrt{2}}(|u\downarrow\rangle - |d\uparrow\rangle).
\end{aligned} \tag{4.6}$$

The field equations for the Dirac components become:

$$\frac{du}{dr} = g_\pi h u + (-\epsilon - g_\pi \sigma_h)\, v \ , \tag{4.7}$$

$$\frac{dv}{dr} = -\frac{2}{r} v - g_\pi h v + (\epsilon - g_\pi \sigma_h)\, u \ , \tag{4.8}$$

while for the chiral fields, the equations become:

$$\frac{d^2\sigma_h}{dr^2} = -\frac{2}{r}\frac{d\sigma_h}{dr} + \frac{3g_\pi}{4\pi}(u^2 - v^2) + \frac{\partial V}{\partial \sigma_h} \tag{4.9}$$

$$\frac{d^2 h}{dr^2} = -\frac{2}{r}\frac{dh}{dr} + \frac{2}{r^2} h + \frac{3g_\pi}{2\pi} uv + \frac{\partial V}{\partial h}. \tag{4.10}$$

The solution has been obtained by imposing the following boundary conditions at $r = 0$:

$$\begin{aligned} u'(0) = v(0) = 0, \\ \sigma_h'(0) = h(0) = 0, \end{aligned} \tag{4.11}$$

and at infinity:

$$\begin{aligned} \sigma_h(\infty) = f_\pi,\, h(\infty) = 0, \\ \frac{v(\infty)}{u(\infty)} = \sqrt{\frac{-g f_\pi + \epsilon}{-g f_\pi - \epsilon}} \end{aligned} \tag{4.12}$$

where ϵ is the quark eigenvalue.

The solution for the sigma field developes a bag-like spatial structure where the quark fields become localized. In Fig. 4.1 we plot the Dirac components and the

chiral fields for the $B = 1$ solution. Here it can be seen that the σ field defines two distinct regions with a sharp jump around $r \approx 0.5$ fm, developing a bag-like spatial structure where the quark fields become localized. The pion field on the other hand has the ordinary behaviour, namely it vanishes at the origin, having its maximum exactly where the sigma changes sign, and it extends quite far out. Regarding the quark fields, we see that the upper component $u(r)$ reaches its maximum at the origin, concentrating the energy and the baryon density near $r = 0$, while the lower component has a peak between the origin and the maximum value of the pion field.

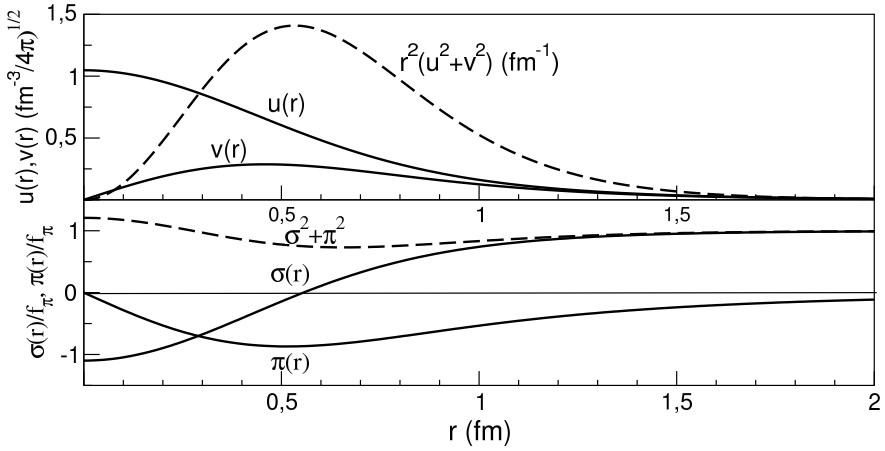

Figure 4.1: Upper and lower components of the Dirac spinor, σ and pion fields for the $B = 1$ solution.

The energy of the soliton in the Hedgehog configuration reads:

$$E_{B=1} = 4\pi \int r^2 dr (E_{int} + E_{kin,Q} + E_\sigma + E_\pi + E_{pot}) \tag{4.13}$$

where the quark-mesons interaction and the quark kinetic energies are:

$$E_{int} = \frac{3}{4\pi}\left[g_\pi \sigma_h (u^2 - v^2) + 2 g_\pi h u v\right] \tag{4.14}$$

$$E_{kin,Q} = \frac{3}{4\pi}\left(u\frac{dv}{dr} - v\frac{du}{dr} + \frac{2}{r}uv\right) \tag{4.15}$$

and the energy density of the meson fields and of the potential read:

$$E_\sigma = \frac{1}{2}\left(-\frac{d\sigma_h}{dr}\right)^2 \tag{4.16}$$

$$E_\pi = \left[\left(\frac{dh}{dr}\right)^2 + \frac{2}{r^2}h^2\right] \tag{4.17}$$

$$E_{pot} = V(\phi_0, \sigma_h, h) \tag{4.18}$$

Making such bag-like structure costs more than 800 MeV in meson field energy, which is compensated by the binding energies of the quarks, as shown in Table 4.1. In total, the whole system has a binding energy of about 400 MeV. The rms radius of the baryon number distribution is about 0.7 fm.

In this model the baryon density is carried exclusively by the quarks, while the energy density gets contributions form both quarks and mesons. n Fig. 4.2 we show on the left the energy density, which is maximum in the interior of the soliton but extends further out due to the pion contribution. On the right we plot the baryon density well localized in the interior of the soliton.

4.2 The two baryon system

In order to study the soliton-soliton interaction we need to construct a $B = 2$ system where two solitons are separated by a certain distance. Assume two

Table 4.1: Contributions to the soliton total energy at mean-field level in the Logarithmic model and in the linear σ model. All quantities are in MeV.

Quantity	Log. Model
Quark eigenvalue	83.1
Quark kinetic energy	1138.0
E_σ (mass+kin.)	334.5
E_π (mass+kin.)	486.0
Potential energy $\sigma - \pi$	105.7
$E_{q\sigma}$	-101.4
$E_{q\pi}$	-787.0
Total energy	1175.6

solitons, each a $B = 1$ hedgehpg solution, whose centers are at $\boldsymbol{r}_1$ and $\boldsymbol{r}_2$ (see Fig. 4.3).

For simplicity we place the centers of the two Hedgehogs symmetrically along the $\hat{z}$ axis at a distance d, hence the explicit expressions for the centers becomes:

$$\boldsymbol{r}_1 = (0, 0, -\frac{d}{2}) \tag{4.19}$$

$$\boldsymbol{r}_2 = (0, 0, \frac{d}{2}). \tag{4.20}$$

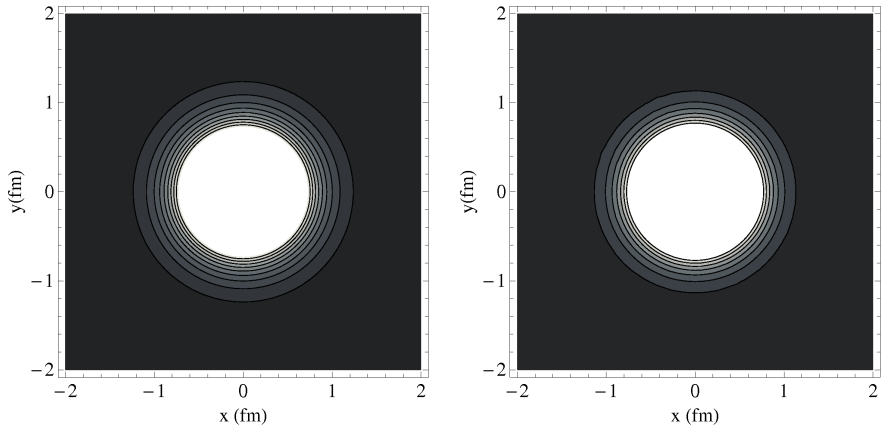

Figure 4.2: Distribution of the energy density (right) and baryon density (left) for the $B = 1$ solution.

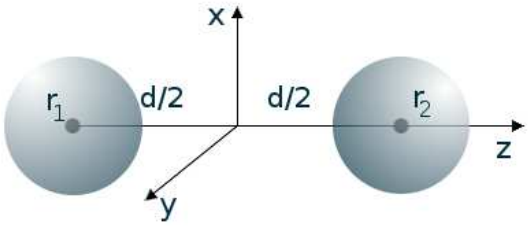

Figure 4.3: Construction of $B = 2$ system. The inter-separation d is along the $\hat{z}$ axis.

Let us define the radial distances measured from these centers:

$$d_1 = |\boldsymbol{r} - \boldsymbol{r}_1| = \sqrt{x^2 + y^2 + \left(z + \frac{d}{2}\right)^2} \tag{4.21}$$

$$d_2 = |\boldsymbol{r} - \boldsymbol{r}_2| = \sqrt{x^2 + y^2 + \left(z - \frac{d}{2}\right)^2}. \tag{4.22}$$

Each radial field of the $B = 1$ soliton solution, displaced in one of the two centers, can be expressed as a function of the distances d_1 and d_2, expressed above. The fields for the soliton placed in $\boldsymbol{r}_1$ become:

$$\sigma_1(\boldsymbol{r} - \boldsymbol{r}_1) = \sigma_h(d_1) \ , \tag{4.23}$$

$$\boldsymbol{\pi}_1(\boldsymbol{r} - \boldsymbol{r}_1) = \left(h(d_1)\frac{x}{d_1}, h(d_1)\frac{y}{d_1}, h(d_1)\frac{z + d/2}{d_1} \right) \ , \tag{4.24}$$

$$\psi_1(\boldsymbol{r} - \boldsymbol{r}_1) = \frac{1}{\sqrt{4\pi}} \begin{pmatrix} u_1(d_1) \\ i\boldsymbol{\sigma} \cdot (\hat{\boldsymbol{r}} - \hat{\boldsymbol{r}}_1) v(d_1) \end{pmatrix} \frac{1}{\sqrt{2}} (|u\downarrow\rangle - |d\uparrow\rangle) \tag{4.25}$$

and similarly for the soliton in $\boldsymbol{r}_2$:

$$\sigma_2(\boldsymbol{r} - \boldsymbol{r}_2) = \sigma_h(d_2) \ , \tag{4.26}$$

$$\boldsymbol{\pi}_2(\boldsymbol{r} - \boldsymbol{r}_2) = \left(h(d_2)\frac{x}{d_2}, h(d_2)\frac{y}{d_2}, h(d_2)\frac{z - d/2}{d_2} \right) \ , \tag{4.27}$$

$$\psi_2(\boldsymbol{r} - \boldsymbol{r}_2) = \frac{1}{\sqrt{4\pi}} \begin{pmatrix} u_2(d_2) \\ i\boldsymbol{\sigma} \cdot (\hat{\boldsymbol{r}} - \hat{\boldsymbol{r}}_2) v(d_2) \end{pmatrix} \frac{1}{\sqrt{2}} (|u\downarrow\rangle - |d\uparrow\rangle). \tag{4.28}$$

The next step is to build, starting from these two soliton configurations, the chiral and the Dirac fields for the $B = 2$ system.

4.2.1 The product ansatz

In order to build up the $B = 2$ soliton system we use the product ansatz following the work of Skyrme in Ref. [46]. In this scheme the chiral fields for the

$B = 2$ configuration are approximated by:

$$\left(\frac{\sigma_{B=2}(\boldsymbol{r}) + i\boldsymbol{\tau}\cdot\boldsymbol{\pi}_{B=2}(\boldsymbol{r})}{f_\pi}\right) = \left(\frac{\sigma_1(\boldsymbol{r}-\boldsymbol{r}_1) + i\boldsymbol{\tau}\cdot\boldsymbol{\pi}_1(\boldsymbol{r}-\boldsymbol{r}_1)}{f_\pi}\right) A \left(\frac{\sigma_2(\boldsymbol{r}-\boldsymbol{r}_2) + i\boldsymbol{\tau}\cdot\boldsymbol{\pi}_2(\boldsymbol{r}-\boldsymbol{r}_2)}{f_\pi}\right) A^\dagger \tag{4.29}$$

where f_π is introduced in order to have the proper dimensions and to recover the correct asymptotic behaviour. The operator A is a $SU(2)$ matrix inserted to take into account the relative orientation in the isospin space of one of the solitons with respect to the other. From eq.(4.29) we can obtain the expressions for the new chiral fields:

$$\begin{aligned}\sigma_{B=2}(\boldsymbol{r}) &= \frac{1}{f_\pi}(\sigma_1\sigma_2 + \boldsymbol{\pi}_1\cdot\boldsymbol{\pi}_2) \ , \\ \pi_{B=2}(\boldsymbol{r}) &= \frac{1}{f_\pi}(\sigma_1\boldsymbol{\pi}_2 + \sigma_2\boldsymbol{\pi}_1 + \boldsymbol{\pi}_1\times\boldsymbol{\pi}_2).\end{aligned} \tag{4.30}$$

In the Skyrme model, taking the product of two $B = 1$ soliton solutions is one of the most convenient ways to obtain the $B = 2$ intersoliton dynamics [134]. However, in the linear Chiral Soliton Model, with explicit quark degrees of freedom, since we are not restricted by a topological winding number, the *product* scheme may not be so essential, though it provides some advantages. First of all, it makes $\sigma_{B=2}$ and $\vec{\pi}_{B=2}$ naturally satisfy the boundary conditions at infinity, as can be seen from eqs.(4.30); that is,

$$\sigma_{B=2}(r\to\infty)\to f_\pi, \qquad \boldsymbol{\pi}_{B=2}(r\to\infty)\to 0 \tag{4.31}$$

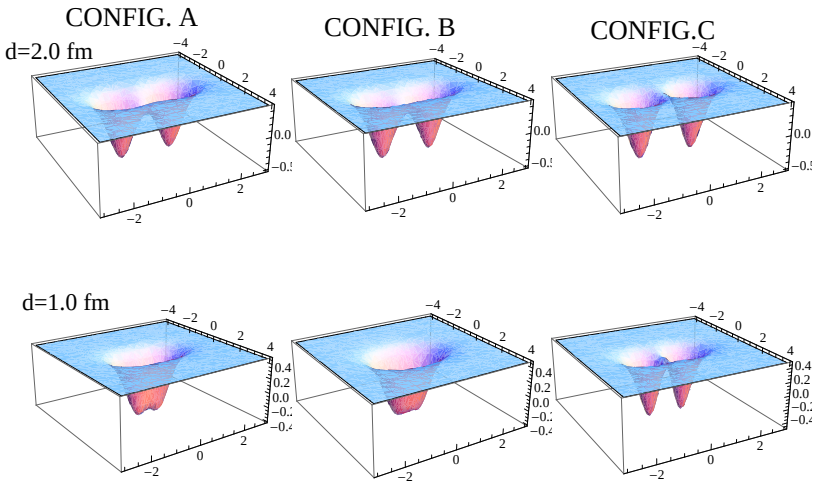

Figure 4.4: The structure of the σ field for B=2, $\sigma_{B=2}$, for the three configurations studied at large (upper figures) and small (lower figures) separation parameter d.

without any further artificial construction. Secondly, when the separation distance between two solitons is sufficiently large, the two solitons will have their own identity. We show in Fig.4.4 the $\sigma_{B=2}$ field obtained by this ansatz (4.30). Note that, at large and intermediate separations, the relative distance is a well defined quantity, while at short separations the fields deform heavily, making complicated overlapping shapes, and the relative distance cannot be well defined.

The relevant difference between the Chiral dilaton Model and Skyrme model is the presence of quark degrees of freedom that also need to be taken into account in the new fields configuration. At zero order, since the meson background configuration shows a reflection symmetry except for an isospin rotation, the quark

fields can be expressed as a linear combination given by:

$$\psi_{\pm}(\boldsymbol{r}) = \frac{1}{\sqrt{2}}(\psi_L(\boldsymbol{r}) \pm \psi_R(\boldsymbol{r})) \ , \tag{4.32}$$

where the left and right spinors read:

$$\begin{aligned} \psi_L(\boldsymbol{r}) &= \psi_1(\boldsymbol{r} - \boldsymbol{r}_1) \ , \\ \psi_R(\boldsymbol{r}) &= A\psi_2(\boldsymbol{r} - \boldsymbol{r}_2). \end{aligned} \tag{4.33}$$

In order to study the soliton-soliton interaction we decide to keep one soliton fixed and rotate the other, namely the one centered in $\boldsymbol{r}_2$. We will consider three different configurations, shown in Fig. 4.5:

1. Configuration A: $A = \mathbb{I}$, i.e. the two solitons are unrotated (panel A in Fig. 4.5).

2. Configuration B: $A = e^{i\frac{\tau_z}{2}\pi} = i\tau_z$, which corresponds to rotating the second soliton by an angle π about the axis parallel to the line joining the two centers (panel B in Fig. 4.5). Under such transformation the vector $\hat{\boldsymbol{r}}_2$ and the pion field become:

$$\begin{aligned} \hat{\boldsymbol{r}}_2 &= \left(-\frac{x}{d_2}, -\frac{y}{d_2}, \frac{z - \frac{d}{2}}{d_2} \right) \ , \\ \boldsymbol{\pi}_2 &= \left(-h(d_2)\frac{x}{d_2}, -h(d_2)\frac{y}{d_2}, h(d_2)\frac{z - d/2}{d_2} \right) \ , \end{aligned} \tag{4.34}$$

3. Configuration C:$A = e^{i\frac{\tau_x}{2}\pi} = i\tau_x$, leading to a rotation of 180 degrees around the axis perpendicular to the line joining the two solitons, in our

case the x axis. For this configuration we obtain:

$$\hat{\boldsymbol{r}}_2 = \left(\frac{x}{d_2}, -\frac{y}{d_2}, -\frac{z-\frac{d}{2}}{d_2} \right) ,$$
$$\boldsymbol{\pi}_2 = \left(h(d_2)\frac{x}{d_2}, -h(d_2)\frac{y}{d_2}, -h(d_2)\frac{z-d/2}{d_2} \right) . \tag{4.35}$$

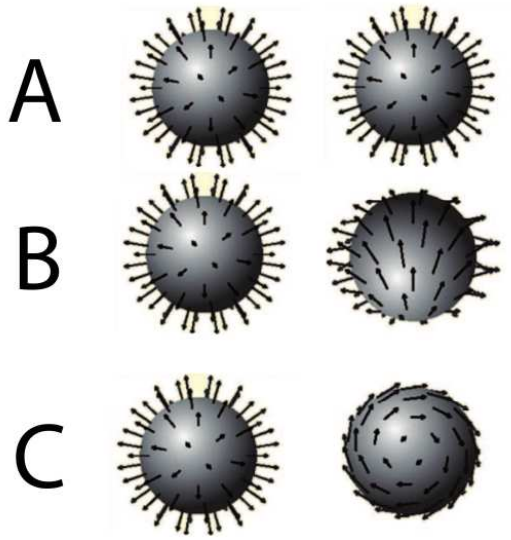

Figure 4.5: The three configurations A, B, and C corrensponding to the different orientation in the isospin space.

For each configuration we calculate the energy of the $B = 2$ soliton using the field expressions given in (4.30) and evaluating the expectation value of the Hamiltonian on the new $B = 2$ state where the valence quarks fill the levels provided by eq. (4.32). The energy hence reads:

$$E_{B=2} = E_{\sigma,B=2} + E_{\pi,B=2} + E_{pot,B=2} + E_{Q,B=2} \tag{4.36}$$

where the meson and potential energy are given by:

$$E_{\sigma,B=2} = \frac{1}{2}\int d^3r \nabla\sigma_{B=2} \cdot \nabla\sigma_{B=2} \ , \tag{4.37}$$

$$E_{\pi,B=2} = \frac{1}{2}\int d^3r \nabla\pi_{B=2} \cdot \nabla\pi_{B=2} \ , \tag{4.38}$$

$$E_{pot,B=2} = \int d^3r V(\sigma_{B=2}, \pi_{B=2}) \ , \tag{4.39}$$

while the quark energy reads:

$$E_{Q,B=2} = \langle B=2| \int d^3r \overline{\psi}[i\boldsymbol{\alpha}\cdot\nabla + g_\pi(\sigma_{B=2} + i\boldsymbol{\tau}\cdot\boldsymbol{\pi}_{B=2})]\psi|B=2\rangle \tag{4.40}$$

The soliton-soliton interaction energy is defined as:

$$V_{int}(d) = E_{B=2} - 2E_{B=1} \tag{4.41}$$

where the energy for the $B = 1$ system is given by eq.(4.13).

4.2.2 Results

In order to analyse how the interaction energy between the two solitons behaves with the different configurations, we study how the $B = 2$ system changes as the distance d gets smaller.

In Fig. 4.6 we show the energy density for all configurations as a function of the separation distance d. The profiles show that for all configurations at large and intermediate distances the two solitons are still well localized and an separation distance d can be defined. As the two solitons approach each other the shape of the halo around the core, provided by the meson fields, starts to deform heavily and the two baryons begin to strongly overlap. The deformation on the outer

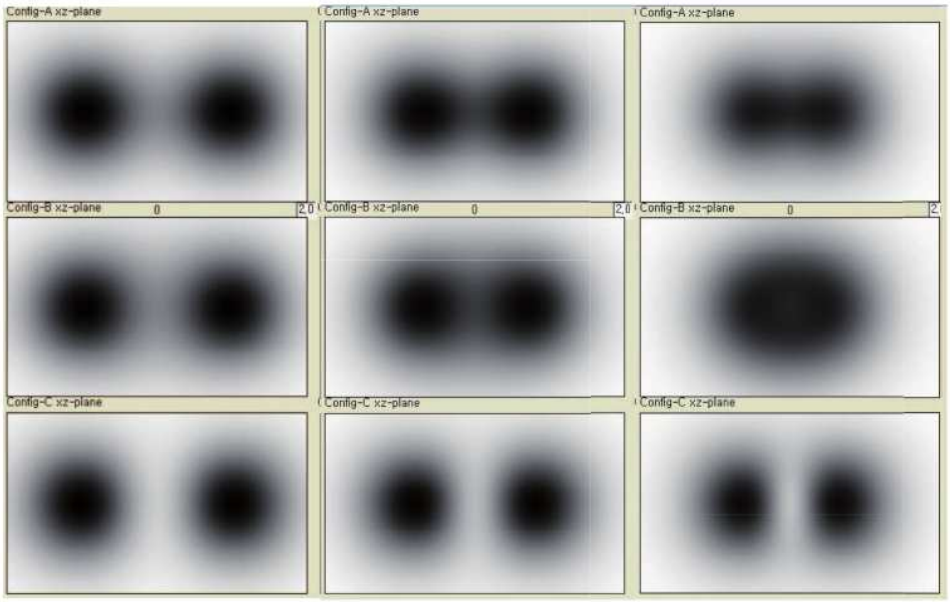

Figure 4.6: Profiles of the energy density of the $B = 2$ system, for all configurations, in the plane $x - z$ as a function of the distance d. The inter-soliton distance decreases from left to right, from the top the configuration are A, B and C in the lower panel.

part of the energy density is mostly due to the long-range contribution coming from the pion fields, while the change of the inner core is given by the repulsion of quarks at short separations. It can be seen that the rotation in isospin space does not affect the system at large d, but it allows to have different behaviours at smaller values of d, some partially attractive and some repulsive.

In order to provide a quantitative analysis of the dependence on isospin, we present in Fig. 4.7 the contribution from meson fields and quarks to the total interaction energy, defined in eq. (4.41) for the three configurations as a function of the separation distance.

First of all it has to be pointed out that the various contributions show very dif-

ferent behaviours in the three configurations, even if the total interaction energy at the end seems quite similar for all the configurations. Both the σ and the π energies are attractive, and for the sigma field the contribution is very large in A configuration while on the contrary the pion provides a huge attraction in rotated arrangements such as B and C and a very small one in the unrotated system. The quarks always show the mostly large repulsive contribution at all values of d which leads to the repulsion at short distances and the potential energy interaction has always small values in all configurations. Moreover it has to be noticed that at large distances, namely when the two solitons are far apart, we recover twice the energies of the $B = 1$ system. This should not be surprising since, as already stressed in the Skyrme's work [46], the product ansatz represents a good approximation when the two baryons are well-separated and there is no interaction between them. Hence at large distances the soliton-soliton system is similar to that obtained in the Skyrme model as expected, since when the two solitons are very far apart the interaction between them is mainly through meson exchange.

In Fig. 4.8 we present the total interaction energy for the three configurations. There is no significant difference in shape between the three cases but the three curves show very different behaviours as d decreases. Configurations A and B are the repulsive for all d while at large distances C is the most stable configuration.

As the two baryons get closer there is a transition from the C to the B configuration around $d \approx 1.5$ fm, just at the point where $V_{int.,C}$ rises (see Fig. 4.8).Configuration B seems to be the lowest energy state only in the region where the interaction is repulsive. It seems that the quark fields plays a crucial role at short separation.

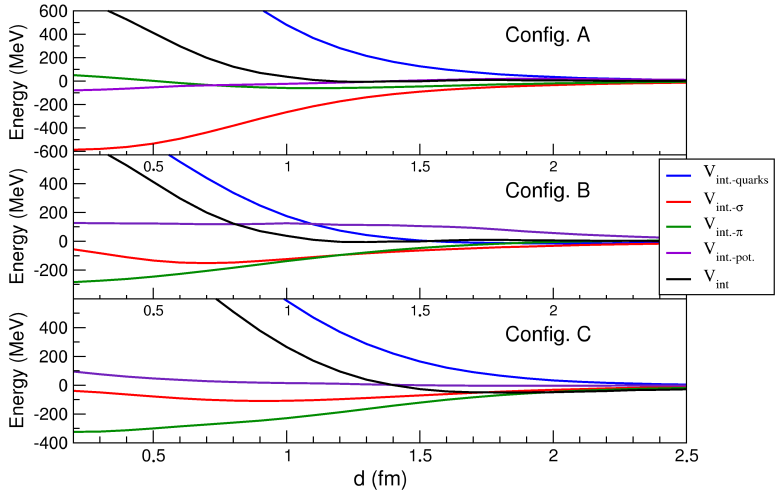

Figure 4.7: Contributions to the total soliton-soliton interaction energy (black line) as a function of the distance d for the three configurations A, B and C.

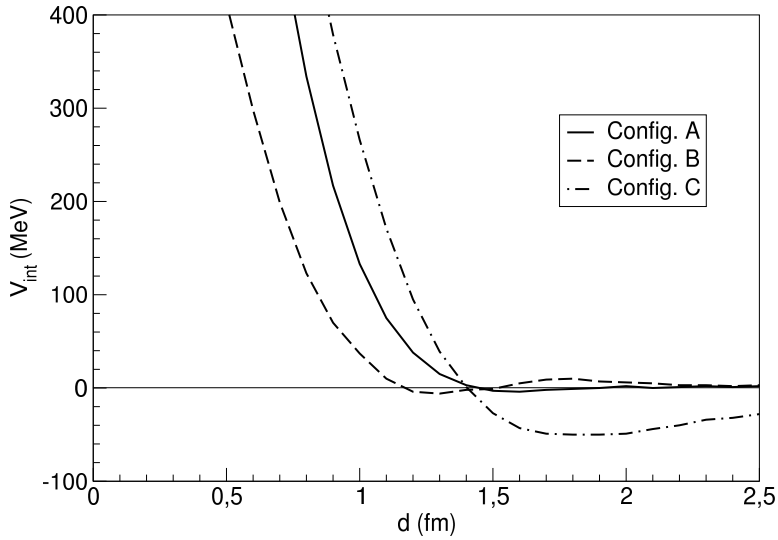

Figure 4.8: Soliton-soliton interaction energy as a function of the distance d for the three configurations A, B and C.

However, our first order calculations, without any modifications on the quark wave function, are too primitive to draw any conclusion for the short distance behaviour of the potential and the inclusion of quark excited states can be relevant in order to get more insight into the physical properties of the $B = 2$ soliton system.

Conclusions

In this thesis we used a Lagrangian with quarks degrees of freedom based on chiral and scale invariance to study how the soliton behaves in vacuum and at finite density. The main aim of the work was, besides checking that the model is able to reproduce a good description of the nucleon at zero density, to verify that the new logarithmic potential allows to reach higher densities in comparison to the linear σ model and that the introduction of vector mesons stabilises the soliton at high densities and provides the necessary repulsion to obtain saturation of chiral matter.
Here we presented results for the simple model with just chiral fields and also for the model including vector mesons.

To describe the single nucleon properties in vacuum we have used a projection technique. The main results obtained in vacuum are the following:

- *the interplay between quarks, chiral fields and vector mesons leads to values of the static observables in the present model that are comparable to the ones obtained using the linear σ model, when compared to the experimental values.*

For the description of the soliton at finite density we have employed the Wigner-Seitz approximation. We have shown that:

- *the new potential, which includes a logarithmic term originating from the breaking of scale invariance, allows the system, for each given m_σ, to reach densities larger than the ones obtained with the σ-model;*

- *as expected, the addition of the vector mesons plays a double role in the study at finite density: on one hand it stabilizes the solution and allows to reach even higher densities, on the other hand it partially provides the repulsion necessary to obtain saturation.The remaining repulsive contribution originates from the band effect.*

The possibility to obtain saturation seems to be a firm result of the model, at the level of the Wigner-Seitz approximation. In fact, by exploring the space of parameters,we have shown that the interplay between attraction, provided by the chiral fields, and repulsion, given by the omega field, allows the model to get saturation for a rather extended range of parameter values.

At sub-nuclear densities the dynamics should be dominated by the chiral fields and the modifications of the nucleon observables obtained in our work can therefore be physically relevant in the low-density range. In particular the isoscalar radius presents a slight swelling, of the order of 5%. This trend is in agreement with previous calculations [30, 123, 126].

The present work will be extended in several directions. First a more precise and accurate calculation of the band in the soliton crystal will be done following Ref. [36]. Work is in progress in order to study this same model by using the technique developed in Ref. [138], which provides a more precise description of a multi-soliton system. Finally, the model can also be studied at finite temperature, including the dynamics of the dilaton field. We can expect that the effect of the finite temperature on the soliton lattice will be to reduce the stability, by lowering

the value of the dilaton field and therefore making it more easy for the chiral fields to fluctuate. It will be interesting to compare the obtained phase diagram with the one proposed by McLerran and Pisarski [26].

Acknowledgements

I would like to thank my supervisors Dr. Alessandro Drago for and Prof. Vicente Vento, who supported me throughout this work with their patience and knowledge. It is a pleasure to also thank Prof. B.Y.Park for many stimulating discussions and for his fundamental contribution in the last part of this project. I would also like to thank M.Birse and J.McGovern for useful comments and tips on calculations.

Finally I wish also to say thank you to all my friends and colleagues who helped during this three years. Last but not least I thank my family, for everything.

Appendix I: Coherent states

In this appendix we discuss the main properties of the coherent states which have been used to describe the meson fields in the Hedgehog baryon wave function and to calculate the nucleon observables [27, 97]. In the following general discussion we define σ as a scalar-isoscalar field and $\boldsymbol{\omega}$ as a vector-isovector field.
In order to define a coherent state, we first need to expand in the plane-wave basis the chosen fields and its conjugate momentum as:

$$\begin{aligned}\sigma(\boldsymbol{r}) &= \int \frac{d^3k}{(2\pi)^3}\frac{1}{\sqrt{2\omega_\sigma}}\left[b(\boldsymbol{k})e^{i\boldsymbol{k}\cdot\boldsymbol{r}} + b(\boldsymbol{k})^\dagger e^{-i\boldsymbol{k}\cdot\boldsymbol{r}}\right] \ , \\ p_\sigma(\boldsymbol{r}) &= -i\int \frac{d^3k}{(2\pi)^3}\sqrt{\frac{\omega_\sigma}{2}}\left[b(\boldsymbol{k})e^{i\boldsymbol{k}\cdot\boldsymbol{r}} + b(\boldsymbol{k})^\dagger e^{-i\boldsymbol{k}\cdot\boldsymbol{r}}\right] \ , \end{aligned} \tag{4.42}$$

and in and analogous way for the ω field:

$$\begin{aligned}\boldsymbol{\omega}(\boldsymbol{r}) &= \int \frac{d^3k}{(2\pi)^3}\frac{1}{\sqrt{2\omega_\omega}}\left[\left(\frac{\boldsymbol{k}}{k}\frac{\omega_\omega}{m_\omega}b_L(\boldsymbol{k}) + \sum_T \hat{\boldsymbol{e}}_t(\boldsymbol{k})b_T(\boldsymbol{k})\right)e^{i\boldsymbol{k}\cdot\boldsymbol{r}} + h.c\right] \ , \\ \boldsymbol{p}_\omega(\boldsymbol{r}) &= -i\int \frac{d^3k}{(2\pi)^3}\sqrt{\frac{\omega_\omega}{2}}\left[\left(\frac{\boldsymbol{k}}{k}\frac{\omega_\omega}{m_\omega}b_L(\boldsymbol{k}) + \sum_T \hat{\boldsymbol{e}}_t(\boldsymbol{k})b_T(\boldsymbol{k})\right)e^{i\boldsymbol{k}\cdot\boldsymbol{r}} + h.c\right], \end{aligned} \tag{4.43}$$

where $h.c$ stands for hermitian conjugate. For the $\boldsymbol{\omega}$ we use the polarization basis given by the transversal unit vectors $\boldsymbol{e}_T (T = 1, 2)$ and the unit vector $\boldsymbol{k}/k$. The frequencies ω_i are defined by the dispersion relation $\omega_i = \sqrt{\boldsymbol{k}^2 + m_i^2}$. The choice of the plane-wave basis allows to obtain a vacuum both translationally and rotationally invariant. The rotational invariance leads to a more simple evaluation of matrix elements and overlaps between projected states.
The vacuum state $|0\rangle$ can be obtained by the application of the annihilation

operators $b(\boldsymbol{k})$:

$$b(\boldsymbol{k})|0\rangle = b_L(\boldsymbol{k})|0\rangle = b_T(\boldsymbol{k})|0\rangle = 0. \tag{4.44}$$

The coherent state is defined by translating in function space this vacuum state, so that it is centered on the classical field configuration σ_{cl} and ω_{cl} (given by eqs. (2.53) in chapter 2):

$$\begin{aligned} |\sigma\rangle &= U(\sigma, p_\sigma)|0\rangle \ , \\ |\omega\rangle &= U(\boldsymbol{\omega}, \boldsymbol{p}_\omega)|0\rangle \ , \end{aligned} \tag{4.45}$$

where the operator U reads:

$$\begin{aligned} U(\sigma, p_\sigma) &= exp\left(-i \int d^3r \left[\sigma_{cl}(\boldsymbol{r}) p_\sigma(\boldsymbol{r}) + p_{\sigma,cl}(\boldsymbol{r})\sigma(\boldsymbol{r})\right]\right) \ , \\ U(\boldsymbol{\omega}, \boldsymbol{p}_\omega) &= exp\left(-i \int d^3r \left[\boldsymbol{\omega}_{cl}(\boldsymbol{r}) p_\omega(\boldsymbol{r}) + \boldsymbol{p}_{\omega,cl}(\boldsymbol{r})\boldsymbol{\omega}(\boldsymbol{r})\right]\right) \ . \end{aligned} \tag{4.46}$$

In terms of the creation and annihilation operators the coherent states become:

$$\begin{aligned} |\sigma\rangle &= \frac{1}{N_s} \exp\left(\int d^3k b(\boldsymbol{k})^\dagger \sigma(\boldsymbol{k})\right)|0\rangle \ , \\ |\omega\rangle &= \frac{1}{N_o} \exp\left(\int d^3k \sum_\lambda b_\lambda(\boldsymbol{k})^\dagger \Omega_\lambda(\boldsymbol{k})\right)|0\rangle \ , \end{aligned} \tag{4.47}$$

where N_s, N_o are normalization factors and the polarization index $\lambda = 1, 2, L$. The coherent states $|\sigma\rangle$ and $|\omega\rangle$ are eigenstates of the annihilation operators $b(\boldsymbol{k})$ and $b_\lambda(\boldsymbol{k})$ and the amplitudes $\sigma(\boldsymbol{k})$ and $\Omega(\boldsymbol{k})$ are the corresponding eigenvalues.

Similar expressions hold for the other meson fields ρ, A_S and A_T and more details about the construction of coherent states can be found in [139, 140].
For the meson fields present in the Lagrangian in eq. (2.35) , the amplitudes of the corresponding coherent states read:

$$\begin{aligned}
\sigma(\boldsymbol{k}) &= \sqrt{\frac{\omega_\sigma}{\pi}} \int r^2 dr j_0(kr)\sigma_h(r) \\
\pi_a(\boldsymbol{k}) &= -i\hat{k}_a \sqrt{\frac{\omega_\pi}{\pi}} \int r^2 dr j_1(kr)h(r) \ , \\
\Omega_L(\boldsymbol{k}) &= \sqrt{\frac{\omega_\omega}{\pi}} \frac{1}{m_\omega k} \int r^2 dr j_1(kr)\omega(r) \ , \\
\Omega_T(\boldsymbol{k}) &= 0 \ , \\
\rho^a_T(\boldsymbol{k}) &= 0 \ , \\
\rho^a_L(\boldsymbol{k}) &= -i\hat{k}^a \sqrt{\frac{\omega_\rho}{\pi}} (\hat{e}_T \wedge \hat{\boldsymbol{k}})_a \int r^2 dr j_1(kr)\rho(r) \ , \\
A^a_L(\boldsymbol{k}) &= \frac{m_\rho}{\sqrt{\pi\omega_\rho}} \hat{k}^a \int r^2 dr \left[j_0(kr)A_S(r) - \frac{2}{3} j_2(kr)A_T(r) \right] \ , \\
A^a_T(\boldsymbol{k}) &= \hat{e}^a_T \sqrt{\frac{\omega_\rho}{\pi}} \int r^2 dr \left[j_0(kr)A_S(r) + \frac{1}{3} j_2(kr)A_T(r) \right] \ , \qquad (4.48)
\end{aligned}$$

where the radial fields $\sigma_h(r)$, $h(r)$, $\omega(r)$, $\rho(r)$, $A_S(r)$ and $A_T(r)$ are defined in chapter 2.
The average number of mesons is evaluated in the following way:

$$\begin{aligned}
\overline{N}_\sigma &= 2\pi \int r^2 dr \sigma_h(r)\tilde{\sigma}_h(r) \ , \\
\overline{N}_\pi &= 2\pi \int r^2 dr h(r)\tilde{h}(r) \ , \\
\overline{N}_\omega &= 2\pi \int r^2 dr \omega(r)\tilde{\omega}(r) \ ,
\end{aligned}$$

$$\overline{N}_\rho = 4\pi \int r^2 dr \rho(r)\tilde{\rho}(r) \ ,$$
$$\overline{N}_A = 4\pi \int r^2 dr \left[3A_S(r)\tilde{A}_S(r) + \frac{2}{3}A_T(r)\tilde{A}_T(r)\right] \ , \tag{4.49}$$

where the tilde fields are given by:

$$\begin{aligned}
\tilde{\sigma}_h(r) =& \frac{2}{\pi}\int dk k^2 \omega_\sigma j_0(kr) \int dr' r'^2 j_0(kr')\sigma_h(r') \ , \\
\tilde{h}(r) =& \frac{2}{\pi}\int dk k^2 \omega_\pi j_1(kr) \int dr' r'^2 j_1(kr')h(r') \ , \\
\tilde{\omega}_h(r) =& \frac{2}{\pi}\int dk k^2 \omega_\omega j_0(kr) \int dr' r'^2 j_0(kr')\omega(r') \ , \\
\tilde{\rho}(r) =& \frac{2}{\pi}\int dk k^2 \omega_\rho j_1(kr) \int dr' r'^2 j_1(kr')\rho(r') \ , \\
\tilde{A}_S(r) =& \frac{2}{\pi}\int dk k^2 dr' r'^2 j_0(kr) \\
& \times \frac{1}{3}\left[\left(2\omega_\rho + \frac{m_\rho^2}{\omega_\rho}\right) j_0(kr')A_S(r') \right. \\
& \left. + \frac{2}{3}\left(\omega_\rho - \frac{m_\rho^2}{\omega_\rho}\right) j_2(kr')A_T(r')\right] \ , \\
\tilde{A}_T(r) =& \frac{2}{\pi}\int dk k^2 dr' r'^2 j_2(kr) \\
& \times \left[\left(\omega_\rho - \frac{m_\rho^2}{\omega_\rho}\right) j_0(kr')A_S(r') + \frac{1}{3}\left(\omega_\rho + \frac{2m_\rho^2}{\omega_\rho}\right) j_2(kr')A_T(r')\right] .
\end{aligned} \tag{4.50}$$

References

[1] J. Blaizot and E. Iancu, *QCD perspectives on hot and dense matter* NATO science series: Mathematics, physics, and chemistry (Kluwer Academic Publishers, 2002).

[2] J.-P. Blaizot and E. Iancu, Phys.Rept. **359**, 355 (2002).

[3] A. Lacour, J. Oller, and U.-G. Meissner, Annals Phys. **326**, 241 (2011).

[4] M. G. Alford, A. Schmitt, K. Rajagopal, and T. Schafer, Rev.Mod.Phys. **80**, 1455 (2008).

[5] P. van Baal, AIP Conf.Proc. **892**, 241 (2007).

[6] M. Cheng *et al.*, Phys.Rev. **D75**, 034506 (2007).

[7] M. Cheng *et al.*, Phys.Rev. **D74**, 054507 (2006).

[8] S. Borsanyi *et al.*, JHEP **1011**, 077 (2010).

[9] Y. Nambu and G. Jona-Lasinio, Phys. Rev. **122**, 345 (1961).

[10] D. Diakonov and V. Petrov, Nucl.Phys. **B272**, 457 (1986).

[11] D. Diakonov, V. Petrov, and P. Pobylitsa, Nucl.Phys. **B306**, 809 (1988).

[12] M. C. Birse and M. K. Banerjee, Phys. Lett. **B136**, 284 (1984).

[13] G. Kahana, Nuclear Physics A **429**, 462 (1984).

[14] S. Kahana, G. Ripka, and V. Soni, Nucl.Phys. **A415**, 351 (1984).

[15] R. J. Furnstahl, B. D. Serot, and H.-B. Tang, Nucl. Phys. **A598**, 539 (1996).

[16] R. J. Furnstahl and B. D. Serot, Phys. Rev. **C47**, 2338 (1993).

[17] S. Weinberg, Phys. Rev. Lett. **18**, 507 (1967).

[18] R. J. Furnstahl, B. D. Serot, and H.-B. Tang, Nucl. Phys. **A598**, 539 (1996).

[19] J. Schechter, Phys.Rev. **D21**, 3393 (1980).

[20] A. A. Migdal and M. A. Shifman, Phys.Lett. **B114**, 445 (1982).

[21] E. Heide, S. Rudaz, and P. Ellis, Nuclear Physics A **571**, 713 (1994).

[22] G. Carter and P. Ellis, Nuclear Physics A **628**, 325 (1998).

[23] G. Carter, P. Ellis, and S. Rudaz, Nuclear Physics A **618**, 317 (1997).

[24] G. Carter, P. Ellis, and S. Rudaz, Nuclear Physics A **603**, 367 (1996).

[25] L. Bonanno and A. Drago, Phys. Rev. **C79**, 045801 (2009).

[26] L. McLerran and R. D. Pisarski, Nucl. Phys. **A796**, 83 (2007).

[27] M. C. Birse, Phys. Rev. **D33**, 1934 (1986).

[28] S. Phatak, Phys.Rev. **C44**, 875 (1991).

[29] K. Saito and A. W. Thomas, Phys. Rev. **C51**, 2757 (1995).

[30] J. R. Smith and G. A. Miller, Phys.Rev. **C70**, 065205 (2004).

[31] J. Achtzehnter, W. Scheid, and L. Wilets, Phys. Rev. **D32**, 2414 (1985).

[32] B. Glendenning, N. K., Phys. Rev. **C34**, 1072 (1986).

[33] D. Hahn and N. K. Glendenning, Phys. Rev. **C36**, 1181 (1987).

[34] M. C. Birse, J. J. Rehr, and L. Wilets, Phys. Rev. **C38**, 359 (1988).

[35] M. Birse, Progress in Particle and Nuclear Physics **25**, 1 (1990).

[36] U. Weber and J. A. McGovern, Phys. Rev. **C57**, 3376 (1998).

[37] P. Amore and A. De Pace, Phys. Rev. **C61**, 055201 (2000).

[38] CP-PACS Collaboration, A. Ali Khan *et al.*, Phys.Rev. **D65**, 054505 (2002).

[39] QCDSF/UKQCD Collaboration, M. Gockeler *et al.*, PoS **LAT2009**, 125 (2009), 0912.0167.

[40] A. Chodos, R. Jaffe, K. Johnson, and C. Thorn, Physical Review D **10**, 2599 (1974).

[41] A. Chodos, R. Jaffe, K. Johnson, C. Thorn, and V. Weisskopf, Physical Review D **9**, 3471 (1974).

[42] R. Friedberg and T. Lee, Physical Review D **15**, 1694 (1977).

[43] R. Friedberg and T. Lee, Physical Review D **18**, 2623 (1978).

[44] G. Chanfray and H. Pirner, Physical Review C **35**, 760 (1987).

[45] M. Gell-Mann and M. Levy, Nuovo Cim. **16**, 705 (1960).

[46] T. H. R. Skyrme, Nucl. Phys. **31**, 556 (1962).

[47] J. K. Perring and T. H. R. Skyrme, Nucl. Phys. **31**, 550 (1962).

[48] M. Fiolhais, J. Urbano, and K. Goeke, Phys.Lett. **B150**, 253 (1985).

[49] E. Ruiz Arriola, P. Alberto, J. N. Urbano, and K. Goeke, Z. Phys. **A333**, 203 (1989).

[50] R. Goldflam and L. Wilets, Physical Review D **25**, 1951 (1982).

[51] A. G. Williams, L. R. Dodd, and A. W. Thomas, Phys. Lett. **B176**, 158 (1986).

[52] K. Braeuer, A. Drago, and A. Faessler, Nucl. Phys. **A511**, 558 (1990).

[53] H.-J. Pirner, Prog.Part.Nucl.Phys. **29**, 33 (1992).

[54] E. Naar and M. C. Birse, J. Phys. **G19**, 555 (1993).

[55] L. R. Dodd, A. G. Williams, and A. W. Thomas, Phys. Rev. D **35**, 1040 (1987).

[56] A. Drago, K. Brauer, and A. Faessler, J.Phys.G **G15**, L7 (1989).

[57] R. Álvarez-Estrada, *Models of hadron structure based on quantum chromodynamics,* Lecture notes in physics (Springer-Verlag, 1986).

[58] C. DeTar and T. Kunihiro, Phys. Rev. D **39**, 2805 (1989).

[59] D. Zschiesche, L. Tolos, J. Schaffner-Bielich, and R. D. Pisarski, Phys.Rev. **C75**, 055202 (2007).

[60] V. Dexheimer, S. Schramm, and D. Zschiesche, Phys.Rev. **C77**, 025803 (2008).

[61] M. C. Birse and M. K. Banerjee, Phys. Rev. **D31**, 118 (1985).

[62] W. Broniowski and M. Banerjee, Physical Review D **34**, 849 (1986).

[63] J. Sakurai, Physical Review Letters **17**, 1021 (1966).

[64] G. 't Hooft, Nucl. Phys. **B72**, 461 (1974).

[65] J. Wess and B. Zumino, Phys.Lett. **B37**, 95 (1971).

[66] S. Coleman, *Aspects of symmetry* (Cambridge University Press, 1985).

[67] J.-B. Z. Claude Itzykson, *Quantum Field Theory* (Dover, 1980).

[68] J. Callan, Curtis G., S. R. Coleman, and R. Jackiw, Ann. Phys. **59**, 42 (1970).

[69] R. J. Crewther, Phys. Rev. Lett. **28**, 1421 (1972).

[70] M. S. Chanowitz and J. R. Ellis, Phys. Lett. **B40**, 397 (1972).

[71] J. C. Collins, A. Duncan, and S. D. Joglekar, Phys. Rev. **D16**, 438 (1977).

[72] M. A. Shifman, A. Vainshtein, and V. I. Zakharov, Nucl.Phys. **B147**, 448 (1979).

[73] M. A. Shifman, A. Vainshtein, and V. I. Zakharov, Nucl.Phys. **B147**, 385 (1979).

[74] H. Gomm and J. Schechter, Phys.Lett. **B158**, 449 (1985).

[75] E. K. Heide, S. Rudaz, and P. J. Ellis, Phys. Lett. **B293**, 259 (1992).

[76] J. R. Smith and G. A. Miller, Phys. Rev. Lett. **91**, 212301 (2003).

[77] J. R. Smith and G. A. Miller, Phys. Rev. C **70**, 065205 (2004).

[78] Y. Nambu, Phys. Rev. **106**, 1366 (1957).

[79] W. R. Frazer and J. R. Fulco, Phys. Rev. Lett. **2**, 365 (1959).

[80] N. M. Kroll, T. D. Lee, and B. Zumino, Phys. Rev. **157**, 1376 (1967).

[81] R. Machleidt, K. Holinde, and C. Elster, Phys. Rept. **149**, 1 (1987).

[82] K. Kawarabayashi and M. Suzuki, Phys. Rev. Lett. **16**, 255 (1966).

[83] Fayyazuddin and Riazuddin, Phys. Rev. **182**, 1617 (1969).

[84] M. Bando, T. Kugo, S. Uehara, K. Yamawaki, and T. Yanagida, Phys. Rev. Lett. **54**, 1215 (1985).

[85] M. Bando, T. Kugo, and K. Yamawaki, Prog. Theor. Phys. **73**, 1541 (1985).

[86] U. G. Meissner, Phys. Rept. **161**, 213 (1988).

[87] U. G. Meissner, N. Kaiser, A. Wirzba, and W. Weise, Phys. Rev. Lett. **57**, 1676 (1986).

[88] E. Cremmer and B. Julia, Phys. Lett. **B80**, 48 (1978).

[89] E. Cremmer and B. Julia, Nucl. Phys. **B159**, 141 (1979).

[90] O. Kaymakcalan and J. Schechter, Phys. Rev. **D31**, 1109 (1985).

[91] O. Kaymakcalan, S. Rajeev, and J. Schechter, Phys. Rev. **D30**, 594 (1984).

[92] H. Gomm, O. Kaymakcalan, and J. Schechter, Phys. Rev. **D30**, 2345 (1984).

[93] J. Sakurai, Annals Phys. **11**, 1 (1960).

[94] B. W. Lee and H. T. Nieh, Phys. Rev. **166**, 1507 (1968).

[95] S. Gasiorowicz and D. A. Geffen, Rev. Mod. Phys. **41**, 531 (1969).

[96] P. Ko and S. Rudaz, Phys. Rev. **D50**, 6877 (1994).

[97] E. Ruiz Arriola, P. Alberto, J. Urbano, and K. Goke, Nucl.Phys. **A591**, 561 (1995).

[98] K. Goeke, J. N. Urbano, M. Fiolhais, and M. Harvey, Phys. Lett. **B164**, 249 (1985).

[99] R. E. Peierls and J. Yoccoz, Proc. Phys. Soc. **A70**, 381 (1957).

[100] J. J. Griffin and J. A. Wheeler, Phys. Rev. **108**, 311 (1957).

[101] J. L. Dethier, R. Goldflam, E. M. Henley, and L. Wilets, Phys. Rev. D **27**, 2191 (1983).

[102] M. Abu-Shady and M. Rashdan, Phys.Rev. **C81**, 015203 (2010).

[103] T. S. T. Aly, J. A. McNeil, and S. Pruess, Phys. Rev. D **60**, 114022 (1999).

[104] B. D. Serot and J. D. Walecka, Adv. Nucl. Phys. **16**, 1 (1986).

[105] J. Achtzehnter and L. Wilets, Phys. Rev. **C38**, 5 (1988).

[106] J. Zimanyi and S. A. Moszkowski, Phys. Rev. **C42**, 1416 (1990).

[107] H. Feldmeier and J. Lindner, Z. Phys. **A341**, 83 (1991).

[108] H. J. Pirner, G. Chanfray, and O. Nachtmann, Phys. Lett. **B147**, 249 (1984).

[109] M. K. Banerjee, Phys. Rev. **C45**, 1359 (1992).

[110] E. Wigner and F. Seitz, Phys.Rev. **43**, 804 (1933).

[111] E. M. Nyman, Nucl. Phys. **B17**, 599 (1970).

[112] I. R. Klebanov, Nucl. Phys. **B262**, 133 (1985).

[113] Q. Zhang, C. Derreth, A. Schafer, and W. Greiner, J. Phys. **G12**, L19 (1986).

[114] H. Reinhardt, B. V. Dang, and H. Schulz, Phys. Lett. **B159**, 161 (1985).

[115] N. K. Glendenning and B. Banerjee, Lawrence Berkeley Lab. - LBL-20281 (85,REC.MAR.86) 20p.

[116] D. Hahn and N. K. Glendenning, Phys. Rev. **C36**, 1181 (1987).

[117] E. Wuest, G. E. Brown, and A. D. Jackson, Nucl. Phys. **A468**, 450 (1987).

[118] P. Amore, Nuovo Cim. **A111**, 493 (1998).

[119] C. Kittel, *Introduction to solid state physics* (Wiley, 2005).

[120] K. Shimizu, Rept. Prog. Phys. **52**, 1 (1989).

[121] A. Faessler, Prog. Part. Nucl. Phys. **36**, 337 (1996).

[122] European Muon Collaboration, J. Aubert *et al.*, Phys.Lett. **B123**, 275 (1983).

[123] L. S. Celenza, A. Rosenthal, and C. M. Shakin, Phys. Rev. Lett. **53**, 892 (1984).

[124] M. Ericson and M. Rosa-Clot, Phys.Lett. **B188**, 11 (1987).

[125] P. Mulders, Phys.Rept. **185**, 83 (1990).

[126] D.-H. Lu, K. Tsushima, A. W. Thomas, A. G. Williams, and K. Saito, Phys.Rev. **C60**, 068201 (1999).

[127] T. D. Cohen and W. Broniowski, Phys.Rev. **D34**, 3472 (1986).

[128] V. M. Sarti, A. Drago, V. Vento, and B.-Y. Park, (2012), 1201.0675.

[129] E. Braaten and L. Carson, Phys. Rev. Lett. **56**, 1897 (1986).

[130] J. J. M. Verbaarschot, Phys. Lett. **B195**, 235 (1987).

[131] A. J. Schramm, Phys. Rev. **C37**, 1799 (1988).

[132] E. Braaten and L. Carson, Phys. Rev. **D38**, 3525 (1988).

[133] G. E. Brown and M. Rho, (2009), 0907.1963.

[134] H.-J. Lee, B.-Y. Park, D.-P. Min, M. Rho, and V. Vento, Nucl. Phys. **A723**, 427 (2003).

[135] B.-Y. Park and V. Vento, (2009), 0906.3263.

[136] B. Blattel, J. Kunz, U. Mosel, and T. Reitz, Nucl. Phys. **A466**, 560 (1987).

[137] N. Sawado and S. Oryu, Phys. Rev. **C58**, 3046 (1998).

[138] B.-Y. Park, H.-J. Lee, and V. Vento, Phys.Rev. **D80**, 036001 (2009).

[139] M. C. Birse, E. M. Henley, G. Lubeck, and L. Wilets, Nucl. Phys. **A543**, 337c (1992).

[140] E. G. Lubeck, M. C. Birse, E. M. Henley, and L. Wilets, Phys. Rev. **D33**, 234 (1986).